Drivers of short-term variability in phytoplankton production in an embayment of the southern Benguela upwelling system: an observational and modelling study

Jessica Burger

Dissertation presented for the degree of Master of Science

in the Department of Oceanography

University of Cape Town

December 2018

Supervisors:

Dr. Sarah Fawcett

Associate Prof. Coleen Moloney

Plagiarism Declaration

I know the meaning of plagiarism and declare that all of the work in this dissertation, except for that which is properly acknowledged, is my own.

Signed by candidate

.....

Jessica Burger

5 December 2018

Acknowledgements

Firstly, I would like to thank my supervisors Dr. Sarah Fawcett and Associate Prof. Coleen Moloney for their guidance, mentorship and moral support throughout my master's degree.

I would like to extend my appreciation to Dr. Katye Altieri and Dr. David Walker, for their advice on various aspects of my dissertation and for always making time to listen to my many questions.

I am also grateful to the members of the Marine Biogeochemistry Laboratory at UCT, for many discussions that were essential to the development of the ideas presented in this thesis.

I am extremely thankful to Pieter Truter, Ruan Parrott, Nicole Dames, Kolisa Sinyanya and Zimkhita Gebe for their assistance in sample collection.

Furthermore, I would like to acknowledge Raquel Flynn, Dr. Raymond Roman, Shantelle Smith and Kurt Spence for their help in the laboratory. Special thanks must go to Shantelle Smith for teaching me many of the python skills I needed to make the model section of my dissertation possible.

I would like to thank my colleagues, Tanya Marshall, Ehlke de Jong, Raquel Flynn and Heather Forrer for their encouragement, and for creating such a motivating and enjoyable working environment.

Lastly, I would like to thank my family, Sandy, Izak, Amy and Robyn, for their support over the past two years.

Support for this study was provided by the National Research Foundation (NRF).

Contents

Abstract

In the southern Benguela upwelling system (SBUS), the wind-driven supply of nutrient-rich water from depth sustains elevated levels of primary productivity. St Helena Bay (SHB), a coastal embayment in the SBUS positioned north of an upwelling centre, is an area of water mass retention. In addition to supporting 40-50% of total SBUS productivity, SHB often experiences harmful algal blooms (HABs) and hypoxic conditions that are difficult to predict given the high sub-seasonal variability that characterises this region. To better understand this variability, net primary production (NPP), nitrate and ammonium uptake, and phytoplankton community composition were measured for ten days during the upwelling season at an anchor station in SHB. A period of active upwelling (days 1-5) was followed by one of relaxation (day 6-10), together constituting an "upwelling cycle". During upwelling, the mixed layer was deeper than the euphotic zone and phytoplankton were light-limited, evidenced by high ambient nutrient concentrations and relatively low rates of NPP and nitrate uptake. During relaxation, water column stratification increased, restricting phytoplankton production to a shallow, well-lit surface layer in which nitrate was exhausted after three days. The subsequent decline in NPP and nitrate uptake rates confirms that nutrient availability succeeded light as the ultimate control on productivity during the relaxation phase. Of the three phytoplankton size classes investigated (0.7-2.7 µm, 2.7-10 µm, >10 µm), the 2.7-10 µm fraction contributed most to the measured increases in biomass and nutrient uptake rates. This was unexpected given that large (>10 µm) diatoms typically dominate in upwelling systems; however, the 2.7-10 µm size fraction achieved a faster growth rate and sustained it for longer than the other size classes. The success of this size fraction may be partly due to a capacity for luxury nitrate uptake, evidenced by a low biomass C:N ratio and a nitrate uptake rate that was decoupled from NPP. Throughout the experiment, the phytoplankton community comprised mainly *Chaetoceros* spp. and *Skeletonema costatum*. These diatoms occupy a large size range (2-80 µm), although it is likely that they mainly occurred in the 2.7-10 µm size class during the experiment. They also produce resting spores that may provide a selective advantage during seeding in highly variable upwelling systems, increasing their chances of proliferating when conditions become favourable. Once the water column stratified, the phytoplankton community diversified, with dinoflagellates and the large diatom, *Coscinodiscus gigas* (200-500 µm), becoming more abundant. The contribution of *C. gigas* to biomass and productivity was not fully accounted for in the measurements because collected seawater was screened (200 µm mesh) prior to incubation. However, a simple N_3P_3 ecological model parameterized with the observations suggests that their contribution would have been minimal. The hydrographic data indicate that another upwelling cycle commenced by day 10 of the experiment. This likely prevented the further proliferation of dinoflagellates, some of which are HAB species, that may have succeeded the small diatoms given a longer period of quiescence. One implication of this is that understanding the rapid cycling between light and nutrient limitation, as induced by an actively upwelling versus stratified water column, may advance our capacity to predict the occurrence of HABs in SHB.

1 Introduction and literature review

1.1 Primary productivity in the ocean

Human activities like fossil fuel combustion and land-use change are playing a significant role in altering Earth's climate. Emissions of greenhouse gases such as carbon dioxide (CO_2) to the atmosphere increase the entrapment of long wavelength radiation emitted from the Earth's surface, leading to global warming (Sarmiento and Gruber 2002). Of the large quantity of CO_2 that has already been emitted, less than half remains in the atmosphere because it is being taken up by the ocean and land biosphere, which act as sinks for atmospheric CO_2 (Sabine et al. 2004).

On ~1000-year timescales, the ocean is the largest active reservoir of carbon on Earth, responsible for removing ~118 $\pm$ 19 Pg C from the atmosphere between ~1800 and 1994, making it the only net sink for atmospheric CO_2 over the last 200 years (Takahashi et al. 2002, 2008; Sabine et al. 2004). Primary production, which is central to the ocean's carbon cycle, is broadly defined as the "production of organic matter by phytoplankton" (Sigman & Hain, 2012), the microscopic, unicellular, autotrophic organisms suspended in the surface layer of the ocean. Phytoplankton use light energy from the sun to convert inorganic carbon (i.e., CO_2) to organic carbon biomass. This organic carbon is then available to support higher trophic levels such as zooplankton, fish, marine mammals and benthic organisms. These are heterotrophic, meaning that the respiration of organic matter is the sole mechanism by which they can obtain energy (Sigman & Hain, 2012).

Gross primary production (GPP) refers to the total rate of organic carbon production by autotrophs, while net primary production (NPP) is GPP minus the rate of autotrophic respiration (Bender et al. 1987); NPP is thus the organic carbon available to higher trophic levels. Finally, net community production (NCP) refers to GPP minus the rate of respiration by all organisms in the ecosystem (Sigman & Hain, 2012); on an annual basis, this quantity should approximate the flux of organic carbon from surface waters into the ocean interior (Falkowski et al., 2003).

1.2 The biological carbon pump and the new production paradigm

The mechanism by which atmospheric CO_2 is exported into the deep ocean after being fixed as organic carbon biomass by phytoplankton in the sunlit upper layer (euphotic zone) is referred to as the "biological carbon pump" (Ducklow et al., 2001). Only a small proportion of the organic matter produced in the euphotic zone eventually reaches the deep ocean because most is respired by heterotrophs in the surface layer. This recycling leads to nutrients being made immediately available for uptake by phytoplankton again (Eppley & Peterson, 1979). The small fraction of organic matter that settles through the interior of the ocean and eventually onto the seafloor is almost entirely decomposed by bacteria and converted back to its dissolved form (Martin et al., 1987). Given that the organisms responsible for decomposition rely on organic matter as their sole source of energy, they are highly efficient, such that less than 1% of organic carbon survives to be buried in the sediments of the deep sea (Sigman & Hain, 2012). The significance of organic carbon burial in the sediments is that CO_2 remains sequestered for decades to centuries or longer (Smetacek et al., 2012).

The flux of sinking organic matter out of the euphotic zone is termed "export production". Export production is difficult to measure directly, but it can be approximated by the rate of "new production". New production, as defined in a seminal study by Dugdale and Goering (1967), is the proportion of total primary production supported by sources of the nutrient, nitrogen (N), that are "new" to the euphotic zone (Fig. 1). The primary source of new N is upwelled nitrate (NO_3^-) (Fig. 1), although N_2 fixation, atmospheric N deposition and riverine N inputs can also contribute to new production (Dugdale & Goering, 1967; Bronk et al., 1994). Conversely, "regenerated production" is the proportion

of total production supported by N that is recycled within the euphotic zone (Fig. 1). Ammonium (NH_4^+) is the primary source of recycled N, although dissolved organic N (DON) and nitrite (NO_2^-) and NO_3^- produced in surface waters may also contribute to regenerated production (Dugdale & Goering, 1967). Eppley and Peterson (1979) demonstrated that, over appropriate space and time scales, the rate of particle flux out of the euphotic zone (measured using sediment traps) generally approximates the rate of new production. When phytoplankton grow, they build their biomass with an molar C:N:P stoichiometry of approximately 106:16:1, which is referred to as the "Redfield ratio" (Redfield 1958). Thus, for every mole of NO_3^- assimilated by phytoplankton, they fix ~6.63 moles of CO_2 as biomass, such that their average biomass C:N ratio is ~6.63:1. As a result, sinking particles that originate from new production in the euphotic zone act as a biological means by which atmospheric CO_2 is transported into the ocean interior (Eppley & Peterson, 1979).

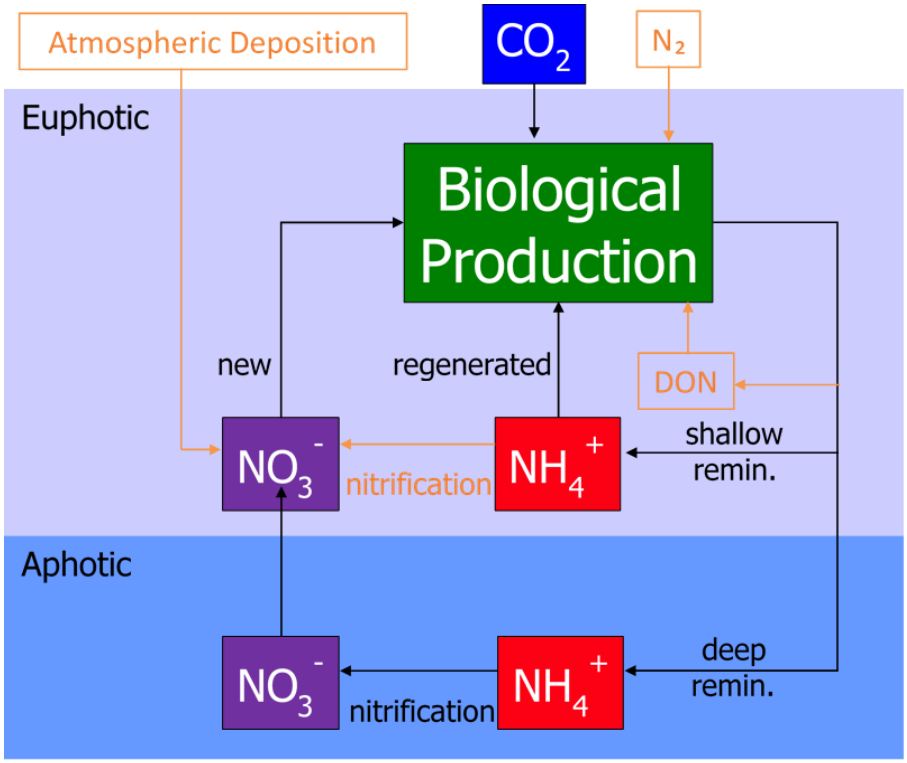

Fig 1. A schematic of the main processes associated with the biological pump, including atmospheric CO_2 fixation, new production, regenerated production, nitrification and shallow and deep remineralisation of sinking organic matter. Possible complications to the 'new production paradigm' such as atmospheric N deposition, dinitrogen (N_2) fixation, dissolved organic nitrogen (DON) cycling and euphotic zone nitrification are highlighted in orange.

Eppley and Peterson (1979) also defined the f-ratio (shorthand for "flux ratio") as the ratio of new production to total production, where total production is the sum of new and regenerated production. Provided a number of assumptions hold true (see section 1.8), the f-ratio provides a metric by which we can quantitatively evaluate the strength of the biological pump and compare the proportion of new production across oceanic regions. For example, an f-ratio greater than 0.5 is indicative of a strong biological carbon pump and high reliance on NO_3^- (Eppley & Peterson, 1979).

1.3 Drivers of productivity

To sustain elevated levels of primary production, phytoplankton require a range of nutrients such as nitrogen, phosphorus (P), iron (Fe) and silicate (Si). When surface ocean nutrient concentrations are low, phytoplankton growth is limited. The major limiting nutrient in much of the global ocean is dissolved inorganic nitrogen (DIN), forms of which include NO_3^-, NO_2^- and NH_4^+. In the absence of upwelling, most of the surface ocean is DIN-poor. Below the nutricline, the concentration of DIN is high due to the oxidation of organic material containing N. This process, nitrification, is the stepwise chemoautotrophic conversion of NH_4^+ to NO_2^- and then to NO_3^- by nitrifying bacteria and archaea.

As a result of nitrification, NH_4^+ and NO_2^- are usually present at low to undetectable concentrations below the nutricline. In surface waters, NH_4^+ is mainly produced by zooplankton grazing and bacterial activity (i.e., the microbial loop; Azam et al., 1983), and rapidly assimilated by phytoplankton such that its ambient concentration is typically very low. Additionally, NH_4^+ can be advected from elsewhere (Wilkerson & Dugdale, 2008) and observations suggest that the concentration of NH_4^+ in the surface waters of the coastal ocean may increase as upwelled water begins to age (Probyn et al., 1990).

The large reservoir of NO_3^- that exists at depth is only made available to phytoplankton following upward vertical advection, the most effective mechanism of which is upwelling. For example, surface NO_3^- concentrations measured in the southern Benguela upwelling system (SBUS) can be up to 25-30 μM (Andrews and Hutchings, 1980; Probyn & Painting, 1985; Shannon & O'Toole, 1999), similar to those measured in other upwelling systems (e.g., 24.8 μM in Monterey Bay, California; Wilkerson et al., 2000).

In addition to nutrients, phytoplankton require light. Sunlight is scattered and absorbed by seawater such that only the very surface of the ocean is illuminated. In oligotrophic, subtropical waters, light can penetrate as deep as 150 m, while in eutrophic, coastal regions there is little to no light below 10 m. As a result, photosynthesis is restricted to the uppermost layer of the ocean (Sigman & Hain, 2012). Solar radiation also warms the surface layer, causing it to become more buoyant than the cold, dense water below that originates from sinking at the poles. As a result, the sunlit upper layers float on top of the dense deeper layers, separated by a pycnocline/thermocline or vertical density/temperature gradient. Most of the ocean is stratified in this way, although mixing across the pycnocline and, by extension, transport of water and its dissolved nutrients can be driven by wind and other energy sources. The success of phytoplankton is strongly determined by this dual effect of light on photosynthesis and water column stratification. Photosynthesis restricts phytoplankton growth to the sunlit upper layers while upper ocean stratification prevents phytoplankton from being mixed down into the deep, dark ocean (Sigman & Hain, 2012). At the same time, water column stratification can act to impose nutrient limitation on productivity. Nutrients are quickly consumed in the euphotic zone while the pycnocline below it prevents nutrients from being reintroduced into the surface at a high enough rate to match consumption (Sigman & Hain, 2012).

According to Liebig's law of the minimum, the success of phytoplankton growth is determined by the "limiting nutrient", which is the least available resource (De Baar 1994), and phytoplankton growth limitation traditionally has been interpreted in this context. However, productivity can also be controlled by interactions between different nutrients as well as between nutrients and light. For example, phytoplankton growth in the Southern Ocean is simultaneously limited by the both iron and light (Sunda and Huntsman 1997), and diatom growth in the Subantarctic by iron, light and silicate (Boyd et al., 1999; Hutchins et al., 2001; Hoffmann et al., 2008).

1.4 Eastern boundary upwelling systems

There are four major eastern boundary upwelling systems (EBUSs), located in the Benguela, California, Iberia/Canary and Humboldt Currents, that exist on the eastern edges of the Atlantic and Pacific subtropical ocean gyres (Chavez & Messié, 2009; Bakun et al., 2015). These EBUSs are among the most productive regions of the world's oceans (Ryther, 1969), supporting more than 20% of the world's marine fish catch despite accounting for less than 1% of the global ocean's surface area (Pauly & Christensen, 1995).

At the eastern edge of the Atlantic and Pacific subtropical gyres, strong equatorward winds drive broad and slow eastern boundary currents. In brief, when a large-scale atmospheric high-pressure system exists near a similarly large low-pressure system, winds are induced that travel from the high pressure to the low pressure regions. Near the coast, these pressure systems may position themselves in a formation that induces alongshore winds that travel towards the equator. If this occurs at the eastern boundary of a major ocean basin, EBUSs are likely to result (García-Reyes et al. 2015).

As they travel along the coast, equatorward winds are deflected from their path by the effect of the Earth's rotation (i.e., the Coriolis effect), which causes winds to deviate to the left (right) of their path in the southern (northern) hemisphere (Ekman, 1923; García-Reyes et al., 2015). In the southern hemisphere, under the influence of steadily blowing equatorward winds, surface waters are set into motion at an angle of 45° to the left of the wind. Momentum introduced at the surface is lost with depth in the water column due to friction. Each successively deeper layer of water is deflected farther to the left until an end point is reached at which a very weak current flows in the opposite direction to that of the motion at the surface. The depth at which this occurs represents the base of the wind-driven mixed layer. The resulting net direction of motion of the full mixed layer is 90° to the left of the wind. This amounts to a net offshore transport of mixed layer waters at the eastern boundaries of ocean basins and is termed Ekman transport (Ernst, 2000). As surface waters are advected offshore, they are replaced by deep water drawn up from below (i.e., upwelling); this water is characteristically cold and nutrient-rich (Chavez & Messié, 2009; García-Reyes et al. 2015). Once supplied to the sunlit upper layer of the coastal zone, upwelled nutrients are available for photosynthesis and regularly support dense phytoplankton blooms. Phytoplankton blooms nourish zooplankton communities, which in turn support large populations of resident small pelagic fish (e.g., sardines and anchovies). Fluctuations in the abundance of such fish exert a top-down and bottom-up control on marine ecosystems by influencing the abundance of zooplankton (Verheye & Richardson, 1998) and the success of higher trophic level marine mammals, seabirds and other commercially-important fish (Bakun et al. 2015).

EBUSs provide various recreational, economic and ecosystem services to the nearly 80 million people that reside at the coast (García-Reyes et al. 2015). However, the productivity of coastal upwelling systems is threatened by climate change. It has been suggested that an increase in spring and summer upwelling intensity as well in the associated rate of offshore advection is to be expected (Bakun et al. 2015). This prediction is generally supported by recent observations (Sydeman et al. 2014) and by global modelling studies that predict an intensification of regional coastal winds during the 21st century (Rykaczewski et al., 2015; Wang et al., 2015). While EBUSs are regarded as relatively resilient oceanic regimes due to their inherent variability (Chavez and Messié 2009), possible climate change-related impacts include an increased frequency of hypoxic events, increased ocean acidity and a decline in the amount of suitably-sized food particles available to juvenile fish. Additionally, changes in primary production and phytoplankton community composition are likely, with direct implications for higher trophic levels (Bakun et al. 2015). Overall, the impact that climate change will have on EBUS

biogeochemistry is known with little confidence and more comprehensive research is required to fully understand both the environmental and societal impacts (García-Reyes et al. 2015).

1.5 The Benguela upwelling system

The Benguela upwelling system (BUS) is bounded by the broad, northward-flowing Benguela current positioned on the southwest coast of Africa that forms the eastern flank of the South Atlantic subtropical gyre (Fennel 1999). It also hosts strong, narrow and fast jets that flow equatorward at the shelf edge, and an under current that flows along the shelf slope and bottom towards the pole (Shillington et al., 2006; Veitch et al., 2018).The BUS extends from the southern tip of Africa (37°S) to about 14°S and is constrained at its northern edge by the Angola-Benguela frontal zone and at its southern edge by the Agulhas current retroflection region (Shannon & Nelson, 1996). The Benguela current differs from other EBUS currents in that it is strongly influenced by the Agulhas current retroflection, a water mass that circulates at the southern tip of the African continent. No other EBUS is influenced by the western boundary current of another ocean basin (Chavez and Messié 2009). In fact, both the northern and southern extents of the BUS are bounded by warm water regimes, making it a unique system (Shannon & O'Toole, 2003; Shannon & Nelson, 1996). In addition, the BUS is arguably the most productive of all the major EBUSs. In a study conducted by Carr (2001), satellite-derived estimates of potential primary production for the four major EBUSs were compared. Using 24 months of SeaWiFs data, primary production estimated for active areas (chlorophyll concentration >1 $mg.m^{-3}$) was greatest in the Benguela current (0.37 Gt C yr^{-1}). For comparison, primary production estimated in the Canary, Humboldt and California Currents was 0.33 Gt C yr^{-1}, 0.20 Gt C yr^{-1} and 0.04 Gt C yr^{-1}, respectively (Carr 2001).

Within the BUS there are several upwelling cells. Upwelling cells are centres of semi-permanent upwelling, usually found near regions of cyclonic wind stress curl and located for the most part where changes occur in the orientation of the coastline (Shannon & Nelson, 1996). In an analysis of satellite-derived sea surface temperature for 1982 to 1985, Lutjeharms and Meeuwis (1987) identified eight distinct upwellings cells, namely the Cunene, Namibia, Walvis Bay, Luderitz, Namaqua, Cape Columbine, Peninsula and Agulhas cells. The Luderitz cell (27°S) experiences the coldest average sea surface temperatures, the greatest westward extent of upwelling, and the greatest frequency of high wind stress and induced upwelling events (Lutjeharms and Meeuwis 1987). In addition, the Luderitz cell separates the BUS into its northern and southern components.

The BUS is driven by large scale wind patterns. The winds over the Benguela are controlled by the anticyclonic motion of the South Atlantic high-pressure cell (a permanent feature of the South Atlantic; Andrews & Hutchings, 1980), the seasonal low pressure cell over the continent and the cyclones that travel eastward across southern Africa. The South Atlantic high-pressure cell exists year-round and shifts seasonally over about 6° of latitude, reaching its northern extent in May and southern extent in February. It also shifts about 13° in longitude, reaching its most westward position in August (Tyson, 1986). Over southern Africa, the air pressure changes significantly between seasons. In summer, surface heat-induced low pressure cells occur over land while in winter, high pressure cells occur over land because the continental heat low and Intertropical Convergence Zone (ITCZ) shift northwards, creating seasonally changing land-sea pressure gradients. The anticyclonic motion associated with the South Atlantic high is steered along the coast by the thermal barrier created by the arid conditions of the coastal region (Nelson & Hutchings, 1983).

During spring, summer and autumn, when the anticyclonic high-pressure cell moves periodically eastwards and south of the continent, south-easterly winds dominate (more than 50% of the time; (Andrews & Hutchings, 1980). Maximum frequencies of south easterly winds occur in spring and late

summer and the upwelling season extends from September to March. In winter, when the South Atlantic high-pressure system shifts northward, the south is exposed to a greater frequency of westerly winds that do not favour upwelling (Andrews & Hutchings, 1980).

Low pressure cells move from west to east, driven by an atmospheric circumpolar wave that travels across the southern tip of South Africa. During this time, north-westerly winds dominate, although not to the same extent as the south-easterly winds in summer. In winter, south-easterly winds do occur, but they persist for a much shorter period (<10% of the time; Andrews & Hutchings, 1980).

In the southern Benguela, upwelling occurs periodically, lasting for 3 to 10 days before winds relax or are reversed due to the passage of eastward mid-latitude cyclones to the south of the African continent (Shillington et al. 2006). In the northern Benguela, the winds are less seasonal and upwelling is perennial (Shannon & Nelson, 1996). This study focuses on the southern Benguela upwelling system (SBUS).

1.6 St Helena Bay

While the SBUS is primarily driven by the strength of upwelling-favourable equatorward winds, coastal topography also plays a key role. Irregularities in the coastline such as bays and capes can significantly alter upwelling processes by causing the coastal winds and alongshore currents to vary, with implications for the chemistry and biology (Chavez and Messié 2009). Capes or headlands are often exposed to intense winds, upwelling and horizontal advection, while on the leeward side of these headlands, bays experience weaker winds, less upwelling and minimal advection. As a result, bays positioned behind headlands (also termed “upwelling shadows” or “retention zones”) often experience large phytoplankton blooms because reduced physical activity and associated water column stratification allow biological processes to occur without biomass continually being advected offshore (Chavez & Messié, 2009).

St Helena Bay (SHB), located off the west coast of South Africa, is a semi-enclosed, shallow (<100 m) bay positioned north of Cape Columbine (Fig. 2). Cape Columbine is one of the major upwelling centres in the SBUS and largely controls the biogeochemical traits of the SHB region (Monteiro & Roychoudhury, 2005). Upwelled waters typically flow north-westward off the tip of Cape Columbine (Shannon & Nelson, 1996), and a sluggish cyclonic gyre is regularly observed in the bay (Touratier et al., 2003).

SHB possesses the hydrodynamic characteristics typical of a retention zone located on the equatorward side of an upwelling cape in an EBUS (Chapman & Bailey, 1991). It also shares several biogeochemical traits with comparable systems in other parts of the world. For example, it acts as a nursery ground for the early life stages of fish (Hutchings, 1992) and often experiences harmful algal blooms (Pitcher et al., 1992) and hypoxic conditions (Chapman & Bailey, 1991). While the surface waters of the SBUS are usually well oxygenated, oxygen (O_2) consumption during bacterial decomposition of phytoplankton cells after they die and sink can result in O_2-deficient bottom waters (Chapman & Shannon, 1985). Anaerobic bacteria can continue to decompose organic matter in O_2-deficient waters using NO_3^- as an electron acceptor instead of O_2, resulting in the stepwise reduction of NO_3^- to NO_2^- and eventually dinitrogen gas (N_2) (i.e., through denitrification) (Devol, 2003). Studies conducted in the BUS suggest that the majority of N loss in its oxygen minimum zones (OMZs) (which typically occur in the northern BUS rather than the SBUS) is due to anammox (the anaerobic oxidation of NH_4^+ with NO_2^- to N_2) rather than canonical denitrification (Kuypers et al., 2005). N loss due to anammox and/or denitrification and the release of P from sediments in O_2-deficient environments

(Kuypers et al., 2005; Flohr et al., 2014) leads to upwelling waters with anomalous nutrient N:P ratios, for which the BUS is well known (Tyrrell & Lucas, 2002).

1.7 Measuring N uptake

Nitrogen has two stable isotopes, ^{15}N and ^{14}N, but most N (> 99%) exists as ^{14}N. To measure rates of N uptake, ^{15}N-labelled DIN (typically NO_3^- or NH_4^+) is added to an incubation bottle containing a natural phytoplankton assemblage. After incubating the assemblage for a known period of time, any ^{15}N incorporated into the phytoplankton biomass can be determined by filtering the sample, oxidising the organic N to N_2 gas via high temperature combustion and measuring its ratio of ^{15}N:^{14}N using mass spectrometry. In this way, ^{15}N-labelled DIN is used to trace uptake into the cell (Lipschultz, 2008; Miller & Wheeler, 2012). The first experiments conducted to determine rates of N uptake using the stable isotope tracer technique were performed by Dugdale and Goering (1967) in the Sargasso Sea. Later, technological advances in mass spectrometry and mass spectrometers designed specifically for the stable isotope tracer technique led to wider use of this method (e.g., Probyn & Painting, 1985; Dugdale & Wilkerson, 1986; Probyn et al., 1990; Bronk & Ward, 1999; Kudela & Dugdale, 2000).

Transport rates (i.e., ρNO_3^- or ρNH_4^+, measured in μmol L^{-1} hr^{-1}) describe phytoplankton community-level assimilation of ambient seawater NO_3^- or NH_4^+ (taken to approximate new or regenerated production) and may change depending on the concentration of particulate organic N biomass (PON) in the water column. Uptake rates can also be reported as "biomass-specific" rates, denoted using the symbol V (i.e., $V_{NO_3^-}$ or $V_{NH_4^+}$, with units of hr^{-1}). Specific uptake rates are intrinsic physiological parameters specific to a phytoplankton species under a particular set of conditions and are commonly normalized to chlorophyll content or PON concentration. Once NO_3^- and NH_4^+ uptake rates have been determined, the proportion of new production (i.e., f-ratio) can be calculated (Eppley & Peterson, 1979; Wilkerson & Dugdale, 2008).

High rates of NO_3^- uptake are typically observed in EBUSs. Moreover, a high ρNO_3^- is usually accompanied by a high $V_{NO_3^-}$ and a high f-ratio. The highest NO_3^- uptake rates measured in the SBUS are on the order of 0.5 μmol L^{-1} hr^{-1} while the highest f-ratio is ~0.7 (Probyn 1985; Probyn 1992). However, there is a great deal of uncertainty associated with these estimates.

1.8 Exceptions to the rule

1.8.1 N_2 Fixation

While widely used to estimate carbon export potential, the new production paradigm has certain limitations. Following Dugdale and Goering (1967), upwelled NO_3^- is assumed to be the main form of new N to the euphotic zone such that NO_3^- assimilation can be equated to new production. Dugdale and Goering (1967) emphasized the potential for additional sources of new N to the euphotic zone but there were few data available at the time to evaluate their relative importance. These potential sources of new N include atmospheric N deposition and N_2 fixation.

Most N on Earth is present in the form of dinitrogen gas (N_2), which is usually unavailable for use by phytoplankton except when fixed to DIN by prokaryotic organisms that possess the enzyme nitrogenase (known as "diazotrophs"). For the most part, N_2 fixation in the ocean is facilitated by free living species of cyanobacteria, mainly *Trichodesmium*, or by bacteria of the genus *Rhizosolenia* that grow in a symbiotic relationship with diatoms (Howarth et al., 1988). There is some evidence that N_2 fixation is a significant input of new N to the euphotic zone in certain ocean regions (Gruber & Sarmiento, 1997; Karl et al., 1997, 2002; Capone et al., 2005), allowing for primary production to occur when other forms of bioavailable N are depleted. However, others suggest that N_2 fixation only has a

minor role to play in supporting new production (Howarth et al., 1988; Needoba et al., 2007; Knapp et al., 2016).

The majority of N_2 fixation research has focused on the tropical and subtropical North Atlantic (e.g., Capone et al., 2005) and North Pacific (e.g., Karl et al., 1997; Dore et al., 2002). This is primarily due to N_2 fixation being historically attributed to *Trichodesmium*, which inhabits warm, stratified and nutrient-poor areas of the surface ocean (Knapp, 2012). However, recent work has begun to challenge the oceanic N_2 fixation paradigm. For example, the use of molecular tools has identified different diazotrophs with different physical and/or chemical traits to those studied previously (Zehr et al., 2001). Additionally, modelling studies (Deutsch et al., 2007) suggest geographic distributions of organisms capable of N_2 fixation (including *Trichodesmium*) that differ from our oligotrophic ocean-centric expectations. Finally, many *in situ* and culture-based studies have questioned the sensitivity of diazotrophs to nutrient concentrations, in particular the extent to which ambient NO_3^- and/ or NH_4^+ inhibits N_2 fixation. In light of this, it is possible that N_2 fixation has a much wider geographic distribution than previous thought, extending beyond the surface layer of oligotrophic ocean gyres (Knapp, 2012). Indeed, one modelling study focused on nutrient ratios in the surface ocean predicted that high rates of N_2 fixation should occur in waters overlying denitrification zones due to the subsequent upwelling of waters with a low nutrient N:P ratio (Deutsch et al., 2007).

Due to its upwelling nutrient ratios, the BUS is a region in which Deutsch et al. (2007) predicted high rates of N_2 fixation should occur. To address this, Sohm et al. (2011) performed a series of $^{15}N_2$ fixation experiments across the South Atlantic gyre and into the northern BUS. Surface N_2 fixation rates were lowest in the gyre and highest in the northern BUS (up to ~8 nmol N L^{-1} d^{-1}) (Sohm et al. 2011). In addition, Fernandez et al. (2011) demonstrated the occurrence of N_2 fixation in the nutrient-rich upwelling system of Peru/Chile. Both regions experience low oxygen conditions and have the potential for denitrification, although this is far more intense in the Peruvian region (Codispoti & Christensen, 1985; Chavez & Messié, 2009). As a result, N_2 fixation could occasionally supplement fixed N in upwelling regions (Fernandez et al., 2011), contributing to new production. If this N_2 fixation is not accounted for, rates of new production could be underestimated. To our knowledge, there are no estimates of N_2 fixation for the SBUS, although work in the northern BUS has shown that, although the N:P ratio of the subsurface nutrient pool should favour N_2 fixation (i.e., N:P < 16:1; Deutsch et al., 2007; Flohr et al., 2014; Knapp et al., 2016), little to no N_2 fixation occurs (Sohm et al., 2011; Wasmund et al., 2015). This has been attributed to iron limitation or to a lack of diazotrophs (Moore et al., 2009; Emeis et al., 2018). Thus, while we cannot completely rule out the possibility of N_2 fixation in the SBUS due to the paucity of measurements, low rates in the surrounding region suggests that it is reasonable to ignore this process when estimating new production in the SBUS.

1.8.2 Atmospheric nitrogen deposition

Atmospheric N deposition, whether direct or indirect (i.e., via runoff), has the potential to influence primary production at the coast (Paerl, 1995), especially considering that coastal waters are generally N-limited and therefore sensitive to N enrichment (Dugdale & Goering, 1967). While initially thought to be of minor importance to oceanic primary production (Knap et al., 1986), some authors suggest that atmospheric N inputs can support a significant proportion of new production (Legendre & Gosselin, 1989; Owens et al., 1992; Paerl, 1995). Using the natural abundance isotopes of N, Paerl & Fogel (1994) emphasized the contribution of atmospheric N deposition to the coastal waters of the north Atlantic Ocean. Furthermore, Owens et al. (1992) suggested, based on a nine year time series of wet deposition, that oceanic primary production may be directly influenced by increases in human

activities like fossil fuel combustion (which increases the inorganic N concentrations in the atmosphere) via the atmospheric N deposition pathway (Owens et al., 1992).

When atmospheric N deposition is significant and not accounted for, new production will be underestimated. To our knowledge, there are no estimates of atmospheric N deposition for the SBUS. According to Duce et al. (2008), the average annual flux of fixed N to the world's oceans in the form of atmospheric deposition is lower than that due to N_2 fixation. In addition, Baker et al. (2010) suggest that atmospheric N deposition is greater in the northern than the southern hemisphere. Another study by Baker et al. (2003) estimates the magnitude of atmospheric N deposition over the entire Atlantic Ocean and finds that the lowest rates of N input occur in the region of the south Atlantic closest to the SBUS. As a result, it is probably reasonable to neglect the contribution of atmospheric N deposition to new production in the SBUS.

1.8.3 Euphotic zone nitrification

Nitrification is the two-step oxidation of NH_4^+ through NO_2^- to NO_3^-. When using the stable isotope tracer technique to determine new production, we assume that all NO_3^- assimilated by phytoplankton is new, originating below the euphotic zone. By extension, we thus assume that there are insignificant rates of nitrification in the euphotic zone (Clark et al., 2008). Nitrification was previously thought to occur in regions of the ocean characterised by relatively high ambient NH_4^+ concentrations and sub-saturating levels of dissolved oxygen, like in oxygen minimum zones (OMZs) (Ward et al., 1989). Additionally, nitrifying microorganisms appear to be outcompeted by phytoplankton for NH_4^+ (Ward 1985; 2005; Smith et al., 2014) and to be inhibited by light (Schön & Engel 1962; Hooper & Terry 1974; Horrigan et al. 1981; Olson 1981), therefore restricting nitrification to deeper waters (Guerrero and Jones 1996; Merbt et al. 2011). However, euphotic zone nitrification has been reported in both coastal and open ocean environments (Ward et al., 1989; Dore and Karl, 1996; Ward, 2005; Clark et al, 2008). For example, experiments conducted in the California upwelling system (Monterey Bay) by Ward (2005) show that subsurface maximum nitrification rates often occur at or near to the base of the euphotic zone. Furthermore, a study conducted by Wankel et al. (2007), also in Monterey Bay, shows that on average, euphotic zone nitrification supports 15% to 27% of NO_3^- based phytoplankton growth in this system (Wankel et al., 2007). NO_3^- derived from euphotic zone nitrification should be considered a regenerated N source. When not accounted for, rates of new production may be overestimated.

1.8.4 DON cycling

Very little is known about dissolved organic nitrogen (DON) cycling in the ocean. This is partly due to the fact that DON fluxes are difficult to measure and that oceanic DON is generally considered to be a highly refractory N pool (Bronk et al., 1994; Bronk, 2002). Nonetheless, DON comprises a large N pool in coastal environments (Sharp, 1983). Small, yet important components of the DON pool include highly labile amino acids and urea, which are consumed by both bacteria and some phytoplankton (Zehr & Ward 2002). While phytoplankton are thought to be the primary source of DON through excretion, decomposition and cell lysis, recent studies suggest that significant fractions of DON also originate from bacterial cell walls. Therefore, bacteria can act as both a source and sink of DON (Zehr & Ward, 2002). When measuring N uptake via the stable isotope incubation technique, we essentially track the amount of ^{15}N-labelled nitrogen that is incorporated into phytoplankton cells. However, this can be complicated by the fact that the ^{15}N label can be released to the DON pool during incubation (Bronk & Glibert, 1993). At this point, the excreted N is no longer part of the PON pool and is therefore not measured as uptake (Bronk et al., 1994). When DON release is not accounted for, $NO_3^-$and NH_4^+

uptake may be underestimated. In fact, in regions of the ocean where phytoplankton are exposed to nutrient or light limitation, viral infection or grazing by heterotrophs, use of the ^{15}N labelling technique has been shown to underestimate rates of nutrient uptake (Bronk & Glibert, 1994). Experiments conducted by Bronk et al. (1994) in both coastal and oligotrophic oceanic environments suggest that new and regenerated production can be underestimated by as much as 74% and 50%, respectively, as a result of DON cycling.

1.9 Cell size and Michaelis-Menten kinetics

The size distribution of phytoplankton assemblages governs the functioning of pelagic food webs and plays an essential role in determining the rate of biological carbon export (Malone, 1980). In most EBUSs, large cells dominate the phytoplankton biomass (Wilkerson et al., 2006) because they are more effective than small cells at utilizing newly upwelled NO_3^- (Probyn & Painting, 1985; Probyn et al., 1990; Probyn, 1992; Wilkerson et al., 2000). Taxonomic studies suggest that the large cells common in EBUSs mainly comprise chain-forming and colonial diatoms ranging in size from 5 μm to 30 μm (Estrada & Blasco, 1985). When EBUS surface waters are replenished with NO_3^- from below, diatom species are the main phytoplankton that proliferate (Malone, 1980) because their physiology makes them well-adapted to exploit the highly variable ambient nutrient concentrations typical of these systems (Hutchings et al., 1995). Diatoms are also likely to dominate the sinking flux because they are large and ballasted by their biogenic silica (Kiørboe 1993; Raven & Waite, 2004).

While their contribution to the sinking flux makes diatoms key players in biological carbon export (Legendre & Rassoulzadegan, 1996), smaller cells like dinoflagellates also play a significant role in NO_3^- uptake. In some EBUSs like Baja, California, less turbulent conditions allow dinoflagellates to flourish. Their ability to migrate vertically between the sunlit surface and the nutrient-rich layer at the base of the euphotic zone enables them to consume large amounts of NO_3^- (MacIsaac 1978). However, new production that occurs in EBUSs dominated by small cells has reduced potential for export. This is because small cells sink more slowly than large cells, allowing more time for them to be remineralized at relatively shallow depths (Guidi et al., 2009). Small cells may contribute to the sinking flux via food web interactions, although this contribution is reduced by the large number of trophic levels between them and the consumers that produce the sinking particles (Michaels & Silver, 1988).

The Michaelis-Menten equation (borrowed from enzyme kinetics) is commonly used to represent cell growth as a function of ambient nutrient concentration. Reaction velocity is plotted against substrate concentration to yield a hyperbolic function (Miller & Wheeler, 2012). The Michaelis-Menten formulation can be applied to NO_3^- and NH_4^+ uptake by phytoplankton in EBUSs using the following equation (shown here for NO_3^-):

$$V_{NO_3^-} = V_{max}(NO_3^-)*[NO_3^-]/(K_s(NO_3^-) + [NO_3^-])$$

where $V_{max}(NO_3^-)$ is the maximum biomass-specific NO_3^- uptake rate, $[NO_3^-]$ is the ambient NO_3^- concentration in seawater, and $K_s(NO_3^-)$ is the half saturation constant or the concentration of NO_3^- at which phytoplankton achieve half their maximum specific uptake rate (MacIsaac & Dugdale, 1972). The half saturation constant can be determined, for example, via ^{15}N tracer incubation experiments and is often used as a measure of substrate affinity. It can also be used to characterise the slope of the initial section of an ecological relationship represented by the hyperbola. A high K_s value is indicative of a low substrate affinity or slow approach to saturation (Miller & Wheeler, 2012).

Phytoplankton in the coastal ocean typically have K_s values of >1 μmol L^{-1} for NO_3^- uptake (Probyn et al., 1995; Kudela & Dugdale, 2000), while open ocean phytoplankton have K_s values on the order of 0.05-0.2 μmol L^{-1} (MacIsaac & Dugdale, 1969; Harrison et al., 1996), suggesting that these cells are

adapted to low ambient NO_3^-concentrations typical of oligotrophic waters (MacIsaac & Dugdale, 1969). Eppley et al. (1969) studied the uptake rates of NO_3^- and NH_4^+ as a function of substrate concentrations for various phytoplankton species. The computed half saturation constants, which indicate the affinity of phytoplankton for a particular nutrient, were found to increase with increasing cell size. This suggests that small cells should outcompete large cells at low concentrations of NO_3^- and NH_4^+ (Eppley et al., 1969). However, a study by Smayda (1997) found that the maximum NO_3^- uptake rates of diatoms are consistently higher than those of dinoflagellates, which enables them to outcompete smaller cells in high-NO_3^- environments.

1.10 Thesis scope

From the literature it is evident that the controls on productivity are complex and multi-faceted, and likely to be even more difficult to disentangle in EBUS because these regions are so variable. A ten-day anchor station experiment was conducted in St Helena Bay during November and December 2016. The objective of this study was to investigate the drivers of short-term temporal variability in phytoplankton primary production in order to understand how this variability impacts C and N cycling in an upwelling shadow zone. In addition, the study aimed to evaluate how such variability might impact the application of the new production paradigm to this region, particularly its effectiveness as a proxy for potential carbon export. To achieve this, an attempt was made to quantify primary productivity and N uptake and characterise the biogeochemistry and phytoplankton community composition in SHB over an active upwelling cycle. Below, the results of the present study will be discussed, along with how they compare to those of the first anchor station experiment performed in SHB in April 1987 (Chapman & Bailey, 1991).

More specifically, section 4.1 describes the upwelling cycle in SHB using hydrographic and nutrient data. In this section, NH_4^+ and PO_4^{3-} efflux from the sediments is discussed, as well as potential sources of the high NO_2^- concentrations observed in surface waters. Section 4.2 highlights the response of phytoplankton to upwelling in SHB, as evidenced by phytoplankton biomass and rates of NPP and NO_3^- and NH_4^+ uptake, and highlights the dominance of the 2.7 to 10 µm size class. It also discusses the potential drivers of short-term variability in phytoplankton production in SHB, which are predominantly light and nutrients. Section 4.3 describes the phytoplankton community in terms of species abundance and diversity and discusses community size structure as a potential third driver of primary productivity. Lastly, section 4.3 deals with the degree of coupling between carbon and N uptake in SHB, arguing that phytoplankton engage in luxury NO_3^- uptake during active upwelling. The observational data raise two questions regarding the importance of large diatom cells and heterotrophic bacteria for biomass and total N uptake that cannot be addressed with the available measurements. These questions are explored through the application of a simple ecological model in section 4.4. Once fitted to the data, the model is also used to estimate the mortality rates of each phytoplankton size class during the anchor station experiment, a parameter for which observations are lacking.

1.10.1 Aims and Objectives

Specifically, the aims of this thesis are to:

1) Determine the main drivers of primary production in St Helena Bay.
2) Determine the size class of phytoplankton responsible for most of primary production in St Helena Bay.
3) Identify the species of phytoplankton that occupy the dominant size class.
4) Understand how carbon and nitrogen cycling are influenced by a shallow, semi-enclosed and highly dynamic embayment.
5) Determine whether new production is an appropriate proxy for potential carbon export in this coastal embayment.

2 Methods

2.1 Study site

A ten-day anchor station study was undertaken at a single location in St Helena Bay (latitude: 32.308°E, longitude: 18.275°S) (Fig. 2). This site corresponds to station 2 of the well-established St Helena Bay Monitoring Line (SHBML) that is occupied four times a year by the Department of Environmental Affairs Integrated Ecosystem Programme. Sampling was conducted daily from the 29th of November to the 8th of December 2016; this period was selected to coincide with the peak upwelling season for the SBUS. Ten days of sampling were undertaken in an attempt to capture the evolution of an upwelling cycle, as upwelling events in the SBUS typically occur over a period of three to ten days (Andrews & Hutchings, 1980), and the subsequent initiation and development of a phytoplankton bloom. Each day, sampling was conducted aboard the MA-RE 1 (Department of Oceanography, University of Cape Town). This study is referred to as an "anchor station experiment" because the same site was visited each day, although it should be noted that the boat was not anchored on site for the duration of the study as was the case in the previous SHB anchor station experiment. The sampling site has a bottom depth of ~30 m and all sample types were collected at 0 m, 5 m, 10 m, 15 m and 20 m to ensure that the entire euphotic zone could be well characterised. Fluorescence data from day 1 suggested that most of the phytoplankton activity was occurring in the upper 15 m of the water column; the NPP and N uptake experiments were thus conducted at only 4 depths (0 m, 5 m, 10 m and 15 m) from days 2-10. A hand-held CTD was deployed three times a day from day 5 to day 10 of the experiment. No CTD data are available for days 1 to 4.

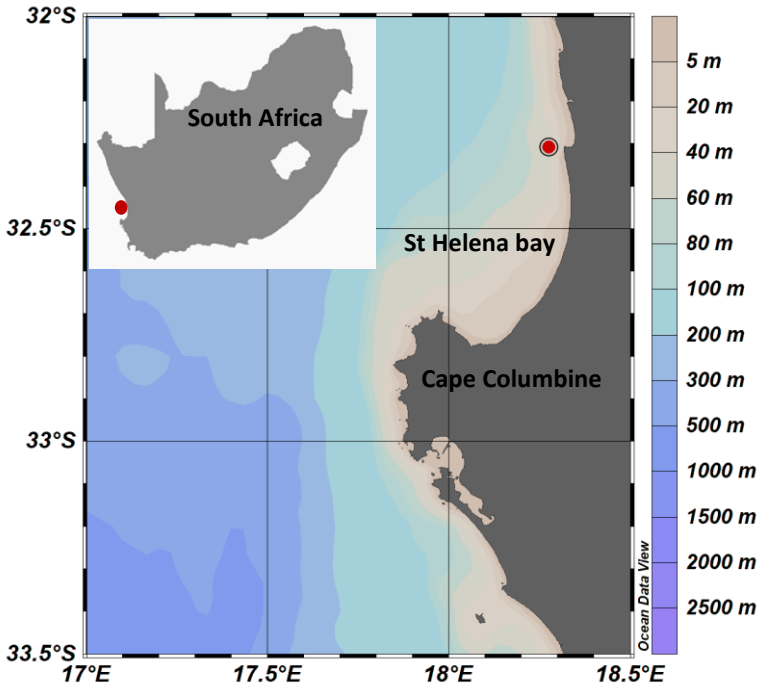

Fig 2. Map showing the study site (32.308°E, 18.275°S) indicated by the red dot in the context of the greater St Helena Bay area, located on the west coast of South Africa. A map of South Africa is included in the top left corner for orientation. The colour represents bathymetry.

2.2 Net primary productivity and nitrogen uptake experiments

On each day of the anchor station study, the stable isotope incubation technique was used to determine size-fractionated rates of NPP and nitrogen (NO_3^- and NH_4^+) uptake. 4 L of seawater were collected at 0 m, 5 m, 10 m, and 15 m using a 5L hand-held Niskin bottle. For each depth, all water was pre-filtered through a 200 µm nylon mesh to remove large grazers, then transferred into four 1 L polycarbonate bottles. ^{13}C-labelled sodium bicarbonate ($NaH^{13}CO_3$) and ^{15}N-labelled ammonium chloride ($^{15}NH_4Cl$) was added to two 1 L bottles to yield a final tracer concentration of 100 µmol L^{-1} and 0.05 µmol L^{-1}, respectively. ^{15}N-labelled potassium nitrate ($K^{15}NO_3$) was added to the other two bottles to yield a final tracer concentration of 0.5 µmol L^{-1}. All bottles were incubated *in situ* at the depth of collection for three to five hours. This was done by attaching the bottles to a line that was weighted at one end and suspended in water column in an upright position using a buoy. Incubations were terminated by filtration; for each 1 L polycarbonate bottle, 300 mL of seawater was filtered through a 25 mm diameter 0.7 µm filter glass fibre filter (GF/F), a second 300 mL aliquot was filtered through a 25 mm diameter 2.7 µm GF/D, and a third 300 mL aliquot was filtered through a 25 mm 10 µm nylon filter. The particulate organic matter (POM) collected on each 10 µm nylon filter was resuspended in approximately 30 mL of filtered (0.2 µm) seawater, then re-filtered onto a 25 mm diameter 0.7 µm GF/F. All GF/Fs were stored in combusted (450°C for 5 hours) foil envelopes and frozen at -20°C until later analysis in the laboratory.

2.2.1 Mass spectrometry

In the Marine Biogeochemistry Laboratory at the University of Cape Town (MBL-UCT), the filters were oven dried for 24 hours at 45°C. Once dry, they were acidified for 24 hours in the presence of 37% hydrochloric acid (HCl) to remove inorganic carbon. After acidification, the filters were oven dried again for 30 minutes at 45°C. Next, the filters were cored with a 20 mm metal punch to remove excess perimeter filter, then folded into tin cups that were placed in clean 96-well trays. Samples were analysed for particulate organic carbon and nitrogen content (POC and PON) and ^{13}C and ^{15}N isotopic enrichment at the Stable Light Isotope Laboratory in the Archaeology Department at UCT using a Thermo DELTA V isotope ratio mass spectrometer interfaced with a Flash 2000 organic elemental analyser (EA-IRMS).

To monitor the stability of the EA-IRMS, a sample blank was run after every 10-20 samples and two laboratory running standards of known weight (CHOC; $\delta^{13}C$ = -17.75 ‰, $\delta^{15}N$= 4.31 ‰ and VALINE; $\delta^{13}C$ = -26.8 ‰, $\delta^{15}N$= 12.14‰) were run after every five samples. Measured carbon isotope ratios were referenced to Vienna Pee-Dee Belemnite (PBD) and nitrogen isotope ratios to N_2 in air, with results expressed in delta notation according to the equations:

$$\delta^{13}C\ (‰\ vs.\ PBD) = [(^{13}C/^{12}C_{\ sample})/(^{13}C/^{12}C_{\ standard}) - 1] \times 1000$$

$$\delta^{15}N\ (‰\ vs.\ N_2) = [(^{15}N/^{14}N_{\ sample})/(^{15}N/^{14}N_{\ standard}) - 1] \times 1000.$$

To determine POC and PON content of the filters, standard curves were obtained by plotting the peak area measured by the IRMS for standards of known weight as a function of that weight in mg. The equation of a regression line fitted to each standard curve was used to calculate sample carbon and nitrogen weight in mg from their measured peak areas. Weight was converted to µ moles and divided by the volume of seawater filtered to obtain the concentration of POC and PON ([POC] and [PON]).

The values of all measurements made using this technique are well above the limit of detection of the EA-IRMS. The pooled standard error for [POC] and [PON] is listed in Table 1.

Table 1: The pooled standard error (SE) for measurements of [POC] and [PON] (µmol L^{-1}), NPP (ρC), nitrate and ammonium uptake (ρNO_3^- and ρNH_4^+; µmol L^{-1} hr^{-1}) for the first five and the last five days of the experiment. The pooled SE is calculated separately for each filter pore size and "n" denotes the number of samples included in the calculation.

Variable	Filter pore size (µm)	SE Days 1 to 5	n	SE Days 6 to 10	n
POC (µmol L^{-1})	0.7	1.72	25	4.61	25
	2.7	2.25	25	3.04	25
	10	1.64	25	3.14	25
PON (µmol L^{-1})	0.7	0.64	25	0.68	25
	2.7	0.40	25	0.45	25
	10	0.19	25	0.26	25
ρC (µmol L^{-1} d^{-1})	0.7	1.25	25	2.19	25
	2.7	2.82	25	2.70	25
	10	0.77	25	2.12	25
ρNO_3^- (µmol L^{-1} d^{-1})	0.7	0.68	24	2.76	25
	2.7	0.78	24	0.84	24
	10	0.31	24	0.46	25
ρNH_4^+ (µmol L^{-1} d^{-1})	0.7	0.23	24	0.18	17
	2.7	0.19	24	0.18	17
	10	0.07	24	0.60	17

2.2.2 Calculating rates of net primary productivity and nitrogen uptake

From the $\delta^{13}C$ and $\delta^{15}N$ data, the atom percent (At%) ^{13}C and ^{15}N were calculated as follows:

$$At\%\ ^{13}C = \delta^{13}C\ (‰)/(1000+1)\times(\text{Nat-abundance C}/100)\times 100$$

$$At\%\ ^{15}N = \delta^{15}N\ (‰)/(1000+1)\times(\text{Nat-abundance N}/100)\times 100$$

where Nat-abundance C = 1.07% and Nat-abundance N = 0.366% (Meija et al. 2016).

For both C and N, $At\%_{enriched}$ was determined by subtracting the Nat-abundance values from the calculated At% values. The rates are then calculated using $At\%_{enriched}$.

The hourly rate of NPP (ρC; µmol L^{-1} hr^{-1}) was calculated according to the original equation of Dugdale and Goering (1967):

$$\rho C = ([POC]*At\%_{enriched})/((At\%_{initial} - 1.07\%)*time)$$

where $At\%_{initial} = (([DIC]_{ambient}*1.07\%) + ([DIC]_{tracer}*99\%))/[DIC]_{initial}$

and $[DIC]_{initial} = [DIC]_{ambient} + [DIC]_{tracer}$

In the equations above, [POC] is the measured concentration of POC biomass (µmol L^{-1}), time is the duration of the incubation (h), $[DIC]_{ambient}$ is the measured ambient concentration of DIC in the water column and $[DIC]_{tracer}$ is the concentration of 99% ^{13}C-labelled $NaHCO_3$ tracer added to the incubation bottles (100 µmol L^{-1}).

The rates of NH_4^+ and NO_3^- uptake (ρNH_4^+ and ρNO_3^-, respectively) were calculated as follows:

$$\rho N = ([PON]*At\%_{enriched})/((At\%_{initial} - 0.366)*time)$$

where $At‰_{initial} = (([DIN]_{ambient}*0.366\%) + ([DIN]_{tracer}*99\%))/[DIN]_{initial}$

and $[DIN]_{initial} = [DIN]_{ambient} + [DIN]_{tracer}$

In the equations above, ρN refers to ρNH_4^+ or ρNO_3^- (µmol L^{-1} hr^{-1}), [PON] is the measured concentration of PON biomass (µmol L^{-1}), time is the duration of the incubation (h), $[DIN]_{ambient}$ is the measured ambient DIN concentration (either $[NH_4^+]$ or $[NO_3^-]$; µmol L^{-1}) and $[DIN]_{tracer}$ is the concentration of $^{15}NH_4^+$ or $^{15}NO_3^-$ added to each bottle (0.05 µmol L^{-1} and 0.5 µmol L^{-1}, respectively).

The specific rates (h^{-1}) of NPP (V_C), NH_4^+ uptake ($V_{NH_4^+}$) and NO_3^- uptake ($V_{NO_3^-}$) were calculated by dividing ρC, ρNH_4^+ and ρNO_3^- at each depth and for each size class by the measured [POC] or [PON] at the same depth and for the same size class. All the calculated uptake rates are well above the limit of detection of this technique, and the pooled standard errors (SE) are listed in Table 1.

2.3 Nutrients

Nutrient samples were collected (unfiltered) in duplicate from five depths (0 m, 5 m, 10 m, 15 m and 20 m) in 50 mL centrifuge tubes. The centrifuge tubes were rinsed 3 times with sample water then filled to just below the 50 ml mark and frozen at -20 °C for later analysis in the MBL-UCT. At each depth, two samples were collected for the analysis of NO_3^-, NO_2^-, Si and PO_4^{3-} concentrations and another two samples were collected for NH_4^+ concentrations.

2.3.1 Ammonium

Ammonium concentrations ($[NH_4^+]$) were measured fluorometrically according to the method of Holmes et al. (1999). In brief, 20 ml aliquots of each sample were decanted into "aged" (i.e., stored containing a solution of Milli-Q water and working reagent) 60 ml HDPE bottles to which 4 ml of working reagent (orthophthaldialdehyde, sodium sulphite and sodium borate) was added. Samples were incubated in the dark for 3 hours, after which their fluorescence was measured using a Turner Designs Trilogy fluorometer (Model number 7200-067). NH_4^+ standards were prepared in Milli-Q and treated similarly to the samples. The matrix effect (ME) was determined to account for the fact that the samples contain sea salt and dissolved organic matter that may cause them to behave differently in terms of fluorescence compared to the standards, which were made up in Milli-Q water. The ME was calculated after Holmes et al. (1999) as follows:

$ME = \Delta F_{std} - (\Delta F_{sample})/ \Delta F_{std}$

Where $\Delta F_{std} = F_{std\_spike} - F_{std\_0}$ and $\Delta F_{sample} = F_{sample\_obs} - F_{sample\_spike}$

ΔF_{std} refers to the change in the fluorescence of a standard following the addition of a known quantity of ammonium (i.e., "spike"). F_{std_spike} is the fluorescence of a known concentration of ammonium chloride (0 to 2 µmol L^{-1}) and F_{std_0} refers to the fluorescence of a standard with no ammonium chloride addition. ΔF_{sample} refers to the change in the fluorescence of a given seawater sample following the addition of that same quantity of ammonium as is added to the standard, while F_{sample_obs} is the observed fluorescence of a sample of seawater and F_{sample_spike} refers to the fluorescence of that same sample after the addition of a known concentration of ammonium chloride.

Ammonium concentrations were then corrected for the ME:

$[NH_4^+]_{corrected} = [NH_4^+]_{sample} + ([NH_4^+]_{sample}*(ME/100))$

The limit of detection was 0.05 µmol L^{-1} and the pooled standard error of all samples measured was 0.10 µmol L^{-1} (n = 47).

2.3.2 Nitrate + nitrite

Sample nitrate + nitrite concentrations ($[NO_3^-]+[NO_2^-]$) were measured using a Lachat QuikChem Flow Injection Analysis platform. The limit of detection for this technique was 0.1 µmol L^{-1} and the pooled standard error for all samples measured was 0.39 µmol L^{-1} (n = 50). In brief, a cadmium column is used to reduce NO_3^- to NO_2^- as follows:

$$NO_3^- + H_2O + EDTA + Cd^o \rightarrow NO_2^- + 2OH + Cd(EDTA)^{2-}$$

Cd^{2+} binds with EDTA (ethylenediaminetetracetic acid), preventing the precipitation of $Cd(OH)_2$ onto the column and allowing the sample to pass through the column with no interference (Margeson et al., 1980). After reduction of NO_3^- to NO_2^-, a mixed reagent of sulphanilamide and N-(1-naphthyl)-ethylenediamine dihydrochloride (N-NED) is added, which allows a colour to develop. The samples were measured according to the colorimetric method of Benschneider & Robinson (1952) at a wavelength of 543 nm.

Nitrite concentrations ($[NO_2^-]$) were measured separately for each sample according to the colorimetric method described by Grasshoff et al. (1983), with absorbance (543 nm) determined using a Thermo Scientific Genesys 30 visible spectrophotometer. In brief, 0.1 mL of 0.2 N sulphanilamide is added to 5 ml of sample, which is then vortexed and allowed to react for 5 to 10 minutes. Next, 0.1 mL of 0.004 N N-NED solution is added, and the sample is vortexed again. The detection limit was 0.05 µmol L^{-1} and the pooled standard error for all the samples measured was 0.06 µmol L^{-1} (n = 48). Sample nitrate concentrations ($[NO_3^-]$) were determined via subtraction, with error propagated according to standard statistical practice.

2.3.3 Silicate

The silicic acid concentration ($[SiO_4]$) was determined via the colorimetric method of Grasshoff (1979) using the Lachet QuikChem Flow Injection Analysis platform. Under acidic conditions, SiO_4 reacts with ammonium molybdate to form a beta molybdosilicic acid, which is then reduced using ascorbic acid, forming a blue solution. Oxalic acid is added to the seawater samples before they are analysed in order to reduce interference caused by PO_4^{3-} in the sample. The final solution is measured at a wavelength of 820 nm. The limit of detection for this technique was 0.5 µmol L^{-1} and the pooled standard error for all the samples measured was 0.46 µmol L^{-1} (n = 50). All nutrient measurements made using the Lachat QuikChem Flow Injection Analysis platform were corrected for instrument drift, which was well characterised by analysing a series of standards of known concentrations after every 10 samples.

2.3.4 Phosphate

The phosphate concentrations ($[PO_4^{3-}]$) for each sample were analysed via a colorimetric method based on Murphy & Riley (1962) whereby 5 mL of sample is mixed with 0.5 mL of mixed reagent (10 mL of 0.15 N ammonium molybdate solution, 25 mL of 8 N sulphuric acid solution, 10 mL of 0.3 N ascorbic acid solution and 5 mL of 0.002 N potassium antimonyl-tartrate solution). The absorbance (885 nm) is then determined using a Thermo Scientific Genesys 30 visible spectrophotometer. The limit of detection of this technique was 0.05 µmol L^{-1} and the pooled standard error of all measured samples was 0.18 µmol L^{-1} (n = 49).

2.4 Chlorophyll-a

To determine the chlorophyll-a concentrations ([Chl-a]), 2 L of seawater was collected from each sampling depth (0 m, 5 m, 10 m, 15 m and 20 m) in opaque HDPE bottles. On land, the bottles were gently and repeatedly inverted to homogenize the sample. 1 L of seawater from each sample was

filtered through a 47 mm diameter 10 µm polycarbonate filter, 500 mL was filtered through a 47 mm diameter 3 µm polycarbonate filter and the remaining 500 mL was filtered through a 47 mm diameter 0.2 µm polycarbonate filter. The filters were transferred to glass test tubes to which 8 mL of 90% acetone was added. The tubes were left in a freezer (-20°C) for 24 hours, after which the extracted chlorophyll was measured fluorometrically according to the method of Welschmeyer (2004) and corrected for the acetone + filter blank.

2.5 CTD data

On days when CTD data are available (i.e., days 5 to 10), they are used to describe the hydrographic conditions of the water column at the anchor station. The potential density anomaly of seawater (kg m^{-3}) was calculated as a function of absolute salinity (g kg^{-1}) and conservative temperature (^{o}C) with respect to a reference pressure of 0 dbar as described by IOC et al. (2010). Absolute salinity and conservative temperature were calculated from the conductivity and temperature recorded by the CTD. On days 1 to 4, no CTD data are available. However, salinity was measured for discrete samples collected on all days of the experiment at 5 m intervals from the surface to 20 m using a Portasal salinometer, model number 8410A; these salinity measurements were used to calibrate the CTD on days 5 to 10. The salinity data from days 1 to 4 were combined with extrapolated temperature (see below) to yield estimates of density for the first few days of the experiment.

To estimate temperature at the beginning of the experiment, a linear regression analysis was performed using ambient [NO_3^-] and CTD temperature data from days 5 to 10 following Waldron & Probyn (1992) and illustrated in Fig. 3. This temperature-nitrate (TN) relationship was then applied to ambient [NO_3^-] data from the beginning of the experiment to estimate the temperature of the water column on days 1 to 4. According to Zentara and Kamykowski (1977), ocean temperature and inorganic nutrient concentrations like NO_3^- typically display highly correlated negative relationships. The estimated temperature for the second half of the experiment (based on the TN relationship) is not significantly different ($p < 0.05$) from the measured CTD temperature over this period. Thus, the TN relationship appears to yield a reasonable approximation of temperature when no CTD data are available.

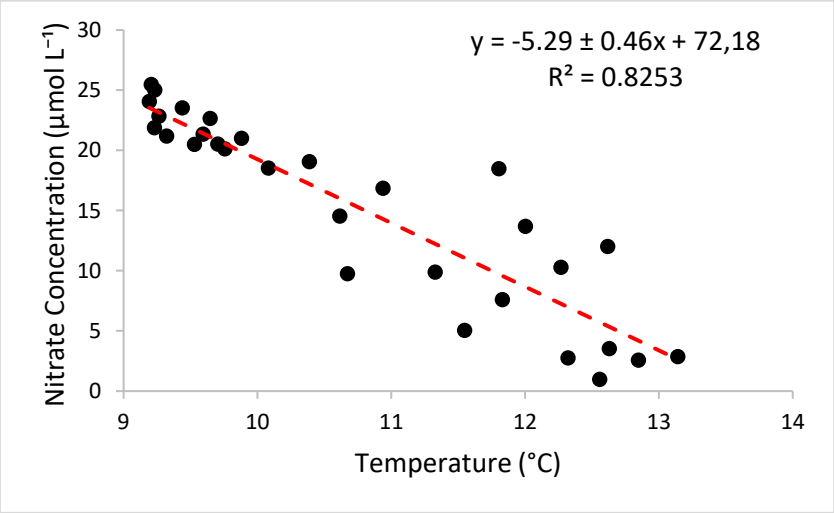

Fig 3. A linear regression of temperature (°C) on nitrate concentration (µmol L^{-1}) for days 6 to 10 of the anchor station study. A linear trend line (shown in red) was fitted to the data, and the equation and R^2 value of the trend line is displayed in the top right-hand corner of the figure.

Where possible, daily mixed layer depth (MLD) was determined according to the criteria outlined by de Boyer Montégut et al. (2004) but using the surface as a reference value given that the water depth was only about 30 m. Successively deeper levels were examined until one was found with a density value that differed from the reference level value by more than 0.03 $kg.m^{-3}$.

2.6 Euphotic zone depth

The depth of the euphotic zone (z_{eu}), taken to be the depth at which photosynthetically active radiation (PAR) falls to 1% of its surface value (Kirk, 1994), was measured four times each day at roughly 7:30 am, 8:30 am, 9:30 am and 11:30 am using a Secchi disk. The Secchi disk depth (SDD) was determined by lowering a weighted black and white disk into the water and recording the depth at which it disappeared from view. Each day, the SDD was taken to be the average of the four deployments. The diffuse attenuation coefficient of PAR (Kd(PAR)) was calculated according to the equation:

$$Kd(PAR) = a/SDD$$

where a is an empirical co-efficient of 1.7 (Idso & Gilbert, 1974). The z_{eu} was then calculated using the equation:

$$I_{Zeu} = I_0 e^{-Kd(PAR)zeu}$$

where I_z = 1% and I_0 = 100%.

3 Results

3.1 Wind speed and direction

For the month of the 10th of November 2016 to the 10th of December 2016, mean (± SE) wind speeds ranged from 2.6 ± 1.5 m s^{-1} to 11.4 ± 2.3 m s^{-1} (Fig. 4A) and the wind direction was predominantly southerly to south easterly (Fig. 4B). In the ~2 weeks prior to the start of the anchor station study, the average (± SE) wind speed was 7.3 ± 2.3 m s^{-1}, while the average wind speed over the duration of the 10-day anchor station study was 6.8 ± 1.8 m s^{-1}. In addition, a general decrease in wind speed was evident over the study period (Fig. 4A), from 9.0 ± 1.4 m s^{-1} on day 3 to 2.6 ± 1.5 m s^{-1} on day 10 of the experiment.

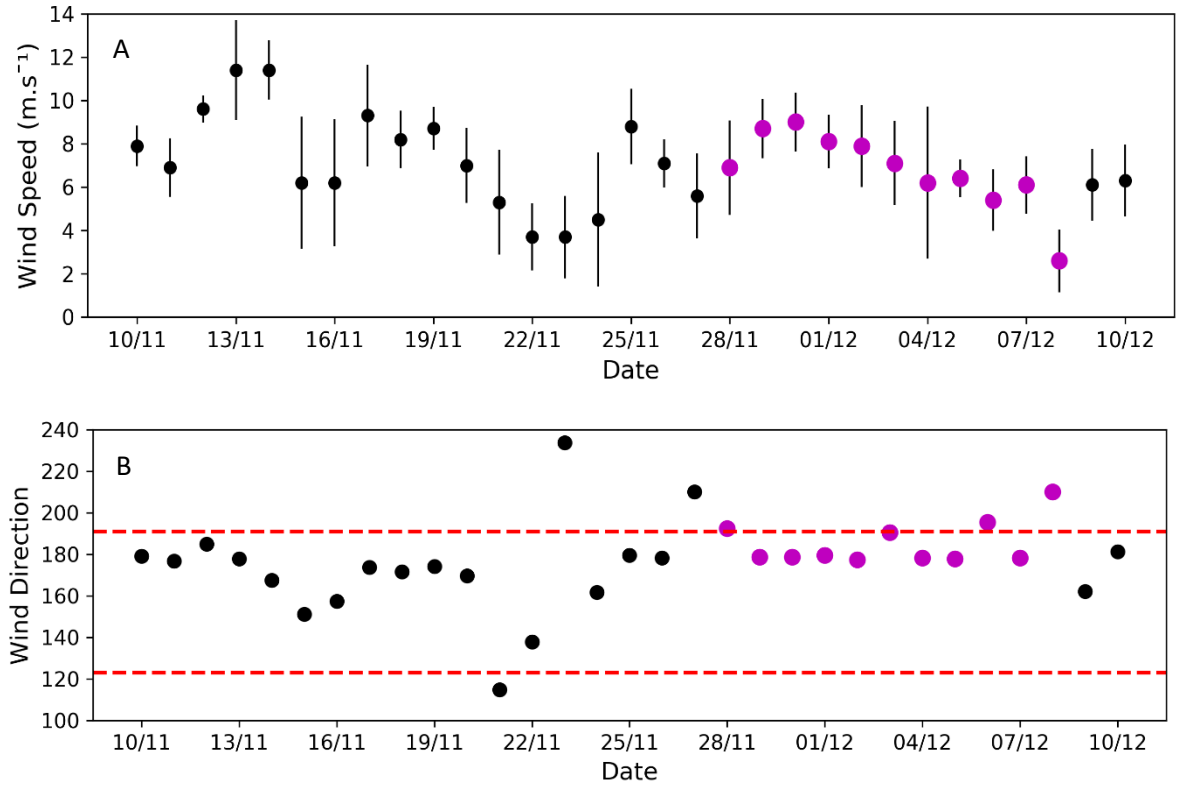

Fig 4. The wind speed in m s^{-1} (A) and the wind direction in degrees clockwise from true north (B) for one month from the 10th of November to the 10th of December 2016. For both A and B, a daily average (n = 24) is shown, with standard error (± 1 SE) indicated by the error bars in panel A. Pink dots highlight values for the dates corresponding to the 10-day anchor station study. In panel B, the dashed red lines indicate the south easterly wind direction (123.75°) and the southerly wind direction (191.24°) as defined by the South African Weather Service (SAWS), such that points falling between the red lines correspond to winds from the south or south east.

3.2 Water column hydrography

Over the first 5 days of the experiment, the water column was well mixed. Cold water existed throughout the upper 20 m with 9°C to 10°C water extending from depth to ~5 m and 10.5°C to 11.5°C water in the very surface layer (Fig. 5). On day 3, cold water was apparent all the way to the surface (Fig. 5). From day 5 to day 10 stratification set in. The surface waters warmed from 12°C to 13°C and the thermocline deepened from ~5 m to 15 m (Fig. 5).

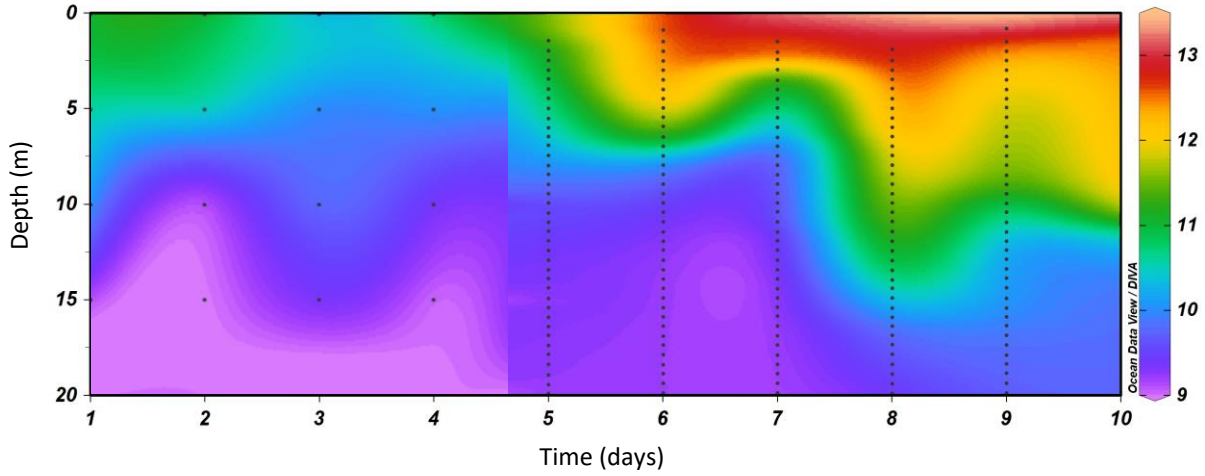

Fig 5. Water column temperature (°C) over the course of the experiment. Black dots indicate the sampling frequency. Temperature on days 1 to 4 was determined by the TN relationship. Temperature on days 5 to 10 was measured by the CTD. The discontinuity between days 4 and 5 results from the merging of two separate data sets with different sampling resolutions, when configuring the temperature section plot.

The potential density anomaly showed a well-mixed water column over the first 4 days of the experiment, with a density range of 26.8 to 27 kg m^{-3} extending from the surface to 20 m (Fig. 6). On day 3, slightly denser water originating from depth appeared to extend to the surface. Over days 5 to 10, the water column became stratified (Fig. 6), as evidenced by the low-density surface waters (26.2 to 26.6 kg m^{-3}) overlying the denser waters below (~ 26.9 kg m^{-3}). During this period, the pycnocline deepened from ~5 m to 15 m.

The euphotic zone depth derived from Secchi disk measurements deepened from 10 m on day 2 to 14 m on day 4 (Fig. 6; white triangles), before it shoaled to 5.4 m on day 8 and then deepened slightly to 8.5 m on day 10. Over the second half of the experiment, the MLD (Fig. 6; white triangles) shoaled from 5 m on day 6 to 2.5 m on day 7. It then deepened to 15 m on day 8 and remained at 10 m for the last two days of the experiment.

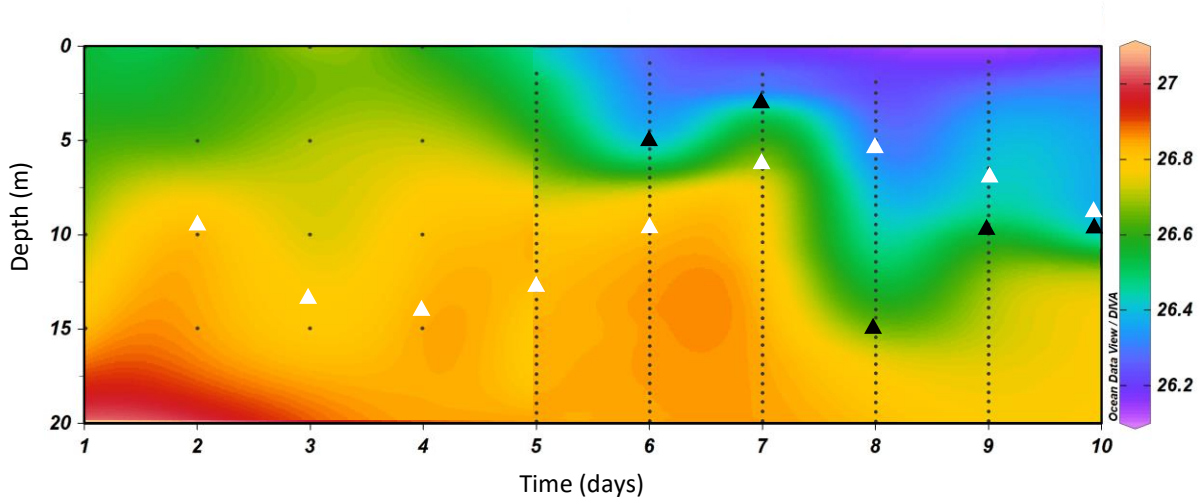

Fig 6. Water column potential density anomaly (kg.m^{-3}) over the course of the experiment. Black dots indicate the sampling frequency. Density on days 1 to 4 was determined from discrete salinity samples and TN-inferred temperature. Density on days 5 to 10 was calculated from CTD measurements of temperature and salinity. White triangles indicate the euphotic zone depth and black triangles indicate the mixed layer depth.

3.3 Nutrients

On each day of the experiment, the nitrate concentration ([NO_3^-]) data showed typical nutrient like profiles with lower [NO_3^-] at the surface compared to depth (Fig. 7A). Over the course of the experiment, the [NO_3^-] below 10 m remained relatively high (18.5 to 26.8 µmol L^{-1}) with little variation over time. In the surface layer (~ 0 m to 10 m), the [NO_3^-] was on average lower than at depth and there was a distinct decline in [NO_3^-] over the second of half of the experiment (days 7 to 10; 0.9 to 21.3 µmol L^{-1}) compared to the first half (days 1 to 6; 9.9 to 24.3 µmol L^{-1}). On day 3, higher [NO_3^-] waters appeared to extend into the very surface layer.

The ammonium concentration ([NH_4^+]) was highly variable over time and with depth (Fig. 7B). High [NH_4^+] (1 to 2 µmol L^{-1}) occurred throughout the water column on days 1 to 3, and from 5 m to 20 m on days 4 to 7 and days 9 to 10. From days 3 to 10, the [NH_4^+] was relatively low in surface waters (0 to 0.75 µmol L^{-1}). This low [NH_4^+] seawater extended to 15 m on day 8.

The nitrite concentration ([NO_2^-]) was typically low (< 1 µmol L^{-1}) throughout the water column over the course of the experiment, except in the upper 5 m on days 3 to 5 where it reached unusually high values (2 to 4 µmol L^{-1}) (Fig. 7C).

The phosphate concentration ([PO_4^{3-}]) was highly variable over the first half of the experiment (Fig. 7D). Relatively high [PO_4^{3-}] (3 to 6 µmol L^{-1}) occurred from 5 m to 20 m on day 2, from 15 m to 20 m on day 4 and in the upper 5 m on day 5. Over the second half of the experiment, the [PO_4^{3-}] was relatively low (1 to 2 µmol L^{-1}) and homogenous throughout the water column, although still slightly higher at depth than in the mixed layer.

The silicate concentration ([Si]) was relatively high (30 to 40 µmol L^{-1}) for most of the experiment (Fig. 7E). The maximum concentration (51.3 µmol L^{-1}) occurred at the surface on day 4, and decreased to relatively low values (17 to 27 µmol L^{-1}) in the upper 5 m of the water column on days 7, 9 and 10, and in the upper 15 m on day 8.

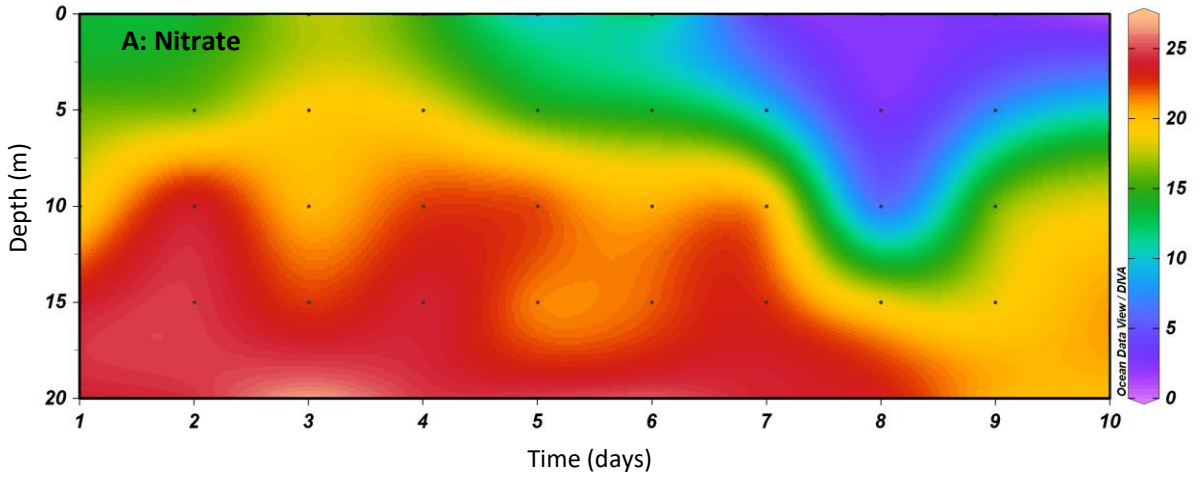
A: Nitrate
Depth (m)
0
5
10
15
20
1
2
3
4
5
6
7
8
9
10
Time (days)
25
20
15
10
5
0
Ocean Data View / DIVA

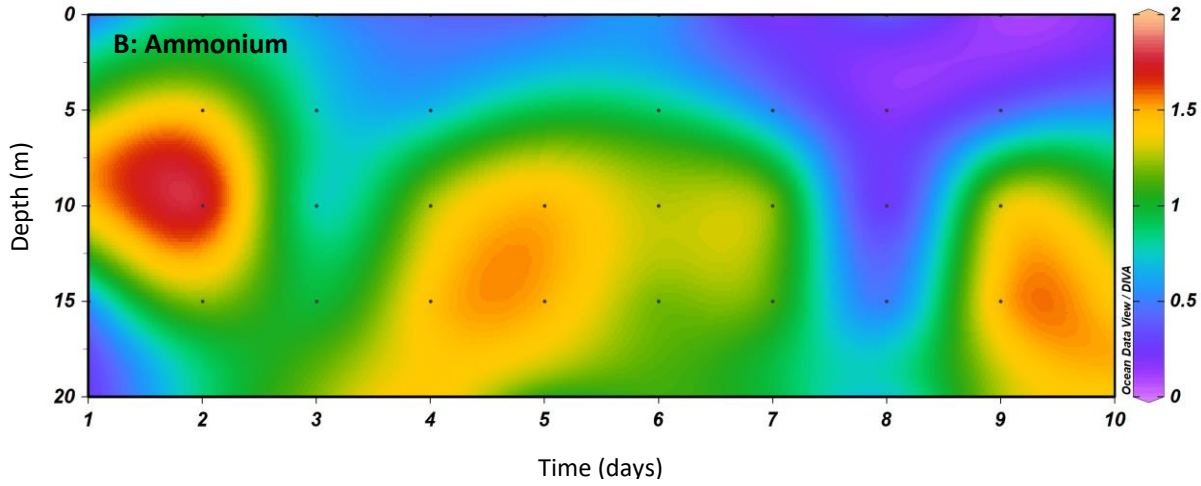
B: Ammonium
Depth (m)
0
5
10
15
20
1
2
3
4
5
6
7
8
9
10
Time (days)
2
1.5
1
0.5
0
Ocean Data View / DIVA

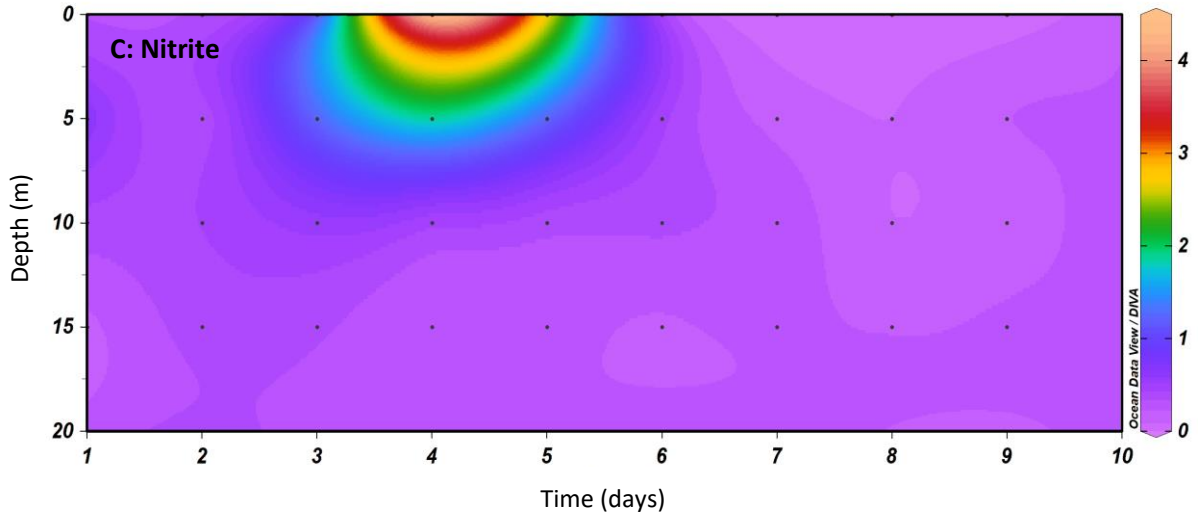
C: Nitrite
Depth (m)
0
5
10
15
20
1
2
3
4
5
6
7
8
9
10
Time (days)
4
3
2
1
0
Ocean Data View / DIVA

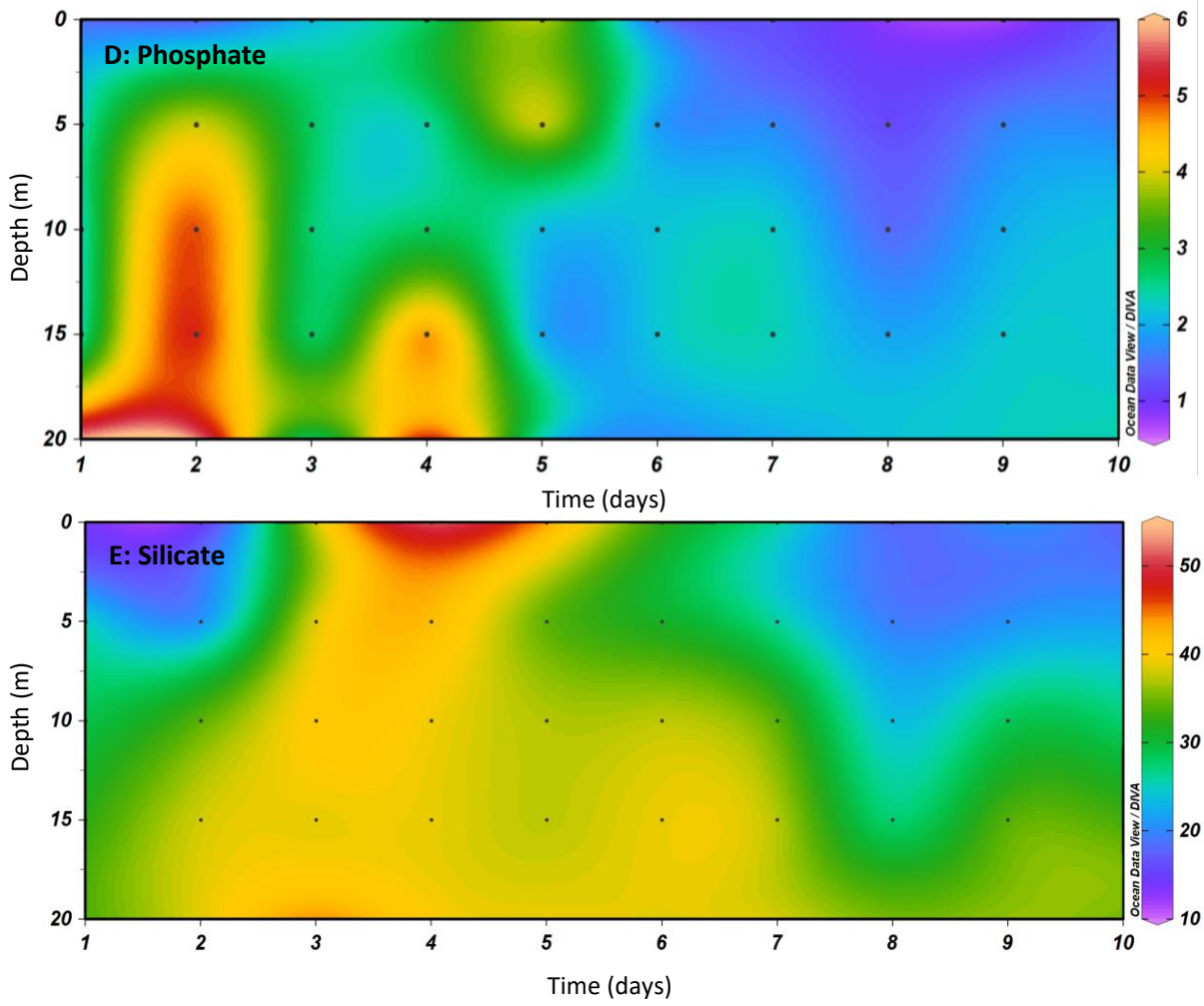

Fig 7. Nitrate (A), ammonium (B), nitrite (C), phosphate (D) and silicate (E) concentrations (µmol L^{-1}) throughout the upper 20 m of the water column over the course of the experiment. Black dots indicate the sampling frequency. In all cases, n = 2.

3.4 Particulate organic carbon and nitrogen concentrations

Over the course of the experiment, the [POC] was highest at the surface and 5 m (avg ± SE), and decreased to <20 µmol L^{-1} at 10 m and 15 m (Fig. 8). At the surface and 5 m, the intermediate size class (2.7 µm – 10 µm) dominated the bulk phytoplankton community biomass (>0.7 µm). The smallest size class (0.7 µm – 2.7 µm) made little to no contribution to phytoplankton biomass. The largest size class (>10 µm) also made a significant contribution to biomass, although its [POC] was for the most part lower than that of the intermediate size class. Variation in the [POC] over time was most prominent at the surface and 5 m, with minor variations occurring at 10 m and 15 m (Fig. 8). At the surface, there was a clear increase in the mean (± SE) bulk community [POC] from 32.1 $\pm$ 1.2 µmol L^{-1} on day 3 to 68.1 $\pm$ 9.5 µmol L^{-1} on day 8, while at 5 m there was an increase from 20.7 $\pm$ 1.3 µmol L^{-1} on day 6 to 70.6 $\pm$ 3.5 µmol L^{-1} on day 8 (Fig. 8). The mean (± SE) [POC] of the intermediate size class, which made the largest contribution to phytoplankton biomass at the surface, increased from 14.0 $\pm$ 1.8 µmol L^{-1} on day 4 to 57.9 $\pm$ 5.1 µmol L^{-1} on day 8 (Fig. 9). The mean (± SE) [POC] of the largest size class was less variable over time, and increased at a slower rate from 9.0 $\pm$ 0.6 µmol L^{-1} on day 3 to 28.5 $\pm$ 2.7 µmol L^{-1} on day 9 (Fig. 9).

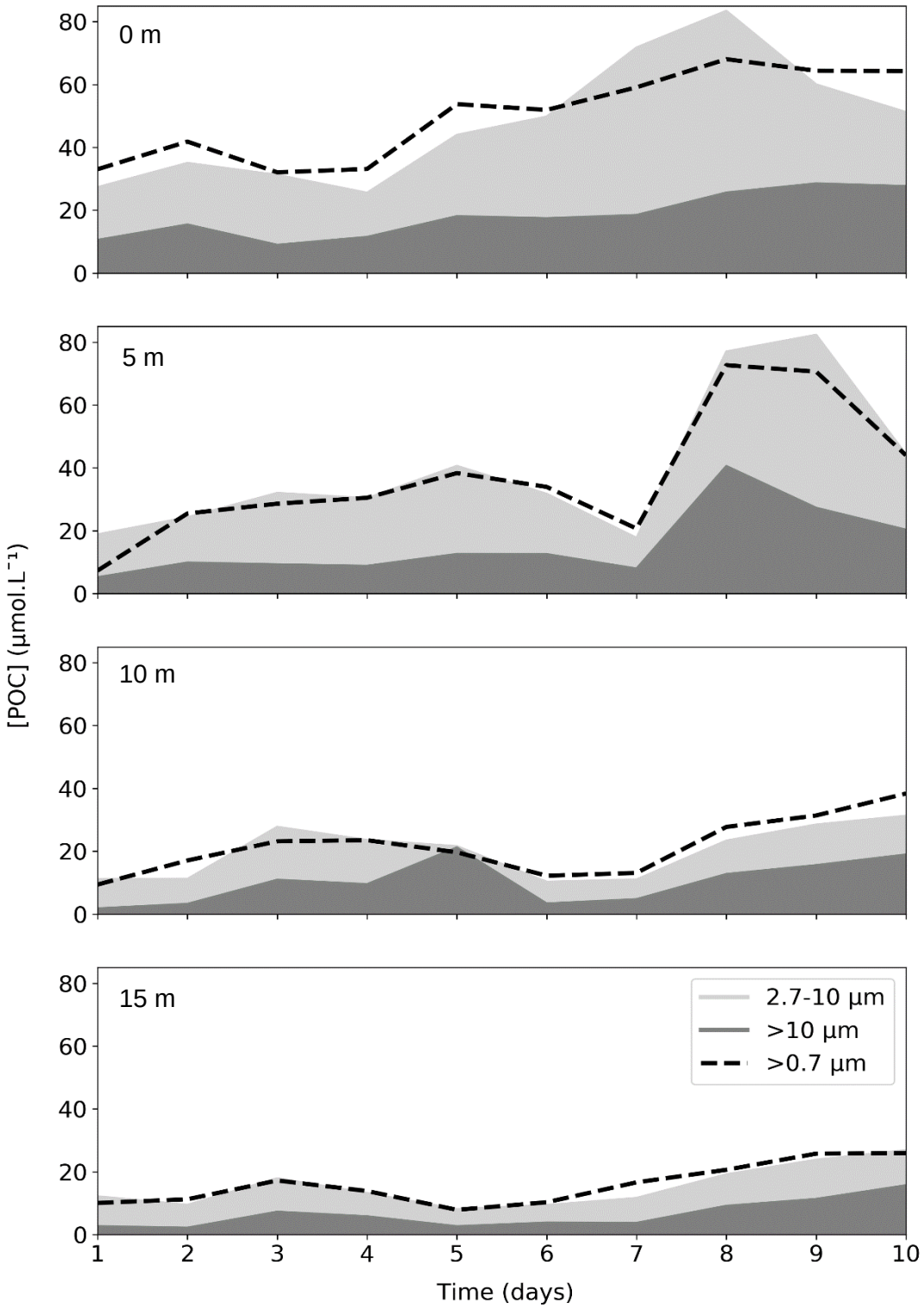

Fig 8. The particulate organic carbon concentration ([POC]) measured at 0 m, 5 m, 10 m and 15 m for the total (>0.7 µm), medium (2.7-10 µm) and large (>10 µm) phytoplankton size classes over the course of the experiment. In all cases, n = 2.

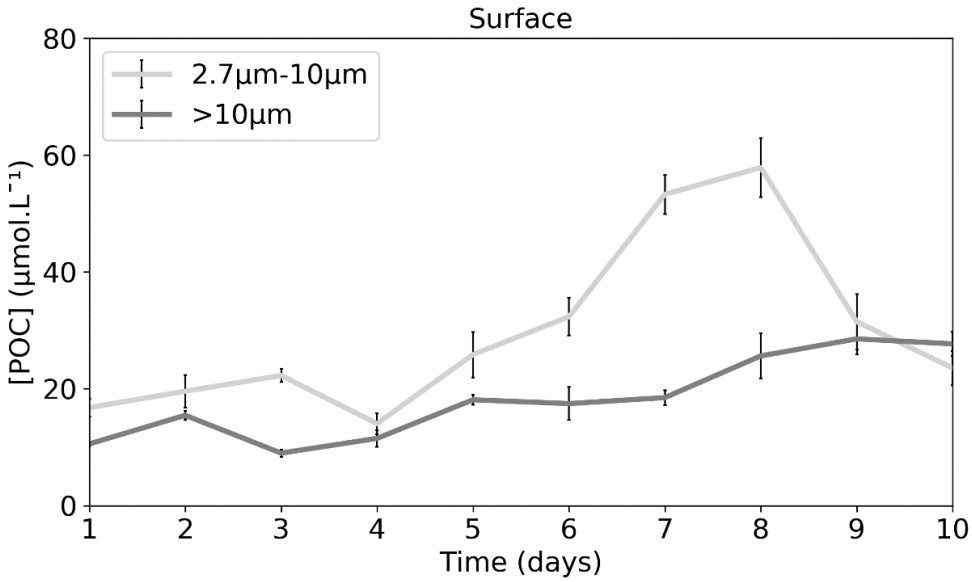

Fig 9. The particulate organic carbon concentration ([POC]) measured at the surface (~0 m) for the medium (2.7-10 µm) and large (>10 µm) phytoplankton size classes over the course of the experiment. The average and associated error is shown (± 1 SE), with n = 4. Where size classes were subtracted from one another, error is propagated according to standard statistical practise.

Similar trends were observed for [PON] (Fig. 10). The smallest phytoplankton size class made little to no contribution to the bulk [PON] while the intermediate size class dominated the biomass. The [PON] varied over time within the upper 10 m of the water column, with minimal variation at 15 m where the [PON] was consistently lower than 5 µmol L^{-1} (Fig. 10). At the surface, there was a clear increase in the mean (± SE) bulk community [PON] from 4.7 ± 0.2 µmol L^{-1} on day 3 to 10.7 ± 3.0 µmol L^{-1} on day 8, while at 5 m there was an increase from 5.6 ± 1.0 µmol L^{-1} on day 6 to 11.5 ± 1.0 µmol L^{-1} on day 9 (Fig. 10). The mean (± SE) [PON] of the intermediate size class increased from 3.7 ± 1.4 µmol L^{-1} on day 5 to 7.5 ± 1.6 µmol L^{-1} on day 8 (Fig. 11). The mean (± SE) [PON] of the largest size class increased from 1.0 ± 0.1 µmol L^{-1} on day 3 to 3.1 ± 0.1 µmol L^{-1} on day 5, then decreased to 2.5 ± 0.1 µmol L^{-1} on day 7 before it increased again to 4.3 ± 0.2 µmol L^{-1} on day 9 (Fig. 11).

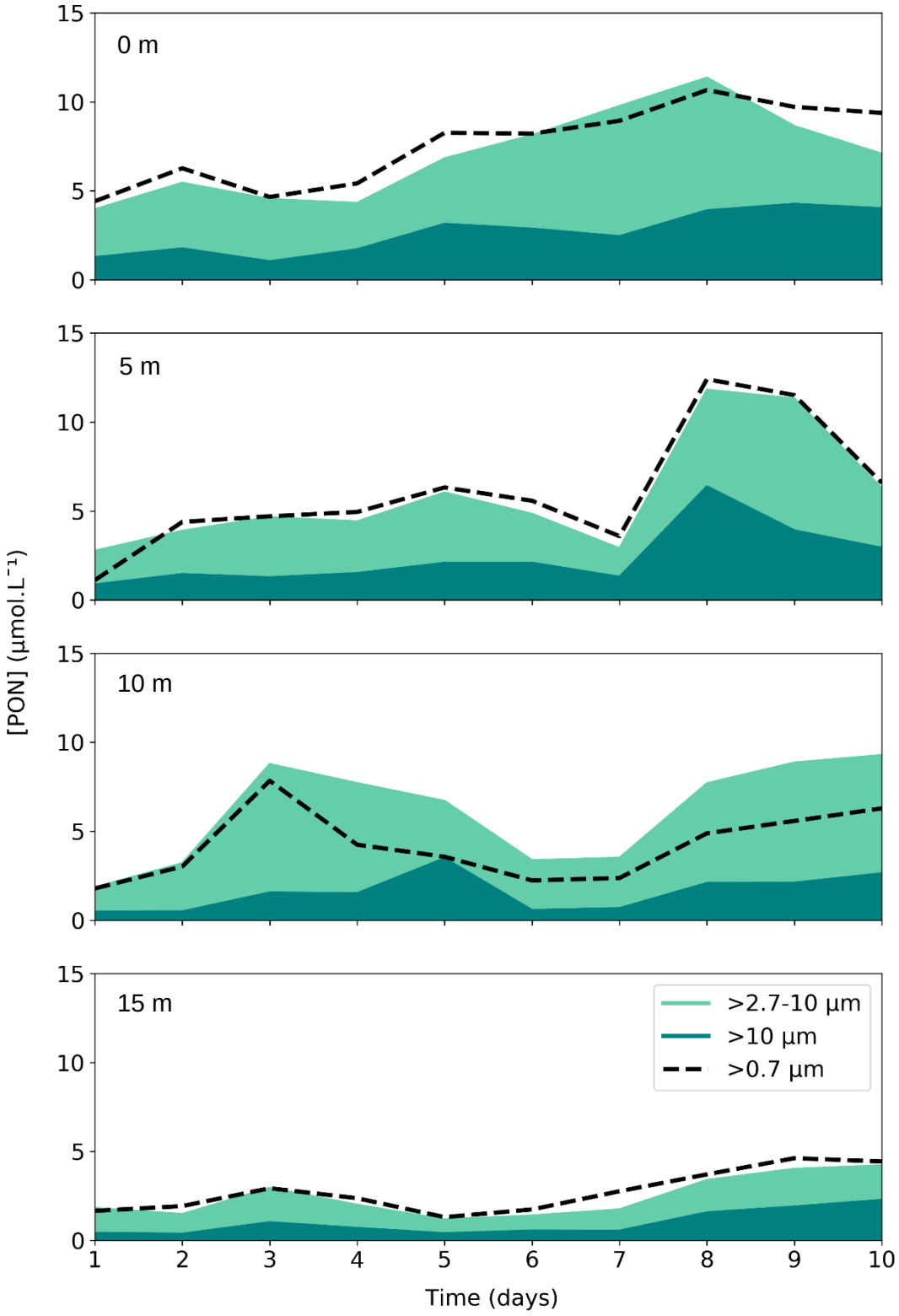

Fig 10. The particulate organic nitrogen concentration ([PON]) measured at 0 m, 5 m, 10 m and 15 m for the total (>0.7 µm), medium (2.7-10 µm) and large (>10 µm) phytoplankton size classes over the course of the experiment. In all cases, n = 4.

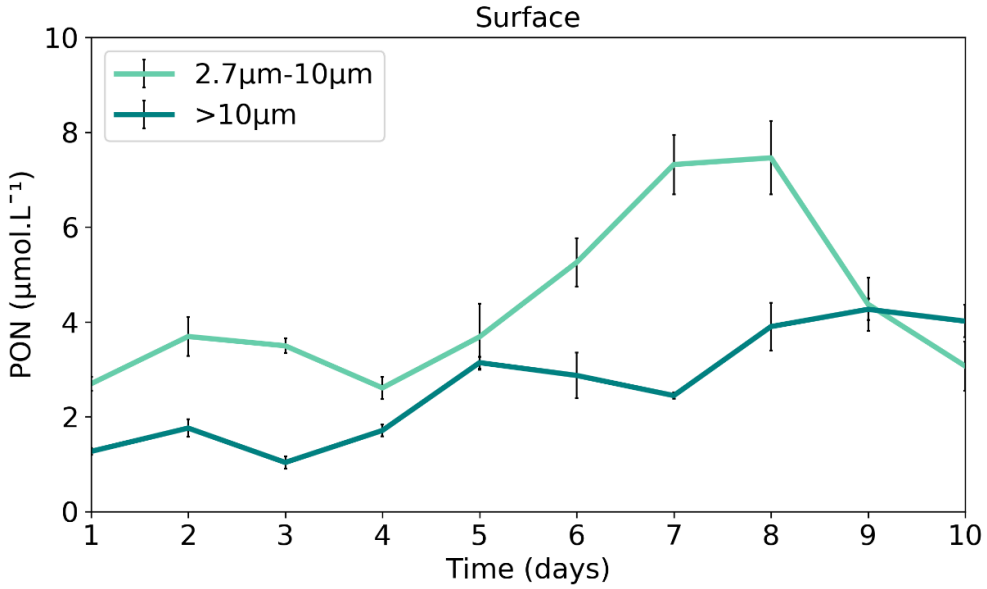

Fig 11. The particulate organic nitrogen concentration ([PON]) measured at the surface (~0 m) for the medium (2.7-10 µm) and large (>10 µm) phytoplankton size classes, over the course of the experiment. The average and associated error is shown (± 1 SE) and in all cases n = 4. Where size classes were subtracted from one another, error is propagated according to standard statistical practise.

3.5 Chlorophyll-a concentrations

The chlorophyll-a concentrations [Chl-a] at and below 10 m were relatively low (typically <10 µg L^{-1}), and displayed little variation over the 10-day time series compared to the [Chl-a] at the surface and 5m (Fig. 12). Here, the contribution of the smallest size class (0.2 µm to 3 µm) to the bulk community (> 0.2 µm) [Chl-a] was low and insignificant in comparison to the contribution of the intermediate (3 µm to 10 µm) and largest (> 10 µm) size classes. In general, the largest size class made the biggest contribution to bulk community [Chl-a], except over the last 3 days of the experiment when most of the Chl-a at the surface was attributed to the medium phytoplankton size class.

At the surface, total [Chl-a] decreased from 12.3µg L^{-1} on day 1 to 4.7 µg L^{-1} on day 3. Over the next 5 days, the [Chl-a] gradually increased to a maximum of 21.9 µg L^{-1} on day 8. Over the last two days of the experiment, the [Chl-a] decreased slightly to 16.3 µg L^{-1}. A similar trend was observed at 5 m where total [Chl-a] decreased from 11.9 µg L^{-1} on day 1 to 7.0 µg L^{-1} on day 3. Next, the [Chl-a] increased to a maximum of 16.9 µg L^{-1} on day 5 and remained relatively high until day 8 before it decreased to 9.0 µg L^{-1} on day 10. Day 7 was characterised by a slightly lower [Chl-a] of 10.3 µg L^{-1}.

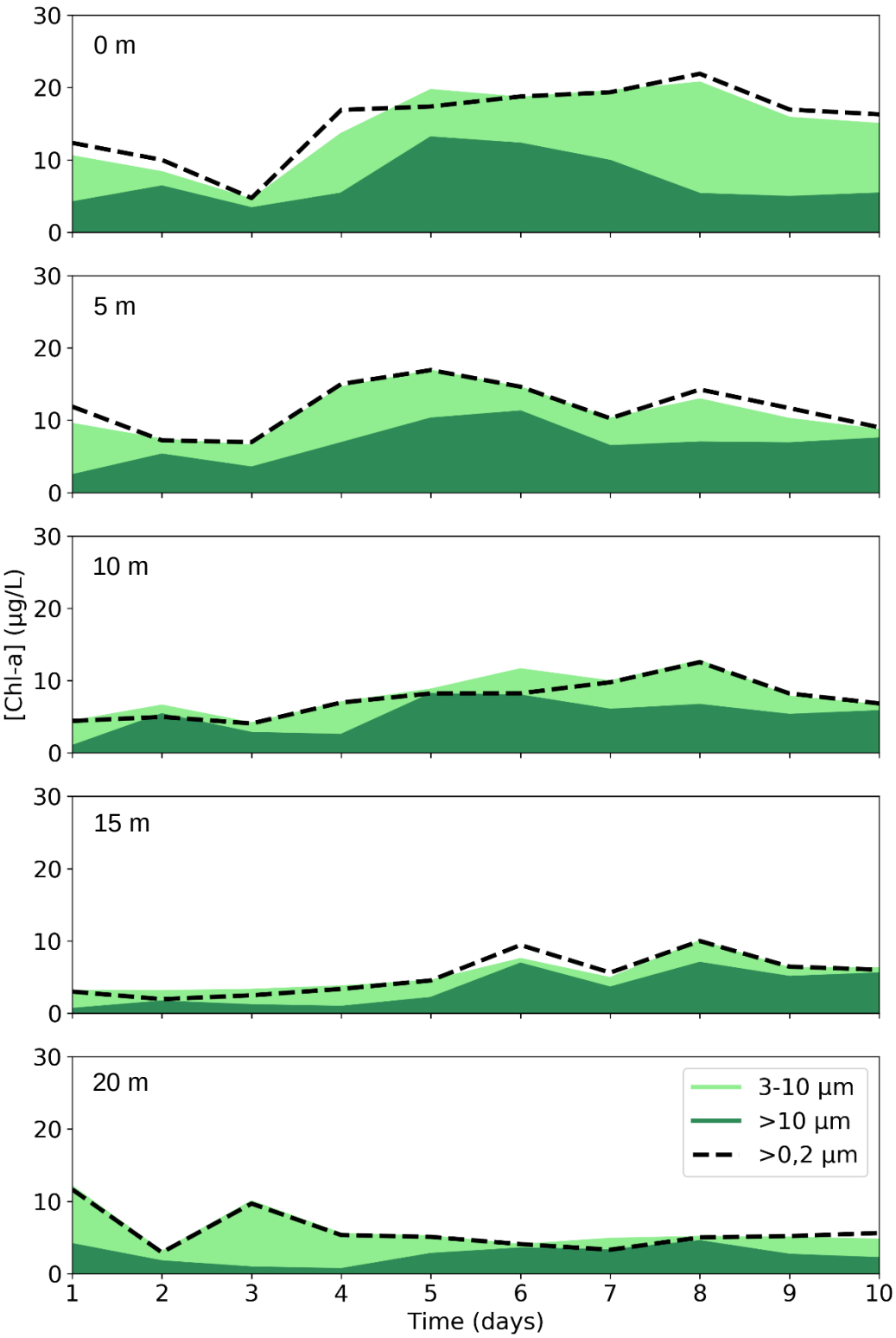

Fig 12. The chlorophyll-a concentration ([Chl-a]) measured at 0 m, 5 m, 10 m, 15 m and 20 m for the total (>0.2 µm), medium (3-10 µm) and large (>10 µm) phytoplankton size classes over the course of the experiment.

3.6 Net primary production, nitrate and ammonium uptake rates

Rates of net primary production (ρC) were dominated by the intermediate phytoplankton size class at all depths and throughout the experiment (Fig. 13). The contribution of the largest phytoplankton size class to bulk ρC was low and the contribution of the smallest phytoplankton size class was negligible compared to the others.

While local maxima in ρC occurred on day 4 and day 10 at 10 m, rates of ρC at and below 10 m were low and relatively invariant with time in comparison to ρC in the surface layer (Fig. 13). Here, there was a general increasing trend in mean (± SE) bulk community ρC from 9.5 $\pm$ 1.5 µmol L^{-1} d^{-1} on day 3 to 63.6 $\pm$ 0.4 µmol L^{-1} d^{-1} on day 8. At 5 m, mean (± SE) bulk community ρC increased from 0.1 $\pm$ 0.2 µmol L^{-1} d^{-1} on day 1 to 29.6 $\pm$ 2.7 µmol L^{-1} d^{-1} on day 5. The mean (± SE) ρC then decreased to 5.9 $\pm$ 0.3 µmol L^{-1} d^{-1} on day 7 before it increased again to 44.9 $\pm$ 6.5 µmol L^{-1} d^{-1} on day 9. The maximum surface ρC (days 7 and 8) was mirrored by a large decline in ρC just below at 5 m.

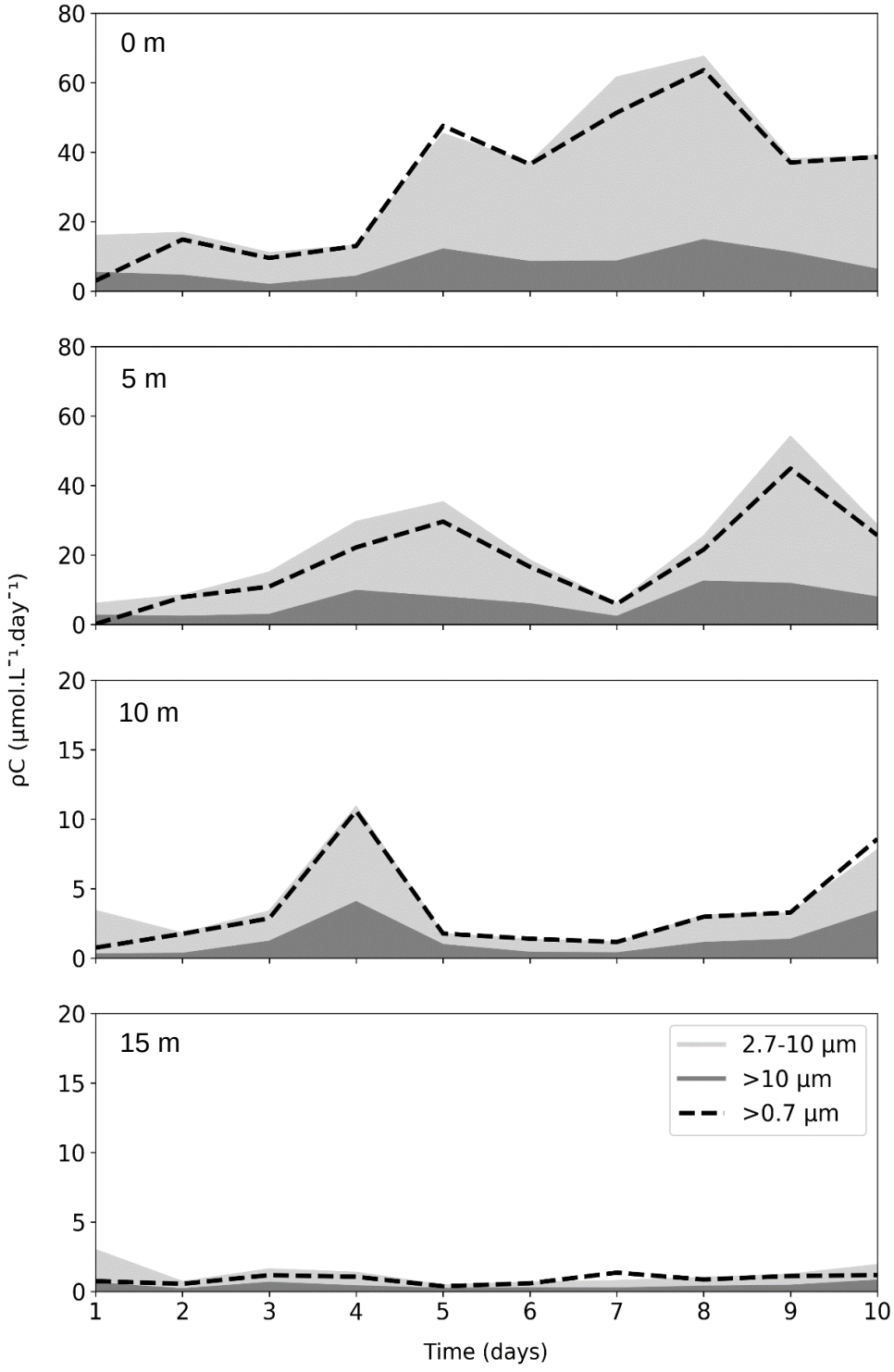

Fig 13. Rates of net primary production (ρC) measured at 0 m, 5 m, 10 m and 15 m for the total (>0.7 µm), medium (2.7-10 µm) and large (>10 µm) phytoplankton size classes over the course of the experiment. Note the change in y-axis scale between the top two and bottom two panels. In all cases, n = 2.

The nitrate uptake rates (ρNO_3^-) showed similar trends to ρC (Fig. 14). ρNO_3^- at and below 10 m was low and varied little over time. The contribution of the smallest phytoplankton size class to bulk community ρNO_3^- was negligible compared to the contribution of the intermediate and large phytoplankton size classes. The intermediate phytoplankton size class dominated ρNO_3^- overall. At the surface, there was a clear increase in the mean (± SE) bulk community ρNO_3^- from 2.0 $\pm$ 0.4 µmol L^{-1} d^{-1} on day 3 to 12.4 $\pm$ 2.0 µmol L^{-1} d^{-1} on day 6. ρNO_3^- then remained relatively constant for two days before it decreased to 3.2 $\pm$ 0.2 µmol L^{-1} d^{-1} on day 9. At 5 m, there were two distinct maxima in ρNO_3^-, on day 5 and day 9, with a decline in ρNO_3^- observed over the days in between, coincident with the maximum ρNO_3^- observed at the surface. At 5 m, the mean (± SE) ρNO_3^- increased from 0.2 $\pm$ 0.1 µmol L^{-1} d^{-1} on day 1 to 7.5 $\pm$ 0.5 µmol L^{-1} d^{-1} on day 5. ρNO_3^- then decreased to 0.6 $\pm$ 0.01 µmol L^{-1} d^{-1} on day 7 before it increased again to 10.7 $\pm$ 0.8 µmol L^{-1} d^{-1} on day 9.

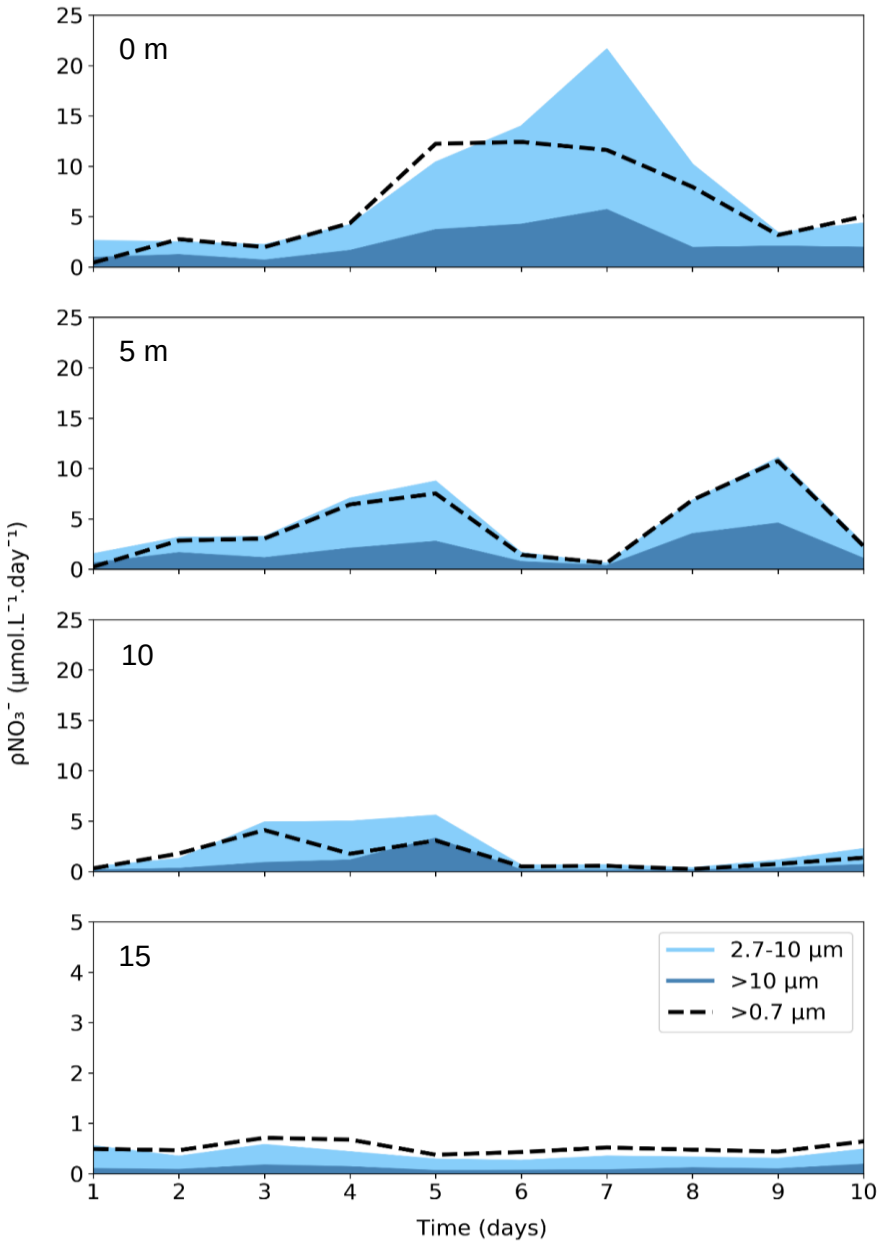

Fig 14. Rates of nitrate uptake (ρNO_3^-) measured at 0 m, 5 m, 10 m and 15 m for the total (>0.7 µm), medium (2.7-10 µm) and large (>10 µm) phytoplankton size classes over the course of the experiment. Note the change in y-axis scale for the bottom-most panel. In all cases, n = 2.

The ammonium uptake rates (ρNH_4^+) were relatively low compared to ρNO_3^- and ρC and appeared to follow a different trend (Fig. 15). ρNH_4^+ at 15 m was low in comparison to the other depths and did not vary much over time. ρNH_4^+ at the surface, 5 m and 10 m was higher and more variable, with a maximum in the mean (± SE) bulk community ρNH_4^+ occurring on day 2 at all of these depths – 2.0 $\pm$ 0.1 µmol L^{-1} d^{-1}, 1.5 $\pm$ 0.06 µmol L^{-1} d^{-1} and 2.9 $\pm$ 0.2 µmol L^{-1} d^{-1} at 0 m, 5 m and 10 m, respectively. At the surface, an increasing trend was apparent in the mean (± SE) bulk community ρNH_4^+, from 0.8 $\pm$ 0.03 µmol L^{-1} d^{-1} on day 3 to 3.1 $\pm$ 0.1 µmol L^{-1} d^{-1} on day 6. Again, the intermediate phytoplankton size class dominated the community ρNH_4^+. The largest phytoplankton size class made a small contribution to bulk ρNH_4^+, and the contribution of the smallest phytoplankton size class was negligible in comparison to that of the other sizes. There are no ρNH_4^+ data available for days 7 and 8 of the experiment.

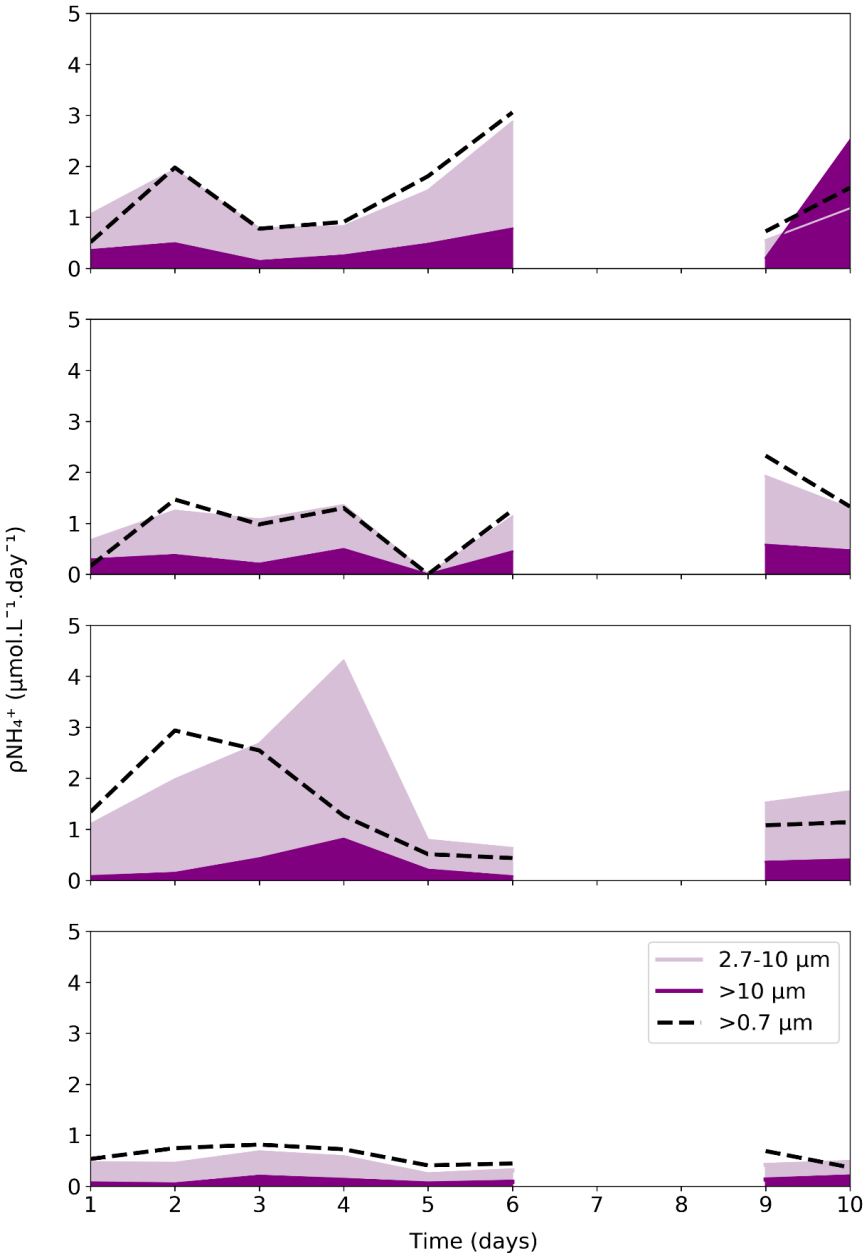

Fig 15. Rates of ammonium uptake (ρNH_4^+) measured at 0 m, 5 m, 10 m and 15 m for the total (>0.7 µm), medium (2.7-10 µm) and large (>10 µm) phytoplankton size classes over the course of the experiment. Where data are not available (days 7 and 8), the plot is left blank. In all cases, n = 2.

3.7 Phytoplankton growth rates

The contribution of the smallest phytoplankton size class to the bulk community biomass, ρC, ρNO_3^- and ρNH_4^+ was clearly unimportant compared to that made by the intermediate and large phytoplankton size classes. For this reason, discussion will focus only on the intermediate and large phytoplankton, hereafter referred to as the medium (2.7_10 μm) and large (> 10 μm) phytoplankton communities.

Size-fractionated specific uptake rates of carbon (Vc) were computed by normalising size-fractionated ρC to [POC] while size-fractionated specific uptake rates of NO_3^- ($V_{NO_3^-}$) and ammonium ($V_{NH_4^+}$) were normalised to [PON]. Vc was highest at the surface and 5 m (Fig. 16). For the most part, the medium phytoplankton community exhibited a higher Vc than the large phytoplankton community, although temporal trends in Vc were similar for both phytoplankton size classes (Fig. 16). At the surface, Vc was relatively constant over the first four days of the experiment. On Day 5, Vc reached a maximum, with values corresponding to a mean (± SE) of 1.3 $\pm$ 0.3 d^{-1} and 0.7 $\pm$ 0.1 d^{-1} for the medium and large phytoplankton communities, respectively, after which Vc decreased slightly before remaining relatively constant until the end of the experiment. The medium phytoplankton community showed a second maximum in Vc on day 10, equivalent to a mean (± SE) of 1.4 $\pm$ 0.2 d^{-1}. Similar results were observed at 5 m. At 10 m, Vc was consistently low and invariable except on day 4 when there was a small maximum in Vc equivalent to a mean (± SE) of 0.5 $\pm$ 0.2 d^{-1} and 0.4 $\pm$ 0.2 d^{-1} for the medium and large phytoplankton communities, respectively. At 15 m, a near zero Vc was observed with very little difference between the medium and large phytoplankton community over time.

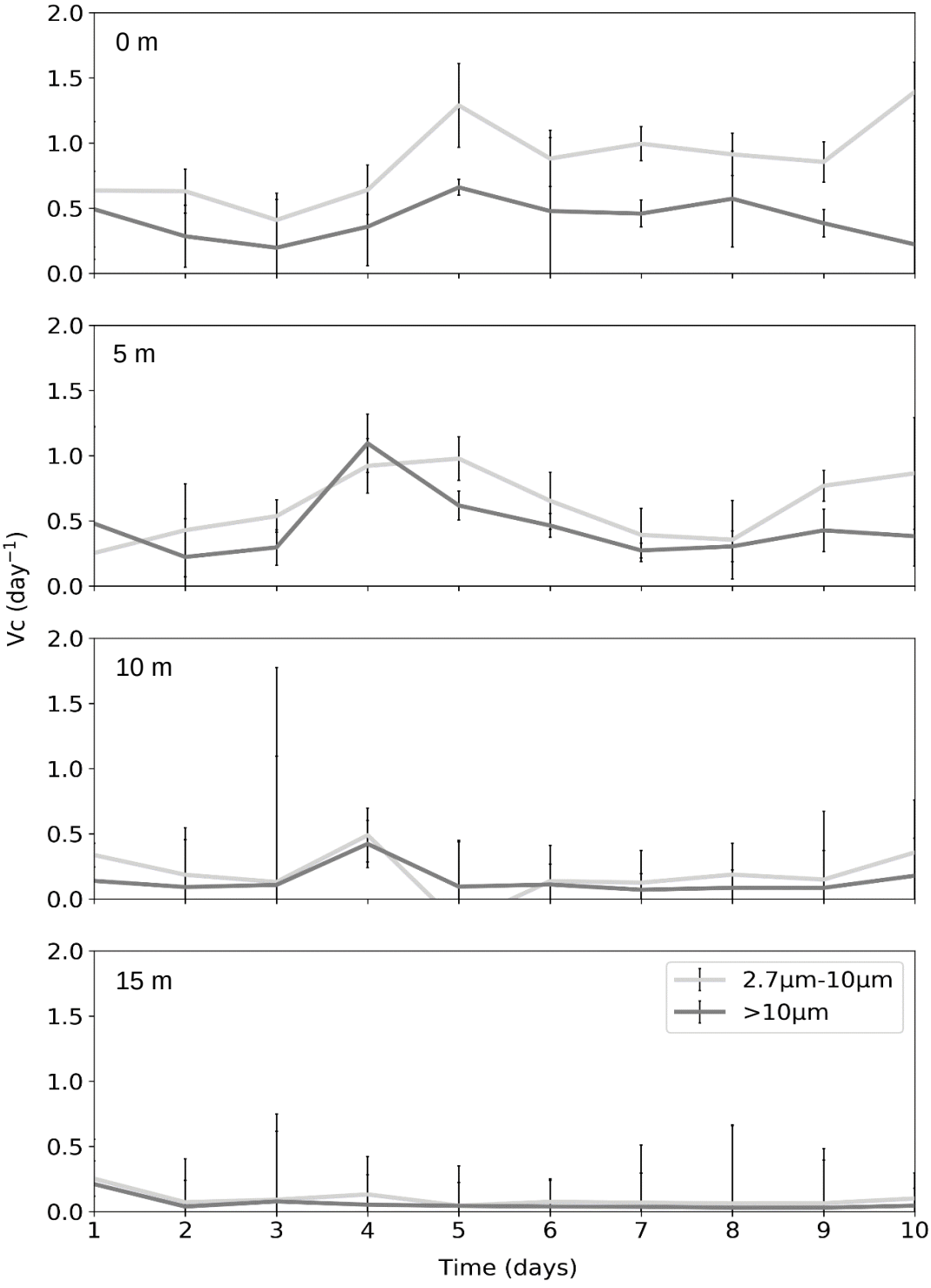

Fig 16. Phytoplankton growth rates based on carbon (Vc) measured at 0 m, 5 m, 10 m and 15 m for the medium (2.7-10 µm) and large (>10 µm) phytoplankton size classes over the course of the experiment. The average and associated error (± 1 SE) is shown for n = 2 in all cases. Values below zero are not shown.

$V_{NO_3^-}$ was highest at the surface and decreased with depth (Fig. 17). At 10 m, $V_{NO_3^-}$ was higher over the first half of the experiment than over the second half. $V_{NO_3^-}$ at 15 m was low compared to the shallower depths and varied little over time. At the surface and 5 m, the large phytoplankton community displayed a higher $V_{NO_3^-}$ than the medium phytoplankton community over the first three days of the experiment. On day 3, the $V_{NO_3^-}$ of both communities began to rise, with the $V_{NO_3^-}$ of the medium phytoplankton community rising faster than that of the large phytoplankton community.

At the surface, the medium phytoplankton community reached a maximum $V_{NO_3^-}$ on day 5 (1.8 $\pm$ 0.4 d^{-1}), which was maintained until day 7, after which $V_{NO_3^-}$ decreased to a mean (± SE) of 0.3 $\pm$ 0.2 d^{-1} by day 9 (Fig. 17). The large community reached a maximum $V_{NO_3^-}$ on day 7 (2.3 $\pm$ 0.1 d^{-1}), which immediately decreased to a mean (± SE) of 0.5 $\pm$ 0.8 d^{-1} on day 8. Both phytoplankton communities attained a similar maximum $V_{NO_3^-}$ (mean (± SE) of 2.2 $\pm$ 0.2 d^{-1} and 2.3 $\pm$ 0.1 d^{-1} for the medium and large phytoplankton communities, respectively).

At 5 m, the medium and large phytoplankton communities attained a maximum $V_{NO_3^-}$ on day 4 (mean (± SE) of 1.7 $\pm$ 0.1 d^{-1} and 1.4 $\pm$ 0.2 d^{-1}, respectively) (Fig. 17). In both cases, this high $V_{NO_3^-}$ was maintained for a day and then decreased to a minimum by day 7 (mean (± SE) of 0.2 $\pm$ 0.3 d^{-1} for the medium phytoplankton community and 0.3 $\pm$ 0.2 d^{-1} for large phytoplankton community). At 5 m, both phytoplankton communities exhibited a second local maximum on day 9, corresponding to a mean (± SE) of 0.9 $\pm$ 0.2 d^{-1} and 1.2 $\pm$ 0.1 d^{-1} for the medium and large phytoplankton communities, respectively.

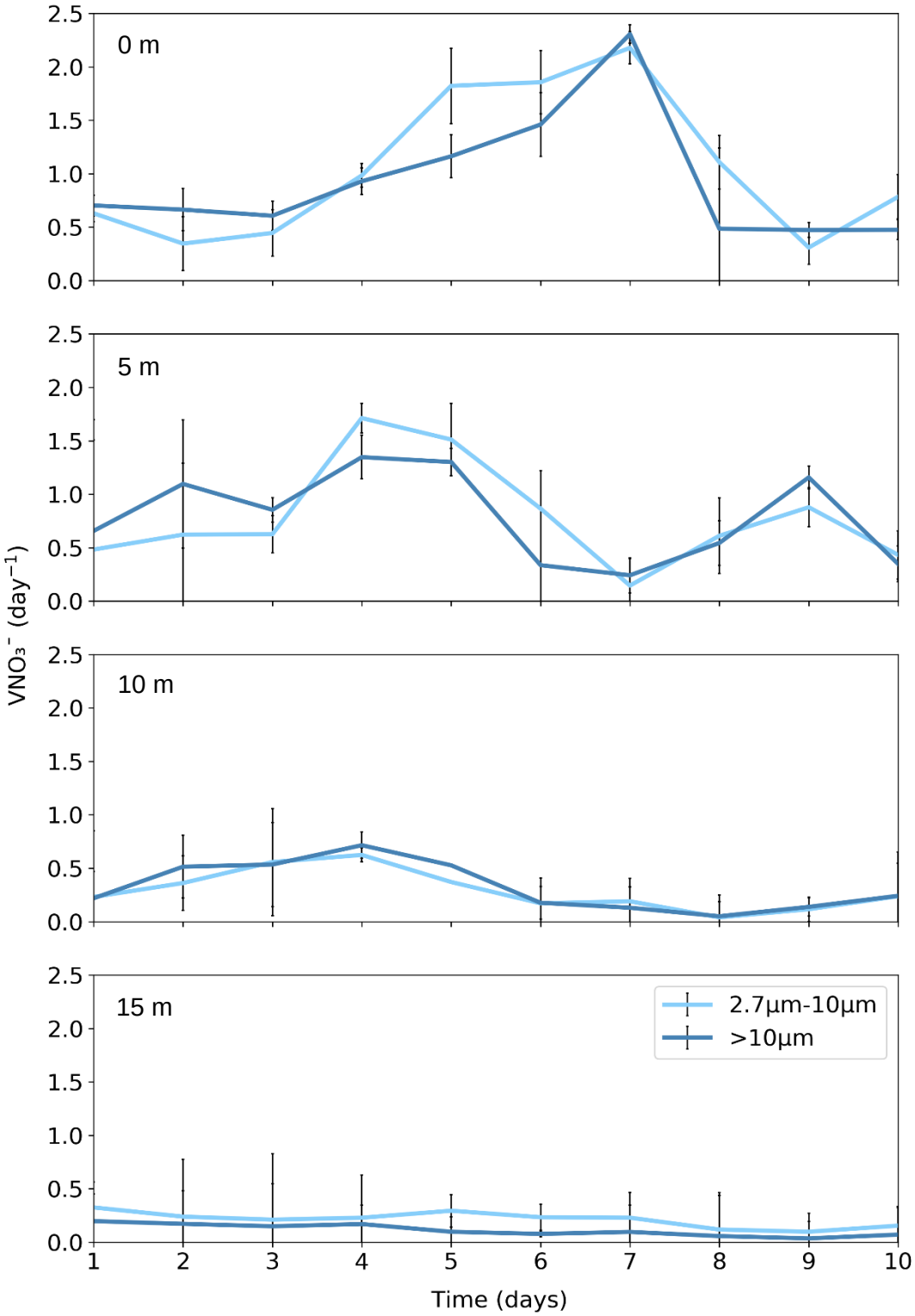

Fig 17. Phytoplankton growth rates based on NO_3^- ($V_{NO_3^-}$) measured at 0 m, 5 m, 10 m and 15 m for the medium (2.7-10 µm) and large (>10 µm) phytoplankton size classes over the course of the experiment. The average and associated error (± 1 SE) is shown for n = 2 in all cases. Values below zero are not shown. On days where no error bars are visible, n = 1.

There are no $V_{NH_4^+}$ data available on days 7 and 8 of the experiment, therefore the following interpretation is true only where $V_{NH_4^+}$ data exist. $V_{NH_4^+}$ for both phytoplankton communities was low and relatively consistent over time compared to Vc and $V_{NO_3^-}$ (Fig. 18). The available data suggest that $V_{NH_4^+}$ rarely exceeded 0.5 d^{-1} and that the $V_{NH_4^+}$ of the medium phytoplankton community was

generally higher than that of the large phytoplankton. There was no real trend in $V_{NH_4^+}$ with depth, although the highest $V_{NH_4^+}$ was observed at 10 m, coincident with high ambient [NH_4^+] (Fig. 7B). The medium phytoplankton community at this depth achieved a maximum $V_{NH_4^+}$ of 0.8 $\pm$ 0.2 d^{-1} (mean ± SE) on day 1, while the large phytoplankton community achieved a maximum $V_{NH_4^+}$ of 0.5 $\pm$ 0.2 d^{-1} (mean ± SE) on day 4.

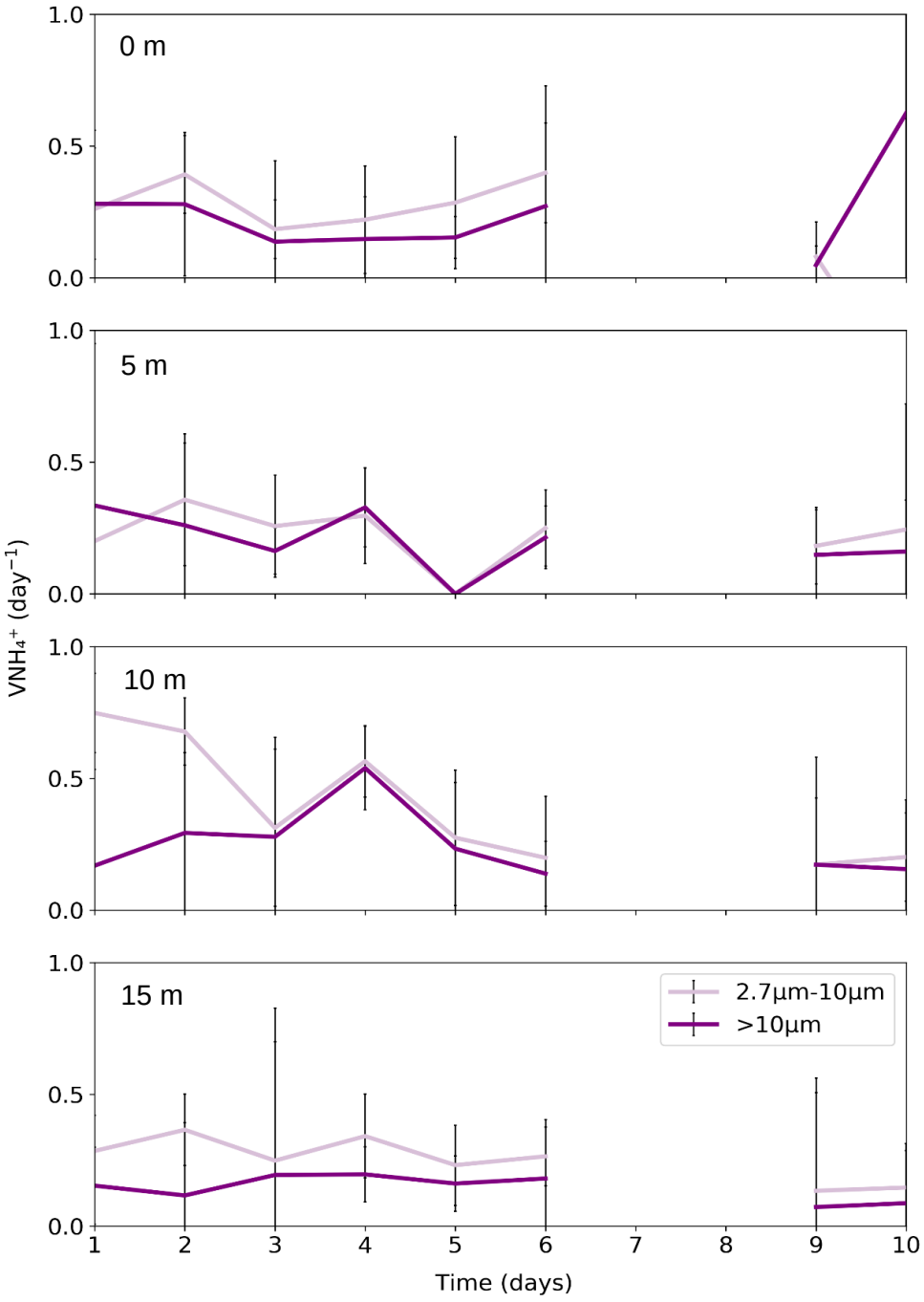

Fig 18. Phytoplankton growth rates based on NH_4^+ ($V_{NH_4^+}$) measured at 0 m, 5 m, 10 m and 15 m for the medium (2.7-10 µm) and large (>10 µm) phytoplankton size classes over the course of the experiment. The average and associated error ($\pm$ 1 SE) is shown for n = 2 in all cases. Values below zero are not shown. On days where no error bars are visible, n = 1. On days 7 and 8, there are no data available.

4. Discussion

4.1 The upwelling cycle in SHB

In March/April 1987, the first simultaneous measurements of physical, chemical and biological parameters were made in SHB during a 27-day anchor station study (Chapman & Bailey 1991). In the absence of upwelling, solar heating of the upper water column resulted in the formation of a two-layered system in SHB. The upper mixed layer (UML) was separated from the bottom mixed layer (BML) by the thermocline (Waldron, 1985). Waters above and below the thermocline differed in their hydrographic properties and nutrient concentrations except during the periodic intrusion of cold, nutrient-rich, low salinity South Atlantic Central Water (SACW). This SACW derived from wind-driven upwelling at the discrete upwelling centre located off Cape Columbine. After being upwelled, SACW extended north/north-eastward into the vicinity of SHB and followed a cyclonic trajectory (Bailey & Chapman, 1991). During active upwelling, the mixed layer of the water column was typically characterised by a uniformly-low temperature and high nutrient concentrations. In between upwelling events, the water column stabilised, and SSTs increased. The thermocline intensified and shoaled, once again establishing a two-layered system. During this time, the concentration of most nutrients in the UML were reduced due to assimilation by growing phytoplankton (Mitchell-Innes & Walker, 1991).

It is well established that pulsed upwelling cycles last 3 to 10 days in the SBUS (Chapman & Shannon, 1985), which is the reason for the 10-day duration of the anchor station experiment discussed in this thesis. Below, hydrographic and nutrient data are presented (section 4.1.1 and 4.1.2, respectively) that suggest the study captured a full upwelling cycle in SHB.

4.1.1 Hydrography: active upwelling and stratification

Where CTD data are available (i.e., days 5 to 10), they are used to describe the hydrography of the water column. Where no CTD data are available (i.e., days 1 to 4), temperature was estimated from the temperature-nitrate (TN) relationship established using data collected after day 4. Density was then determined from TN-derived temperature and discrete salinity measurements. TN relationships have been successfully applied in the SBUS in the past to infer NO_3^- concentrations during upwelling events. For example, Waldron and Probyn (1992) used data obtained from the northern and southern Benguela on various cruises to establish a negative relationship between SST and NO_3^- concentration (R^2 = 0.47). Using this relationship in conjunction with satellite imagery, potential annual new production was estimated for the Benguela. In sum, while estimating temperature from NO_3^- concentration is not ideal, there is a precedent for using this approach when direct measurements are lacking.

The data show that the density structure of the water column is more strongly driven by temperature than salinity and that the water column was well mixed for the first half of the experiment (Fig. 5 and 6). Prior to the experiment, sustained upwelling-favourable winds and relatively higher wind speeds (Fig. 4) would have resulted in the upwelling of cold, low salinity SACW at Cape Columbine. Given the circulation of this region (section 4.1), upwelled SACW was likely advected into SHB, causing the cool SSTs apparent during the first half of the experiment. Bailey and Chapman (1991) found the wind field at their site to be most similar to that at Cape Columbine. They too observed lower SSTs in SHB following southerly wind events, which they attributed to a similar mechanism.

In addition to the generally lower temperatures/higher densities observed over the first half of the experiment, there is a clear signal of vertical advection on day 3 that imported water from below 10 m, with a NO_3^- concentration of up to 20 µmol L^{-1}, to the surface near the anchor station site. This

event may have been induced by local water circulation patterns that facilitated exchange across the thermocline. For example, the passage of shelf waves, Ekman pumping or turbulence induced by the shear between currents flowing in the UML and the BML can result in upward nutrient supply (Bailey & Chapman, 1991). Alternately, the high wind speeds (the highest recorded during the experiment) measured at Cape Columbine on day 3 may have led to the entrainment of high-NO_3^- waters originating at Cape Columbine.

Over the second half of the experiment, the water column stratifies, as evidenced by warming surface waters and the development of a shallow thermocline and pycnocline (Fig. 5 and 6). Stratification is likely due to a relaxation of upwelling favourable winds. Indeed, wind data from Cape Columbine suggest that while winds blew predominantly from a south to south-east direction during the experiment, the wind speed steadily dropped from about 9 m s^{-1} on day 3 to 5 m s^{-1} on day 9 (Fig. 4). During the latter half of the study, the mixed layer depth ranged from ~2.5 m to 15 m, which differs from the first five days when no mixed layer depth could be calculated because the entire water column was well mixed (Fig. 5 and 6). This is consistent with the study of Bailey and Chapman (1991) that observed a stable water column with increased SSTs and an intensified thermocline positioned at ~12 m between successive upwelling events.

What matters for phytoplankton growth, however, is not only the establishment of a shallow surface mixed layer, but also the extent to which light is able to penetrate this mixed layer. The euphotic zone depth, which gives an indication of light penetration, is relatively deep at the beginning of the experiment and shoals towards the end. This suggests that light was initially able to penetrate quite far into the water column but was later rapidly attenuated, probably due to an increase in phytoplankton biomass as discussed in section 4.2 below.

4.1.2 Nutrient supply and consumption

During the first half of the experiment, high NO_3^- concentrations were observed throughout the water column, ranging from ~10 to 25 µmol L^{-1} (Fig. 7A). This can be explained by the intrusion of SACW into the bay that was upwelled at Cape Columbine following persistent upwelling favourable winds (Fig. 4). Once stratification set in, NO_3^- in the UML was quickly reduced to near zero concentrations (Fig. 7A). This can be attributed to phytoplankton consumption during water column stabilisation following a relaxation in the upwelling favourable winds. Similar to NO_3^-, relatively lower concentrations of NH_4^+ (Fig. 7B), Si (Fig. 7E) and PO_4^{3-} (Fig. 7D) were observed in the UML during the second half of the experiment. This, too, can be attributed to assimilation by phytoplankton, and in the case of Si, indicates the presence of diatoms. Unlike other phytoplankton species, diatoms require Si for growth (Brzezinski et al. 1997) in addition to N and P.

4.1.2.1 NH_4^+ and PO_4^{3-} efflux from the sediments

Interestingly, the NH_4^+ and PO_4^{3-} concentrations covary (Fig. 7B and D), at least over the first half of the experiment when relatively high concentrations of NH_4^+ (1-2 µmol L^{-1}) and PO_4^{3-} (3-5 µmol L^{-1}) occur on days 1 to 2 and days 4 to 5 near the bottom of the water column. NH_4^+ is known to accumulate in upwelled water as it ages and large amounts of biomass become available for predation and remineralization (Whitledge, 1981; Alcaraz et al., 1994). In addition, it can accumulate due to efflux from the sediments following the remineralization of fresh organic matter recently supplied from the surface (Dugdale et al., 2006). In the oxygen deficient bottom waters (< 1 mL L^{-1}) of SHB, Bailey (1987) measured NH_4^+ concentrations as high as 3 to 4 µmol L^{-1}, which they attributed to sedimentary efflux. Similar bottom water oxygen concentrations are recorded in the present study, suggesting that here, high bottom water NH_4^+ may also derive from sedimentary efflux.

High PO_4^{3-} concentrations were reported by Tyrrell and Lucas (2002) in shelf waters of the northern Benguela and SBUS, although all sampled sites in the SBUS are north of the anchor station site. They attributed this to cold, nutrient-rich deep water from offshore accumulating regenerated PO_4^{3-} from the continental shelf before being upwelled to the surface. The added regenerated PO_4^{3-} has two possible origins. Firstly, it may derive from the sinking of surface particulate organic matter (POM) that is fuelled by the consumption of nutrients being advected offshore in surface waters. Following nutrient consumption, the now nutrient-deplete waters are transported laterally towards the open ocean while the fresh POM sinks and is remineralized on the continental shelf, thereby "trapping" nutrients that would otherwise be lost offshore. Secondly, the regenerated PO_4^{3-} could be diffused out of the sediment pore waters on the shelf where ambient concentrations are very high.

Option one would act to raise the NO_3^- concentration above that of the source waters along with increasing PO_4^{3-}, which is not observed (Fig. 7). One caveat to this is that no rise in NO_3^- would be observed if coincident benthic denitrification removed a similar quantity of NO_3^- to that added by on-shelf remineralization. While sedimentary oxygen concentrations in SHB are probably low enough to support benthic denitrification year-round, it is highly unlikely that this process could have removed the quantity of regenerated NO_3^- expected (~16-32 μmol L^{-1}) if all the excess PO_4^{3-} in bottom waters (~1-2 μmol L^{-1}) derived from remineralization of surface POM. Remineralization yields NH_4^+ that ultimately gets converted to NO_3^- via nitrification, such that while excess NO_3^- is not observed, the 16-32 μmol L^{-1} N may have accumulated in the NH_4^+ pool. However, no NH_4^+ concentrations of this magnitude are observed. In addition, the high concentrations of PO_4^{3-} and NH_4^+ accumulate on a timescale of one to two days. For option one to hold true, the rate of remineralisation and nitrification would need to be extremely high to account for the rapid changes in PO_4^{3-} and NH_4^+. While it might be possible for remineralisation to occur at such high rates, nitrification is a slow process (Ward, 2000). Thus, the available data argue against sinking POM as the direct origin of high ambient PO_4^{3-} and NH_4^+ concentrations at depth.

Option two involves the efflux of sedimentary PO_4^{3-} (and NH_4^+) into the lower water column, which could raise the concentrations of these nutrient species separately from that of NO_3^-. The origin of the high PO_4^{3-} in bottom waters is thus more likely diffusion from the sediments.

High sedimentary PO_4^{3-} concentrations can derive from the activity of large sulphur bacteria (e.g., *Thiomargarita*) (Schulz & Jørgensen, 2001), which gain energy by oxidising sulphide that accumulates in anoxic marine sediments (Schulz & Schulz, 2005). Under oxic conditions, the bacteria acquire energy from the oxidation of sulphur, while at the same time accumulating polyphosphate (poly-P) and NO_3^- in their large intracellular vacuoles (Schulz & Schulz, 2005). Poly-P and NO_3^- are taken up during brief periods when bottom waters are oxic or when loose sediments become suspended in the water column (i.e., during storms or wave action; Schulz & Jørgensen, 2001). Under anoxic conditions, the absence of a suitable electron acceptor drives sulphur bacteria to reduce internally-stored NO_3^- to NH_4^+ via dissimilatory nitrate reduction to ammonium (DNRA) and to break down internally-stored poly-P to PO_4^{3-} in order that sulphide can be oxidised to elemental sulphur to gain energy (Schulz & Schulz, 2005). As a consequence, PO_4^{3-} is released into the pore waters along with any NH_4^+ that escapes consumption in the sediments, from where it can diffuse into the water column (Goldhammer et al., 2010). Sulphur bacteria are known to inhabit the shelf sediments of the BUS, which frequently experiences oxygen deficient bottom water conditions (Neumann et al., 2016). Therefore, the relatively high concentrations of NH_4^+ and PO_4^{3-} at depth in SHB probably derive from sedimentary efflux.

4.1.2.2 High NO_2^- in surface waters

Throughout the experiment, NO_2^- concentrations are below 1 µmol L^{-1}, except at 0 m and 5 m on days 4 to 5 when unexpectedly high concentrations (2.7 - 4.5 µmol L^{-1}) persist (Fig. 7C). The BUS is typically characterised by NO_2^- concentrations of 0.1 to 0.5 µmol L^{-1} (Verheye, 2000). Higher concentrations (up to 5 µmol L^{-1}) have been observed in the northern BUS (Kuypers et al., 2005) and in other upwelling systems (e.g., off the coast of Peru; Hamersley et al., 2007), although such high concentrations are almost always recorded below the surface layer or near the sediments, associated with low to zero oxygen conditions. High NO_2^- concentrations at the surface are unusual given that NO_2^- is an intermediate species in the N cycle, existing temporarily during nitrification or denitrification (Wada & Hattori, 1971). Moreover, the surface waters are well oxygenated, ruling out a denitrification source.

At elevated concentrations, NO_2^- can be toxic to phytoplankton (Abe et al., 2002; Yang et al., 2004), such that they are unlikely to allow it to accumulate or to flourish in waters where high NO_2^- concentrations persist. In studies conducted by Chen et al., (2009) on the fresh water, bloom-forming cyanobacterium, *Microcystis aeruginosa*, increased ambient NO_3^- concentrations were observed to coincide with an increase in intracellular NO_2^- concentration and a decrease in growth rate and photosynthesis. This was attributed to the fact that nitrate reductase (NR) enzymatic activity increases with increasing NO_3^- concentrations, while nitrite reductase (NiR) enzymatic activity does not increase to the same extent. When the flux of NO_2^- produced by NR exceeds that reduced by NiR, NO_2^- accumulates in the cell (Chen et al., 2009). While excess NO_3^- can be stored intracellularly with no negative effect, NO_2^- is an inorganic monovalent anion capable of inhibiting photosynthetic electron transport (Spiller & Boger, 1997; Loranger & Carpentier, 1994). It can also change the pH inside algal cells and cause damage to their cell membranes (Almeida et al., 1995; Sijbesma et al., 1996; Yang et al., 2004).

NO_2^- in seawater is typically produced via biological means. For example, the decomposition of POM releases NH_4^+ that then becomes available for microbial oxidation to NO_2^- through the process of nitrification. Additionally, in parts of the ocean where phytoplankton biomass is high and NO_3^- is not limiting, phytoplankton are known to excrete NO_2^- (Carlucci et al., 1970). Lomas and Glibert (1999) hypothesized that diatoms in an N-replete environment may take up and reduce NO_3^- independently of their nutritional requirements in response to environmental conditions that cause them to possess more energy than they need. Any NO_3^- that gets reduced for non-nutritional purposes must be released from the cell into the surrounding waters to prevent it causing damage to the photosynthetic apparatus (Neale et al., 1993).

Experimental data have shown that rates of NO_2^- and NH_4^+ release from diatom cells increases when they are exposed to rapid increases in irradiance (Lomas et al., 2000). However, even after NO2- was released during these experiments, the media concentration of NO_2^- remained low (<0.5 µmol L^{-1}) (Lomas et al., 2000). In most cases, the release of NO_2^- by phytoplankton into the water column would yield much lower concentrations of ambient NO_2^- than the surface NO_2^- concentrations observed in the present study. Consequently, it is unlikely that the unusually high surface NO_2^- concentrations apparent on days 4 to 5 resulted from *in situ* biological activity.

Further evidence against the *in situ* biological production of surface NO_2^- derives from the fact that ammonia oxidising bacteria (AOB) are traditionally thought to be inhibited by light. Evidence for the photoinhibition of ammonia oxidation has been shown in laboratory cultures of AOB (e.g., Hooper & Terry, 1974; Guerrero & Jones, 1996) and more recently, in ammonia oxidising archaea (AOA), which outnumber AOB in the upper water column (Beman et al., 2008) and appear to be more photosensitive

(Merbt et al., 2011). However, euphotic zone nitrification has been reported in both coastal and open ocean environments (Ward et al., 1989; Dore & Karl, 1996; Ward, 2005; Clark et al, 2008), such that the degree to which AOB are light limited is still a topic of debate. Nonetheless, observations of nitrification in the well-lit surface layer are almost always restricted to the base of the euphotic zone. However, the high NO_2^- concentrations observed in the present study occur at the very surface where light levels are extremely high compared to the base of the euphotic zone.

For NO_2^- to derive from NH_4^+ oxidation, there would also need to be sufficient NH_4^+ present in the upper water column (Ward, 2000). Surface NH_4^+ concentrations were very low throughout the present study. This is usually the case in the surface ocean where NH_4^+ produced by heterotrophic bacteria is rapidly consumed by phytoplankton (Ward, 2000). Furthermore, nitrification is a slow process (Ward, 2000), which is inconsistent with the accumulation of such high NO_2^- concentrations on the timescale of days. Relatively high surface Si and PO_4^{3-} concentrations were observed concurrently with the high NO_2^- concentrations. In the case of Si, the surface concentration was higher than that in the upwelling source waters (Fig. 7E). This, along with the lack of evidence for an *in situ* biologically-mediated source of NO_2^-, suggests that the surface NO_2^- pool may have derived from an external input to the bay. The possible sources are explored in Appendix A. In any case, the anomalously high NO_2^- concentrations did not appear to affect the rates primary productivity or N uptake measured during the experiment.

4.2 The response of phytoplankton to an upwelling event in SHB

POC and PON concentrations indicate that biomass almost doubled over the stratification period of the experiment after remaining relatively constant during active upwelling (Fig. 8 and Fig. 10). A two-fold increase in surface biomass could be responsible for preventing light from penetrating more than a few metres into the water column, driving the shoaling of the euphotic zone depth during the second half of the study, as alluded to in section 4.1.1 (Fig. 6). One might expect phytoplankton growth to be hindered as a result, given that the depth to which light is able to penetrate is limited. However, the shoaling of the euphotic zone depth is matched by a shoaling of the base of the UML. This acts to restrict phytoplankton to the high light surface layer where rapid growth should be favoured.

Rates of NPP (i.e., pC) indicate that phytoplankton growth was rapid during the second half of the experiment, at least at the surface (Fig. 13). As expected, NPP decreased with depth due to the lack of light available for photosynthesis. Furthermore, total community rates of NO_3^- assimilation indicate sustained elevated growth from days 5 to 8 at the surface, coincident with the increasing rates of NPP (Fig. 14). Rates of NO_3^- assimilation were low below 5 m, again likely due to insufficient light availability. NO_3^- is energetically expensive for phytoplankton to reduce compared to NH_4^+ and requires almost a third of the photosynthetically-derived reducing power (Losada & Guerrero, 1979; Syrett, 1981). NO_3^- uptake rates are thus heavily light-dependent. In contrast, NH_4^+ uptake rates are less light-dependent because NH_4^+ requires far less energy to assimilate given its lower oxidation state (Dortch, 1990). This can explain the lack of variation in NH_4^+ uptake rates with light intensity imposed by depth in SHB (Fig. 15).

Low rates of NPP and NO_3^- uptake were observed at 5 m during the same time period that high rates were observed at the surface (day 7; Fig. 13 and Fig. 14), underscoring the high degree of spatial variability that characterises this system. Such a mismatch may be due to the two-layered structure of the water column over the stratification period. The nutrient-poor, less dense UML was separated from the nutrient-replete, denser BML below by a strong pycnocline, with the MLD indicating the base of the UML and changing from day to day. As a result, the phytoplankton community sampled at 5 m on one day might not be the same as the phytoplankton community sampled at 5 m the next day. For example, low rates of NPP on day 7 at 5 m can be explained by an extremely shallow MLD (2.5 m)

compared to that observed on day 6 (5 m) and day 8 (15 m). In other words, the 5 m phytoplankton community on day 7 is probably different from that sampled at the same depth one day before or one day later. Because of its position in the BML, the 5 m phytoplankton community on day 7 would have been restricted to low light conditions less conducive to growth. On days 6 and 7, the 10 m and 15 m sampling depths fell within the BML, while over the last 3 days of the experiment, they occurred in the UML. Therefore, one might expect the uptake rates at these depths to be lower on days 6 and 7 and higher later on, which is not the case. However, euphotic zone depths on the order of 5-10 m indicate that light availability was limited by 10 m; thus, water column stratification is not expected to significantly change the uptake rates at 10 m and 15 m.

The POC concentrations suggest that the biomass comprised phytoplankton primarily from the intermediate and largest size classes, with almost no biomass occurring in the smallest size class. In addition, the contribution by small phytoplankton to NPP was insignificant. While POC biomass was comprised of relatively equal quantities of intermediate- and large-sized phytoplankton, NPP was clearly dominated by the intermediate-sized phytoplankton (Fig. 8 and Fig. 13). In the surface, these phytoplankton exhibited rates of NPP that were roughly double those of the large phytoplankton. This suggests that the specific growth rates based on carbon (i.e., growth rates) of intermediate-sized phytoplankton must be higher than those of large sized phytoplankton, which is confirmed by the data (Fig. 16), at least in the surface and at 5 m.

The intermediate and largest phytoplankton contributed fairly evenly to the PON biomass and total community NO_3^- assimilation rates. While the specific NO_3^- assimilation rates ($V_{NO_3^-}$) of both size classes were fairly similar when averaged over time, the intermediate-sized phytoplankton displayed a more rapid increase in their growth rate (on days 3 to 5) and were able to maintain their maximum growth rate for longer (Fig. 17). This likely enabled them to outcompete the larger cells for NO_3^-. The intermediate-sized phytoplankton comprised mainly small diatoms (see section 4.3.3 below), which are NO_3^- specialists (Andrews & Hutchings, 1980; Pitcher et al., 1992; Litchman, 2007; Fawcett & Ward, 2011) that tend to dominate the phytoplankton biomass under nutrient replete conditions because of their ability to respond more rapidly than other groups to increased NO_3^- concentrations. In a mesocosm experiment conducted by Fawcett and Ward (2011) in the Californian upwelling system, diatoms were observed to increase their $V_{NO_3^-}$ before the rest of the phytoplankton community and maintain this elevated $V_{NO_3^-}$ for a longer period of time, allowing them to outcompete all other phytoplankton, access a disproportionate fraction of the available nutrients, and attain very high levels of biomass. Furthermore, cells that can increase their biomass quickly experience reduced grazing pressure (Cermeno, et al., 2005) allowing them to flourish for longer. In contrast to the present study, the fast-growing diatoms that were dominant in the Californian experiment were >20 µm while the contribution of the intermediate size class (5-20 µm) to biomass, NPP, and N uptake was minor (Fawcett & Ward 2011). Nonetheless, a similar ecological framework best explains the results of the present study, but with medium-sized diatoms (3-10 µm) responding most rapidly to elevated NO_3^-, thus coming to dominate the phytoplankton community.

During the previous SHB anchor station study, primary production was measured using the ^{14}C technique (Strickland & Parsons, 1972; Brown, 1984). Water column integrated NPP varied between 0.99 and 7.85 g C m^{-2} day^{-1} (Mitchell-Innes & Walker, 1991) and, as in the present study, tracked changes in biomass (evidenced by chlorophyll concentrations rather than POC). The 2016 water column integrated rates of bulk community NPP ranged from 13.7 to 336.2 mmol m^{-2} day^{-1}, which equates to roughly 0.18 to 4.3 g C m^{-2} day^{-1}. While slightly lower than the rates of NPP measured previously (Mitchell-Innes & Walker, 1991), these estimates fall within a similar range. Lamont et al. (2014) also determined daily integrated rates of NPP in the SBUS using ^{14}C and reported 0.71 to 6.98

g C m^{-2} day^{-1} for mid-spring and 0.7 to 3.35 g C m^{-2} day^{-1} for autumn. Again, higher rates of NPP occurred coincident with higher phytoplankton biomass, while lower rates of NPP were observed when biomass was low. In addition, Lamont et al. (2014) observed the highest integrated biomass and rates of NPP in SHB, consistent with previous estimates of elevated phytoplankton biomass (Weeks et al., 2006 in summer; Demarcq et al., 2007 all year round) and NPP (Mitchell-Innes et al., 2000 in summer) in this region compared to the surrounding waters. Furthermore, in a recent study conducted at 6 stations across the SBUS in winter, the highest rates of NPP and N uptake and the greatest biomass accumulation were observed in the surfaces waters of SHB (Flynn et al., 2018). SHB is thus clearly responsible for a large proportion of total SBUS productivity, irrespective of the time of year, which highlights the importance of SHB to the fertility of the broader SBUS.

The NH_4^+ uptake rates follow a different trend from that of NPP and NO_3^- assimilation. NH_4^+ uptake was relatively high and variable over the upper 10 m, and relatively low and consistent over time at 15 m, although always about 5-fold lower than the rates of NO_3^- assimilation. The highest NH_4^+ uptake rates appear to correspond with high concentrations of ambient NH_4^+, at least at the surface (e.g., day 2 and days 4 - 6), although NH_4^+ uptake rates were not measured on days 7 to 8 when NPP (and NO_3^- uptake) was highest. In their California upwelling experiment, Fawcett and Ward (2011) observed rates of NPP, NO_3^- and NH_4^+ uptake that, while low immediately following simulated upwelling and subsequently rising over time, all changed in concert (Fawcett & Ward, 2011). That the NH_4^+ uptake rates in the present study did not follow the same trend as NPP and NO_3^- uptake suggests that the driver(s) of NH_4^+ uptake may be different. In any case, total community NH_4^+ uptake rates compare well with previous estimates from the SBUS in summer (Probyn, 1985; Probyn et al, 1996) as well as with recent wintertime estimates from SHB itself (Flynn et al. 2018).

One might expect NH_4^+ uptake rates to be higher in summer and lower in winter due to seasonal changes in temperature, irradiance and daylength (Eppley et al., 1979). However, the results of the present study suggest that NH_4^+ uptake rates in SHB are similar in summer and in winter. This could be due to the relatively minor effect of light availability on NH_4^+ uptake and/or to dominance of intermediate sized phytoplankton in SHB, which achieved the highest rates of NH_4^+ uptake during the study, at least on the days for which data are available (Fig. 18).

According to the literature, the presence of NH_4^+ can inhibit the consumption of NO_3^- by phytoplankton cells (Dortch, 1990; Cochlan & Harrison, 1991), leading phytoplankton to reduce the NH_4^+ concentrations through uptake prior to consuming NO_3^-. Indeed, a trend often observed in EBUS is a decline in $V_{NO_3^-}$ that coincides with an increase in NH_4^+ concentration (Wilkerson & Dugdale, 2008). The most cited NH_4^+ concentration threshold above which $V_{NO_3^-}$ is significantly decreased is 1 µmol L^{-1} (Dortch 1990). Interestingly, despite the high ambient NH_4^+ concentrations observed in this study (0.1-1.8 µmol L^{-1}), there is little evidence that NO_3^- uptake was inhibited. This may be because the highest rates of NPP and NO_3^- uptake (i.e., of phytoplankton activity) occurred at 0 m and 5 m where ambient NH_4^+ concentrations were lower (0.1 – 1.4 µmol L^{-1}). It should also be noted, however, that the degree to which $V_{NO_3^-}$ is affected by NH_4^+ is highly variable, and NO_3^- uptake rates in the presence of 1 µmol L^{-1} NH_4^+ can equal or exceed NH_4^+ uptake rates (Dortch, 1990). There are also many cases where the ambient NH4+ concentration did not affect NO_3^- uptake (e.g., Goering et al., 1970; Kokkinakis & Wheeler, 1987) as well as situations in which NO_3^- uptake was stimulated by NH_4^+ (Glibert et al., 1982b).

In sum, during the anchor station study, phytoplankton responded to upwelling by doubling their biomass in 3 to 4 days as conditions became more favourable for growth. This increase in biomass was matched by a significant increase in the rates of NPP and NO_3^- uptake. Medium sized phytoplankton

were able to outcompete both smaller and larger cells by increasing their growth rate more rapidly and maintaining an elevated growth rate for longer than the other phytoplankton. Phytoplankton in SHB also appeared to avoid NH_4^+ inhibition of NO_3^- uptake, possibly due to the vertical separation of phytoplankton cells and high NH_4^+ concentrations in the water column.

As discussed above, for phytoplankton to grow and synthesise new organic matter, they need to be able to take up nutrients. In addition to consuming nutrients, they also need to be able to absorb light. Therefore, both nutrient and light availability can limit growth, such that both likely exert a strong control on productivity in SHB. The conditions under which phytoplankton growth is limited by light and/or nutrients is discussed in section 4.2.1 below.

4.2.1 Light limitation versus nutrient limitation

In order to sustain elevated levels of primary production, phytoplankton rely heavily on the availability of nutrients (often primarily DIN) and light (Wilkerson & Dugdale, 2008; Sigman & Hain, 2012). During the active upwelling period, water column integrated rates of total community NO_3^- assimilation increased almost 5-fold (Fig. 19; bars). At the same time, the water column integrated dissolved inorganic nitrogen concentration ([DIN]; inclusive of NO_3^-, NO_2^- and NH_4^+) remained relatively constant (Fig. 19; dashed line). The fact that the ambient [DIN] did not decrease despite a significant rise in NO_3^- uptake rates suggests that NO_3^- was being continually resupplied; the ambient NO_3^- concentration could thus be maintained despite consumption by phytoplankton. From day 5 to 8, the water column integrated [DIN] decreased to almost one third of its starting concentration. This suggests that the physical nutrient supply ceased or at least slowed, resulting in the ambient NO_3^- concentration declining due to consumption by phytoplankton. When the water column integrated [DIN] reached a minimum (97 mmol m^{-2}; day 8), NO_3^- assimilation rates began to decline. [DIN] then began to increase again, likely due both to the decrease in phytoplankton consumption and an increase in NO_3^- supply driven by the onset of another upwelling cycle. This is supported by the increase in NO_3^- concentration at depth on days 9 and 10 (Fig. 7A) coincident with the outcropping of isopycnals that occurs during upwelling (Fig. 6). Over the relaxation period, it appears that NO_3^- uptake was modulated largely by the ambient NO_3^- concentration. Brown and Field (1986) similarly observed nutrient limitation driving a reduction in phytoplankton growth that was accompanied by a decrease in nutrient concentrations in the upwelling region off the Cape Peninsula. These data are consistent with the hypothesis that, in the Benguela region, nutrient limitation sets in at NO_3^- concentrations of less than 4 to 5 µmol L^{-1} (Andrew & Hutchings, 1980).

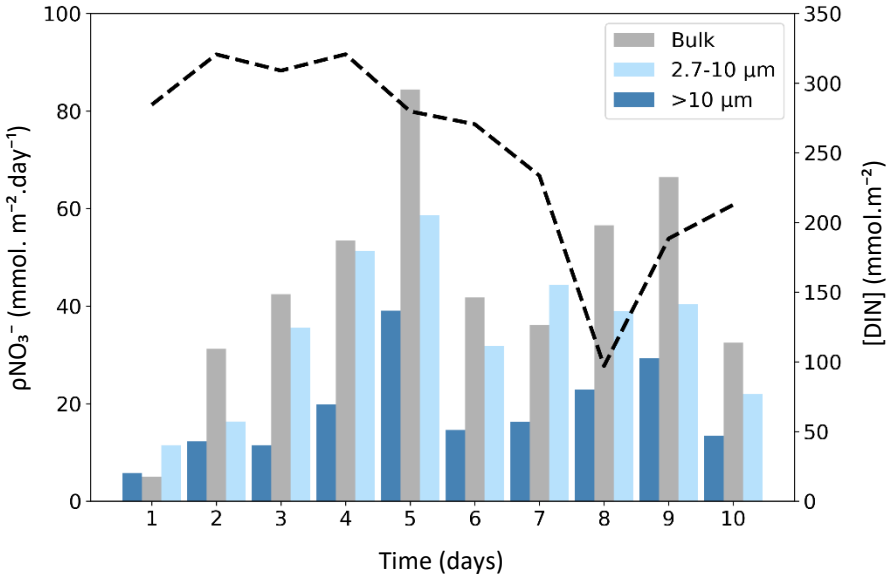

Fig 19. Nitrogen supply and consumption. Bars represent the water column integrated rates of total community NO_3^- assimilation (ρNO_3^-) for the bulk phytoplankton community, which includes all cells > 0.7 µm (grey), phytoplankton that range in size from 2.7 µm to 10 µm (light blue) and phytoplankton > 10 µm (dark blue) over the course of the experiment. The dashed black line indicates the water column integrated dissolved inorganic nitrogen ([DIN]) concentration, which is the sum of NO_3^- NO_2^- and NH_4^+.

While nutrient limitation controls phytoplankton growth during the relaxation period, light appears to control growth during the active upwelling period. The euphotic zone was deeper during active upwelling, shoaling during the relaxation period of the study. Additionally, there was no well-defined mixed layer during the active upwelling period because the entire water column was mixed. However, a well-stratified mixed layer characterised the relaxation period. What matters for phytoplankton growth is not just how deep light is able to penetrate the water column, but where the base of the euphotic zone is located in relation to the depth of the mixed layer. Downstream of upwelling centres, as for SHB, wind stress and turbulence are at times reduced (Bailey, 1991), much like during the relaxation phase of the present study. The resultant warming of surface waters allows a thermocline to develop, which enhances water column stability and reduces the depth of the mixed layer to above the critical depth. According to the critical-depth hypothesis proposed by Sverdrup (1953), this allows phytoplankton to bloom because cells are maintained in the euphotic zone instead of being mixed below the compensation depth, as occurs during turbulent conditions (Bailey, 1991). During the active upwelling period, the MLD was always deeper than the euphotic zone, while during the relaxation period, the MLD was shallower than or similar to the euphotic zone depth, expect on day 8. In accordance with Sverdrup (1953), phytoplankton growth should be limited during the active upwelling period due to their reduced light exposure.

The active upwelling period was also characterised by lower particulate organic carbon to chlorophyll-a ratios (POC: Chl-a) compared to those observed over the relaxation period (Fig. 20). The relationship between chl-a concentration and phytoplankton carbon biomass is influenced by the complex interactions of light, nutrients and temperature in the euphotic zone (Geider et al., 1997). While the combined effects of these variables on POC: Chl-a ratios in the ocean are not well understood (Wang et al., 2009), laboratory studies have shown that phytoplankton respond to changes in them by adjusting their chl-a concentrations. For example, phytoplankton increase their chl-a content under

low light, which decreases their POC:Chl-a ratio (Geider, 1987), while POC:Chl-a ratios increase under conditions of N limitation (Riemann et al., 1989; Geider et al., 1993). The effect of temperature on the POC:Chl-a ratio is more complicated. For example, phytoplankton POC:Chl-a decreased from 130 to 10 as temperature increased from 0°C to 30°C under nutrient-replete, light saturated conditions (Geider, 1987). This study was based on multiple phytoplankton types most of which were diatoms (Geider, 1987). However, nutrient depletion reversed this response, such that the POC:Chl-a ratio decreased in response to decreasing temperatures (Geider, 1987). The plasticity of their POC:Chl-a ratio allows phytoplankton to adapt to and photosynthesize in almost any new environment, even if it is less favourable for growth than their previous environment (Geider, 1987; Macintyre et al., 2002). For example, phytoplankton POC:Chl-a ratios tend to decrease from high-light to low-light environments when nutrients are plentiful as phytoplankton increase their per-cell chl-a in order to harvest more light. This well-studied coping mechanism is referred to as “photoacclimation” (Anning et al. 2000).

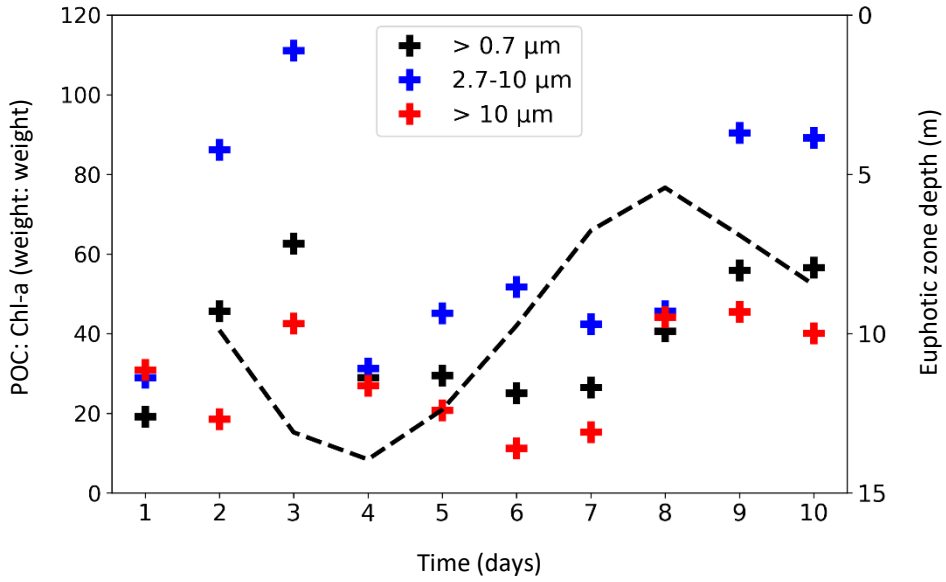

Fig 20. Phytoplankton carbon-to-chlorophyll ratios. Crosses show the water column integrated particulate organic carbon (POC) to chlorophyll-a (Chl-a) ratios (POC:Chl-a) for phytoplankton cells > 0.7 µm (black), phytoplankton cells from 2.7 µm to 10 µm (blue) and phytoplankton cells > 10 µm (red) over the course of the experiment. The dashed black line shows the depth of the base of the euphotic zone.

In the present study, while light penetrated deeper into the water column over the active upwelling period, the POC:Chl-a ratio was on average lower during this time. This may be attributed to the turbulent nature of the water column. If phytoplankton were being mixed below the depth of the euphotic zone, spending significant time in the dark, then even though nutrients were readily available, the total amount of light that they experienced may have been insufficient for phytoplankton to sustain high rates of photosynthesis (Sverdrup, 1953; Bailey, 1991). The lack of light may have caused phytoplankton to produce more chl-a, therefore decreasing the POC:Chl-a ratio, such that photosynthesis could continue, albeit at a much lower rate. Their low POC:Chl-a ratio, coupled with the observation of fairly low rates of NPP and N uptake, suggests that light modulated the growth of phytoplankton during the active upwelling phase. During water column relaxation, light was not able to penetrate as deeply but stratification likely restricted biomass to the well-lit surface layer. This would have ensured that phytoplankton spent much of their time in the light, requiring less light-harvesting chl-a and resulting in higher POC:Chl-a ratios. One exception is day 3 of the study, when a high POC:Chl-a ratio is observed. One option is that, by day 3, phytoplankton still had not had enough time to acclimate to the variable light conditions, thus their chl-a content was still low,

resulting in an elevated POC:Chl-a ratio. A more likely explanation is that the high POC:Chl-a ratio derived from the upward vertical mixing of detritus and other organic matter from the sediments, which had a high POC:Chl-a ratios because of their high concentration of non-autotrophic carbon. It should be noted, however, that on day 3, the POC and chl-a concentrations are low, such that small variations in either relative to the day before and after could have led to large changes in the ratio of POC:Chl-a. For example, a small decrease in the water column integrated chl-a concentration coupled with a small increase in the water column integrated POC concentration would yield a high POC:Chl-a ratio.

Our data suggest that SHB is highly physically and biogeochemically variable, switching rapidly from a system where phytoplankton growth is dominantly controlled by light availability to one where nutrient availability constrains production. Similar results were obtained in a study conducted by Brown and Field (1986) in an active upwelling zone off the Cape Peninsula in the SBUS. This work highlighted the rapid and short-term changes that occur in SST, nutrients and phytoplankton production and biomass in response to variations in the winds that control upwelling versus quiescence. Upwelling disrupted the thermocline and caused the depth of the mixed layer and euphotic zone to increase, leading to high NO_3^- (± 20 µmol L^{-1}) and very low biomass concentrations (as indicated by chl-a concentrations <1 mg m^{-3}). When upwelling favourable winds reversed, a shallow thermocline developed, and the water column appeared to stabilize. NO_3^- concentrations decreased (< 1 µmol L^{-1}) as the upwelled waters warmed and aged, and biomass accumulated to high levels (ranging from 11.4 to 18.4 mg m^{-3} of Chl-a).

Similar to the present study, the rate of primary production measured by Brown and Field (1986) was lower during active upwelling and higher when the wind stress relaxed and the water column stabilized. In contrast to the present study, however, the low rates of primary productivity were attributed to the small seed population of phytoplankton present in the upwelled water and not to light limitation. In fact, Brown and Field (1986) suggest that close to the shore in an active upwelling area where the source water is generally biomass-poor, primary production may be more severely limited by low biomass than by light and/or nutrients.

The biomass at the start of the present study is relatively low, but increases quickly once stratification sets in. In SHB, upwelling is followed by periods of quiescence which, when aided by the retentive circulation of the bay, allow phytoplankton time to grow and increase their biomass. In contrast, other areas of the southern Benguela, characterised by semi-permanent upwelling in summer, may never experience quiescence for long enough to allow for a significant increase in biomass and associated productivity. Therefore, the hypothesis of Brown and Field (1986) that low biomass limits productivity is probably not relevant to the case of SHB. One could argue, however, that the success of the medium phytoplankton size class in terms of its contribution to total community nutrient uptake could be related to the fact that it comprises such a large proportion of the initial biomass of the total assemblage (Fig. 21). As a result, once stratification sets in, medium phytoplankton already have an advantage over both smaller and larger cells due to their higher biomass such that they are effectively predisposed to outcompeting all other phytoplankton. However, this is unlikely to be the only reason for the success of the medium size class; other possible explanations are explored in detail below.

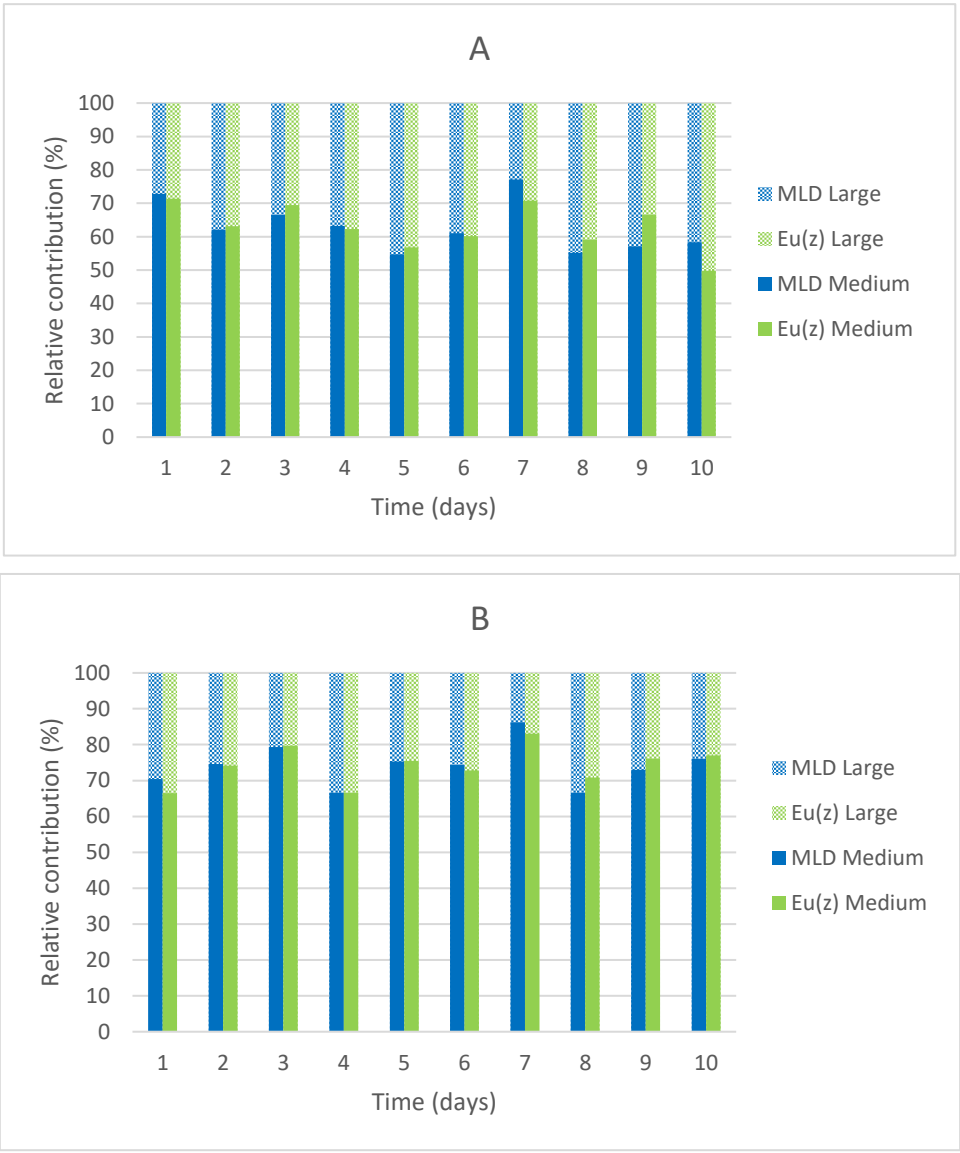

Fig 21. The percent contribution (%) of cells 0.7 µm to 2.7 µm (solid fill) and cells > 10 µm (dotted fill) to the total euphotic zone integrated (blue) and mixed layer depth integrated (green), particulate organic carbon concentration (A; [POC]) and rate of net primary production (B; NPP).

4.3 Phytoplankton community composition - an additional driver of primary production

4.3.1 The importance of phytoplankton cell size

Cell size influences many aspects of phytoplankton physiology and ecology, such as resource acquisition and food web structure (Marañón et al., 2009). Size-fractionated NPP and nitrogen uptake experiments thus allow for a deeper investigation of the structure and functioning of a phytoplankton community compared to the insights offered by bulk community measurements alone.

In the present study, medium sized phytoplankton (2.7 µm to 10 µm) performed best, contributing most significantly to biomass accumulation and nutrient uptake throughout the study, as evidenced by the euphotic zone and MLD integrated POC concentrations and NPP rates in Fig. 21. Given the evidence that small phytoplankton cells (e.g., naked flagellates) generally occupy vertically stratified, oligotrophic waters, while large phytoplankton cells (e.g., diatoms) tend to dominate in eutrophic

environments where the water column is well mixed (Margalef, 1978; Malone, 1980) like SHB, large phytoplankton (> 10 µm) might have been expected to perform best. However, medium sized phytoplankton possess a number of selective advantages over smaller and larger cells (Marañón et al., 2009), which may have aided their success in a highly variable system like SHB.

For example, the rate at which phytoplankton can assimilate nutrients depends on cell surface area. Therefore, nutrient uptake is most efficient in small cells that have high specific surface areas (i.e., surface area-to-volume ratios) (Smetacek, 1985; Kiørboe, 1993). Phytoplankton nutrient uptake and growth are often described as a saturating function of the nutrient, using Michealis-Menten kinetics (Litchman 2007). The two key parameters that characterise the efficiency of nutrient uptake are the maximum specific uptake rate (V_{max}) and the half saturation constant (K_s) (Litchman, 2007). The K_s is a measure of the ability of phytoplankton to utilise low concentrations of nutrients. This parameter varies with cell size, such that small cells have a lower K_s than larger cells like diatoms (Eppley & Thomas, 1969), giving small cells a competitive advantage under nutrient-limited conditions. However, large cells possess a significantly higher V_{max}, which enables them to effectively utilise pulses of high nutrients, outcompeting smaller cells that are constrained by a lower V_{max} (Litchman, 2007). Therefore, while smaller cells may be better nutrient competitors under low nutrient conditions, the pulsed nutrient supply that characterises SHB should favour larger cells.

In addition to the concentration and composition of pigments, light absorption also depends on the surface area of the cell (Banse 1976; Taguchi 1976). The amount of light absorbed per unit of pigment decreases as cell size increases and as the intracellular pigment concentration increases (Kirk, 1976; Morel & Bricaud, 1981). This is attributed to an increased package effect (Sathyendranath et al., 1987; Babin et al., 1993), which refers to a reduction in the ratio between actual absorption of intracelluar pigments and the absorption potential (maximum absorption possible) for the pigment in solution (Kirk, 1976, 1994; Geider & Osborne, 1987). As a result, large cells are less efficient than small cells at absorbing light (Kiørboe, 1993), such that low light conditions should favour growth of small cells.

Nutrient and light availabilty are, in turn, strongly controlled by the stabilty of the water column, such that the extent of water column stratification versus mixing could be regarded as the ultimate determinant of cell size. For example, a well mixed water column can supply nutrients to the euphotic zone from below the thermocline, thus allowing the biomass and NPP of large-sized phytoplankton to increase (Chrisholm, 1992). The degree of water column stabilisation also determines the residence time of various sized phytoplankton in the euphotic zone because phytoplankton need to be able to remain suspended in order to be able to grow in the euphotic zone. Larger cells sink faster than smaller cells; therefore, without the necessary turbulence to keep them suspended, their residence time in the surface will always be reduced compared to that of smaller cells (Marañón et al., 2009).

While small phytoplankton are better at acquiring resources and avoiding sedimentation, large phytoplankton have a competitive advantage in that their size offers a refuge from predation (Kiørboe 1993). In fact, one of the most widely accepted hypotheses for the dominance of large over small cells in upwelling zones is their ability to avoid predation by zooplankton (Geider et al., 1986). Small phytoplankton cells are generally consumed by nano- and microzooplankton (e.g., unicellular ciliates and heterotrophic flagellates), which have generation times that are similar to those of their prey. Larger phytoplankton cells, by contrast, are typically grazed on by larger mesozooplankton predators (e.g., copepods and euphausiaceans) that have much longer generation times than their prey, on the order of weeks to months (Kiørboe 1993). As a result, the abundance of smaller cells is constrained by constant microzooplankton grazing while larger cells are able to form dense phytoplankton blooms, outpacing the growth of their predators (Cermeno et al. 2006).

The success of the intermediate phytoplankton size class throughout the present study might thus be attributed to the fact that they were large enough to avoid predation by any zooplankton that surpassed pre-screening during sample collection. In addition, turbulence during the active upwelling period probably allowed medium sized cells to remain suspended in the euphotic zone, and they are small enough to avoid being negatively affected by the variable light environment as larger cells would have been. Furthermore, the medium sized phytoplankton were probably small enough to avoid sedimentation during the relaxation period. Finally, their intermediate size also provides this phytoplankton size class with the ideal combination of physiological parameters to outcompete smaller and larger cells in a high nutrient environment. For example, they have a higher V_{max} than smaller cells, coupled with a higher growth rate, which allows them to utilise nutrient pulses and grow fast (Litchman, 2007). While larger cells also have a high V_{max}, their growth rate is reduced compared to that of medium sized phytoplankton due to the unimodal distribution of growth rate with cell size (Marañón et al., 2013); this is consistent with the proxies for growth rate (i.e., specific uptake rates) measured in the present study.

The dominance of medium sized phytoplankton in SHB is consistent with observations made by Estrada and Blasco (1985) on a review of the literature from multiple upwelling systems (i.e., Baja California, Peru, northwest and southwest Africa). The authors found that chain-forming and colonial diatoms with individual cell diameters of 5 to 30 µm typically dominate in upwelling systems. In addition, in an observational study, Probyn (1992) suggests that the SBUS is dominated by small diatoms, <10 µm in diameter.

That SHB is dominated by medium sized phytoplankton has many implications for the ecosystem, firstly because the size structure of the phytoplankton community plays a key role in determining the fate of POC (Legendre & Rassoulzadegan, 1996). Where phytoplankton communities are dominated by large-sized phytoplankton, there is greater potential for organic matter transfer to higher trophic levels via short efficient food chains. In contrast, where small-sized phytoplankton dominate, a more complex food web structure persists in which the microbial loop plays a central role. As a result, organic matter is continually recycled within the euphotic zone (Cermeno et al. 2006; Azam et al. 1983; Fenchel 2008).

Secondly, large phytoplankton cells are more at utilising newly upwelled NO_3^- (Hutchings et al., 1995; Legendre & Rassoulzadegan, 1995; Cermeno et al., 2005; Fawcett & Ward, 2011), such that ecosystems dominated by large cells are also typically characterised by higher f-ratios (Hutchings et al. 1995). Given that from a mass balance perspective, NO_3^--based phytoplankton growth (i.e., new production) equates to organic matter export to the ocean interior and that large cells sink more rapidly than small cells, large cells tend to facilitate more carbon export (Michaels & Silver, 1988; Montero et al., 2007; Fawcett et al., 2011). In this way, phytoplankton community size structure can modulate the strength of the biological carbon pump, thus influencing atmospheric CO_2 sequestration (Marañón et al., 2009).

The present study suggests that the SHB water column is dominated by smaller cells than one would expect for a study site located in an upwelling system. In sum, this is because medium sized phytoplankton possess a high V_{max} and growth rate and are the ideal shape to acquire resources while avoiding sedimentation and grazing. The presence of medium sized phytoplankton could mean that SHB does not experience the maximum carbon export potential that would be achieved by larger cells. However, in this study, NO_3^--based phytoplankton growth far exceeds growth on NH_4^+, such that SHB is characterised by a high f-ratio (~0.6 to 0.85). While such a high f-ratio implies that new production is not negatively impacted by the dominance of medium sized phytoplankton, the degree to which new production can be equated to carbon export potential in SHB is unknown. This is because of the

limitations associated with applying the new production paradigm to such a shallow and highly variable coastal environment. In fact, the f-ratio is unlikely to be a useful proxy for carbon export in SHB.

Medium cells (specifically diatoms) also have several strategies that enable them to achieve high growth rates. One such strategy is the ability to store high concentrations of nutrients in intracellular vacuoles under conditions of intermittent nutrient supply (Marañón et al., 2009).

4.3.2 Luxury nitrate uptake

If N uptake and NPP are tightly coupled, a comparison of V_C and the specific N uptake rate (V_N, which includes both NO_3^- and NH_4^+) should yield a 1:1 relationship because V_C and V_N are both independent estimates of phytoplankton growth. However, for all the size classes, the majority of samples fall below such a 1:1 reference line (Fig. 22), which implies that the phytoplankton community in SHB was assimilating more N than they were fixing C, and that N assimilation and photosynthesis were decoupled. This analysis assumes that N uptake is well described by NO_3^- and NH_4^+ only, and that other potential sources of N (e.g., from urea uptake and N_2 fixation) are unimportant in SHB. If another N source were supporting phytoplankton growth in SHB, the data would deviate even more strongly from the 1:1 line in Fig. 22.

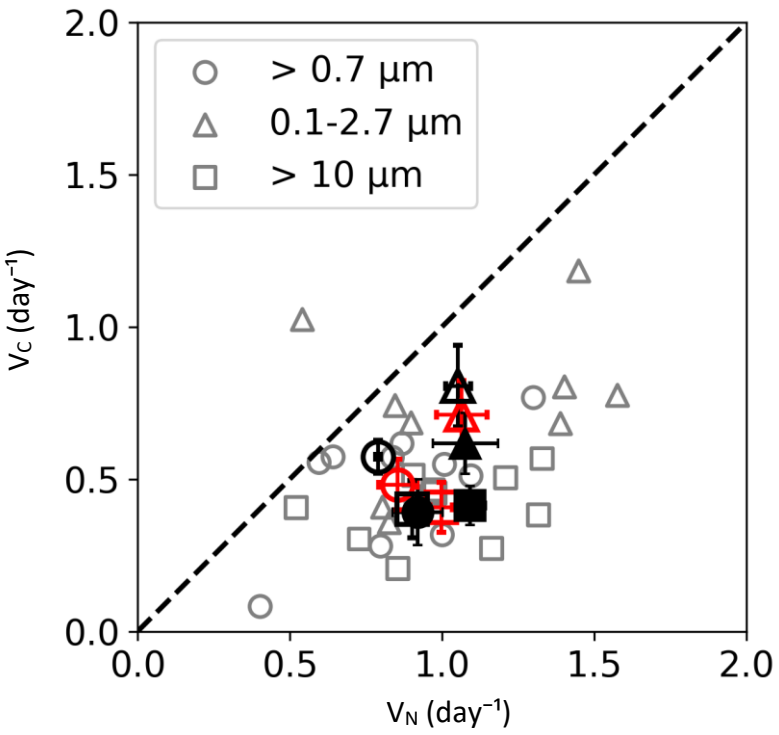

Fig 22. The euphotic zone integrated specific uptake rates of carbon (V_C; day^{-1}) versus the euphotic zone integrated specific uptake rates of total nitrogen ($V_N = V_{NO_3^-} + V_{NH_4^+}$; day^{-1}) for phytoplankton cells > 0.7 µm (circles), 0.7 µm to 2.7 µm (triangles) and > 10 µm (squares). The red symbols show the ten-day average for each size class ± 1 SE (n = 10), while the black filled in symbols show the active upwelling stage average for each size class ± 1 SE (n = 5) and the open black symbols represent the relaxations stage average for each size class ± 1 SE (n = 5). The dashed black line represents a 1:1 relationship, which is expected if NPP and N uptake are coupled.

One possible explanation for the apparent excess N uptake is heterotrophic bacteria assimilating inorganic N without fixing C, which they have been observed to do so at significant rates in some marine environments, particularly during phytoplankton blooms (Kirchman et al., 1991; 1994; Allen et

al., 2002; Bradley et al., 2010; Bronk et al., 1998). Heterotrophic bacteria also typically have a biomass C:N ratio that is lower than that of Redfieldian biomass, on the order of 5:1 (Kirchman et al., 1994). Thus, if heterotrophic bacteria constituted a significant fraction of the total biomass in the present study, they might have been able to lower its C:N ratio (see below) and decouple V_C and V_N. However, a decoupling of carbon fixation and N uptake is observed in all the biomass size classes, not just the smallest size class that would contain the heterotrophic bacteria. While it is possible, and indeed probable, that some heterotrophic bacteria were attached to the larger particles (Iriberri et al., 1987), their contribution to the medium and large phytoplankton biomass is unlikely to have been significant given their small size and associated small volume. Thus, heterotrophic bacteria assimilating inorganic N is unlikely to explain the observed decoupling of carbon fixation and N uptake. Nonetheless, the possible contribution of heterotrophic bacteria to the biomass and N uptake rates of total assemblage is investigated using as ecological model in section 4.4 below.

A decoupling of carbon fixation and N uptake is more likely due to diatoms engaging in luxury NO_3^- uptake. Under nutrient-replete conditions, phytoplankton have been observed to store NO_3^- intracellularly and assimilate it later when ambient nutrients are depleted. For example, a study conducted by Demanche et al. (1979) wherein a batch culture of diatoms was starved of nutrients for 24 hours then resupplied with NO_3^- and NH_4^+ showed initially high NO_3^- uptake rates and the incorporation of NO_3^- into an intracellular pool. When the ambient NO_3^- pool was depleted, the concentration of the intracellular NO_3^- pool decreased. Luxury NO_3^- uptake has also been observed in the environment in response to a pulsed supply of nutrients (Garside, 1981; Glover et al., 2007), and seems to be a strategy characteristic of phytoplankton that periodically experience nutrient limitation. Sommer (1984) describes phytoplankton communities that utilise nutrient pulses for luxury consumption as “storage specialists”. Storage specialists typically have a high maximum uptake velocity (V_{max}) and lower maximum growth rate. This competitive strategy enables them to survive periods of reduced nutrient supply (Sommer, 1984).

Further support for the hypothesis that phytoplankton were engaging in luxury NO_3^- uptake is the biomass C:N ratio of each phytoplankton size class (Fig. 23). At the beginning of the experiment, medium-sized phytoplankton had a C:N ratio very similar to that of typical marine biomass (i.e., Redfieldian biomass; C:N = 6.63:1). During the active upwelling period, their C:N ratio decreased to ~4.3:1, then returned to an approximately Redfield ratio during the relaxation period, with some variability. The low C:N ratio of the medium phytoplankton during active upwelling suggests that they took up NO_3^- in excess of the stoichiometric quantity required to support the observed rate of NPP, which is consistent with luxury NO_3^- uptake. The observed changes in the C:N ratio of medium phytoplankton speaks to their ability to respond rapidly to the introduction of new nutrients. However, luxury NO_3^- uptake alone is not the only factor contributing to the success of medium cells, because large cells are also clearly capable of this strategy (Fig. 22). Rather it is the combination of their ability to store excess NO_3^- along with the other benefits that their size affords them with regards to resource acquisition and suspension compared to larger cells (Section 4.3.1). By extension, even though large cells can store excess NO_3^-, the other disadvantages associated with their size (section 4.3.1) prevent them from dominating in SHB. Kudela and Dugdale (2000) measured a similar rapid decline in the C:N ratio of phytoplankton biomass in an enclosure experiment conducted in Monterey Bay, which they attributed to luxury NO_3^- uptake. The lowest C:N ratios were achieved in the enclosures treated with the highest concentrations of NO_3^-. In the present study, the subsequent increase in the medium phytoplankton C:N ratio above that of Redfield during the relaxation stage is likely due to surface NO_3^- becoming limiting, a condition that Wetz and Wheeler (2003) suggest may eventually lead to excess C fixation.

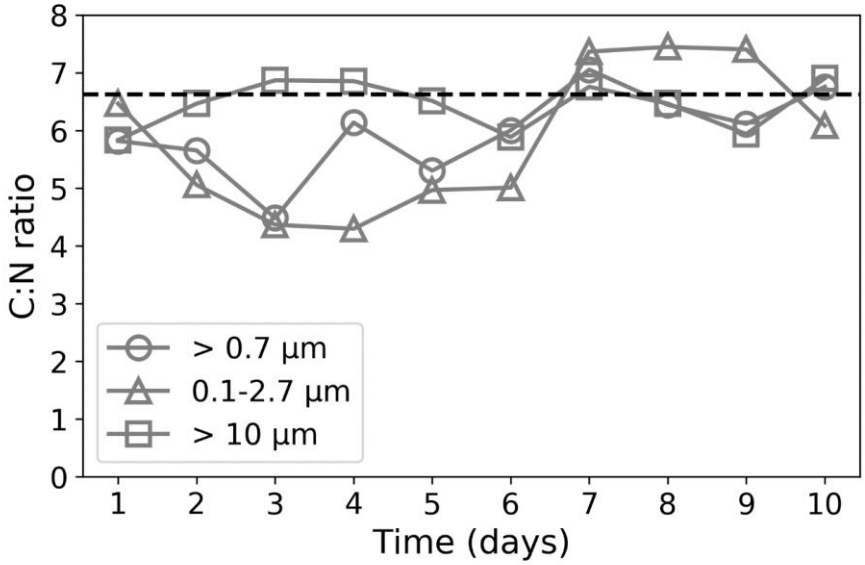

Fig 23. The euphotic zone integrated biomass carbon to nitrogen (C:N) ratio for the phytoplankton cells >0.7 µm (circles), 0.7 µm to 2.7 µm (triangles) and > 10 µm (squares) over the course of the experiment. The dashed black line shows the Redfield ratio.

While the large phytoplankton fall below the 1:1 line in a plot of V_N vs. V_C (Fig. 22), their biomass C:N ratio varied little over the course of the experiment, remaining similar to the Redfield ratio throughout the study. In other words, while large cells appear to be engaging in luxury NO_3^- uptake, this is not reflected in their biomass C:N stoichiometry. While the exact mechanism behind this remains uncertain, one possibility is that the largest size fraction contains a non-trivial quantity of relatively carbon-rich non-autotrophic material like detritus. Detritus would act to raise the combined biomass C:N ratio well above Redfield, such that when averaged with the low C:N ratio of newly synthesized biomass built by large phytoplankton cells engaging in luxury NO_3^- uptake, a ratio similar to that of Redfield could result. Since detritus contains no photosynthesising component, the ratio of V_C to V_N would be unaffected (Dugdale & Wilkerson, 1986; Legendre & Gosselin, 1996).

In contrast to our results, two studies conducted in Monterey Bay report C:N ratios much higher than Redfield at the start of their enclosure/mesocosm experiments (Kudela & Dugdale, 2000; Fawcett & Ward, 2011), although they too gradually converge on the Redfield ratio as the experiments progress. The C:N ratios observed in the present study suggest that given enough time, the elemental composition of phytoplankton biomass will eventually return to that of Redfield after an upwelling event. It may even exceed Redfield due to excess C fixation, which can occur if the water column remains stratified for long enough that nutrients are completely consumed and nutrient limitation sets in (Wetz & Wheeler, 2003).

4.3.3 Species abundance and diversity

While size is a good indicator of phytoplankton function (Marañón et al., 2009), it is not perfect. Community composition tells us a lot more about potential ecological niche. The medium size class may represent many different phytoplankton groups, whose relative and absolute abundances, in terms of numbers and biomass, can vary over time and space (Pitcher et al., 1991). According to Pitcher et al. (1991), short term variations in phytoplankton community composition in response to environmental factors is still relatively unresolved in SHB.

For this study, the relative abundances of different phytoplankton species were enumerated via light microscopy for samples collected on each day of the experiment at the surface and 10 m (Fig. 24). The phytoplankton community comprised mainly *Chaetoceros* spp. and *Skeletonema costatum* at both depths throughout the experiment. Given that these diatoms occupy a large size range (2-80 µm; The phytoplankton encyclopaedia project (2012)), it is possible (and indeed, likely) that the 2.7 µm to 10 µm size class was composed primarily of these species. In addition to the advantages afforded by their size (see section 4.3.1 above), the success of these diatom species in SHB may be related to the fact that both have resting stages (Mcquoid & Hobson, 1996). *Chaetoceros* spp produce resting spores and *Skeletonema costatum* produce specialised resting cells (Mcquoid & Hobson, 1996). This adaptation has been hypothesized to provide a selective advantage during seeding in highly variable upwelling systems, increasing the chances of the resting spore or cell-producing species proliferating when conditions become favourable for growth (Pitcher 1990). Initially, the seed stock is only able to perform physiological processes (e.g., growth and nutrient uptake) at slow rates. However, as the winds relax and stratification sets in, the rates increase in response to higher light and nutrient conditions. This increase in the rate at which physiological processes can be performed is termed "shift up" (Wilkerson & Dugdale, 1987) and is thought to aid biomass accumulation of seed stock species.

Additionally, *Chaetoceros* spp. and *Skeletonema costatum* are both known to form chains. This means that these species likely benefit from the advantages of being smaller in size (e.g., they have a high affinity for nutrients and are more efficient at absorbing light; see section 4.3.1) and, when aggregated into chains, from the advantages of being large (e.g., grazer avoidance). Their ability to form chains is thus another possible reason for the success of *Chaetoceros* spp. and *Skeletonema costatum* in SHB. As the experiment progressed, the phytoplankton community in the surface and at depth became more diverse, with more phytoplankton species observed during the relaxation period than the active upwelling period (Fig. 24). This observation is consistent with the findings of Pitcher (1988), who investigated how phytoplankton community composition and distribution in SHB changes in response to upwelling events, and observed an increase in species diversity as upwelled water began to age. This has been reported for other upwelling systems too. For example, Garrison (1979) observed a significant increase in phytoplankton diversity in Monterey Bay following upwelling as the water column began to resemble more oceanic conditions (as opposed to upwelling conditions).

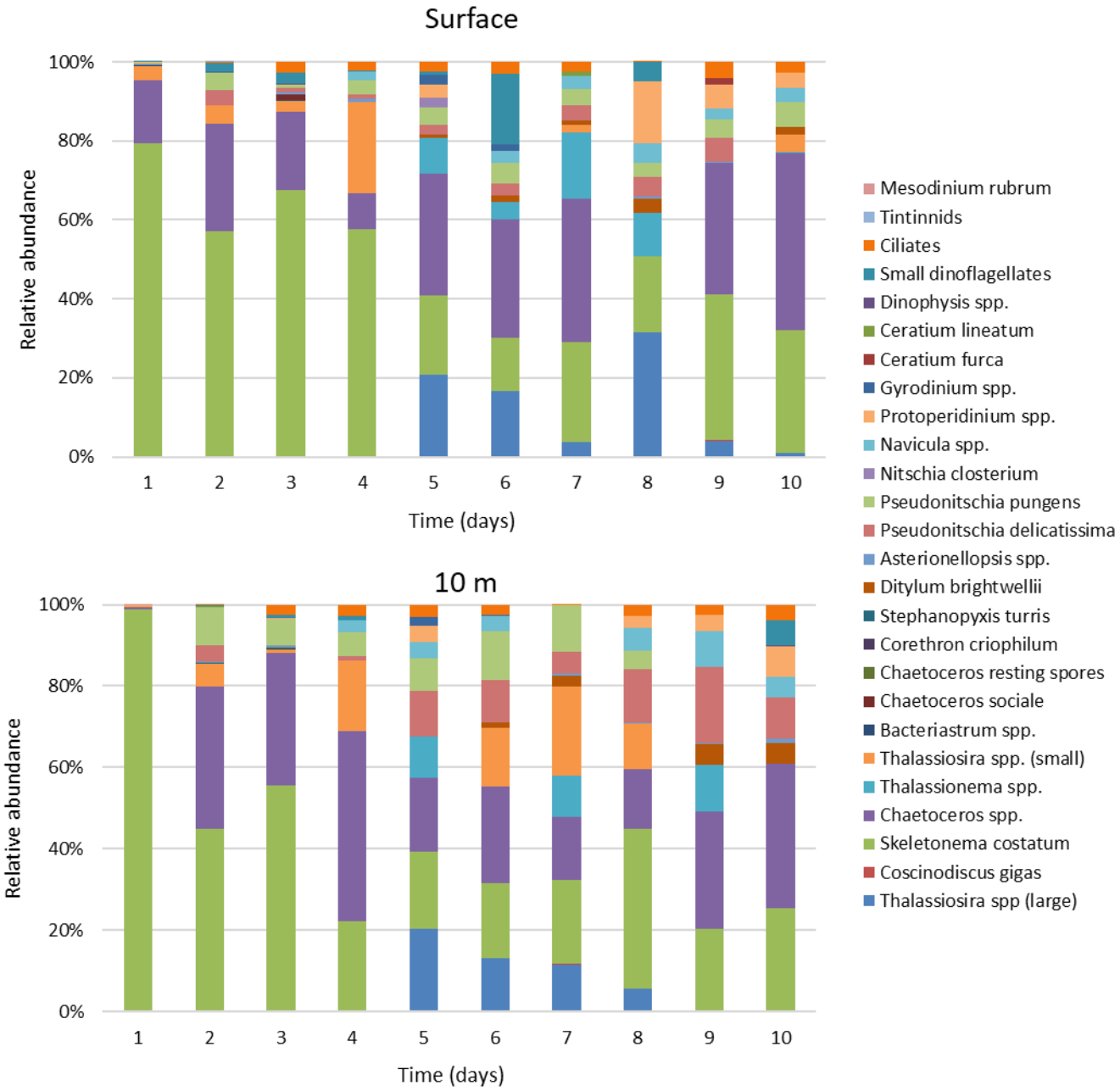

Fig 24. The relative cellular abundance of all phytoplankton species identified in St Helena Bay via light microscopy at the surface (top panel) and at 10 m (bottom panel) over the course of the experiment.

Of particular interest is the large centric diatoms that appeared on day 5 at the surface and 10 m, and persisted for the duration of the relaxation period (Fig. 25). This group consisted of large *Thalassiosira* spp. (40-80 µm) as well as *Coscinodiscus gigas* (100-300 µm). In addition, the relaxation period was characterised by an increased abundance of dinoflagellate cells (Fig. 25).

While the absolute abundance of *C. gigas* was much lower than that of any other species, their large size suggests that they might play a significant role in carbon and N cycling in SHB. Because the NPP and N uptake experiments were pre-screened using a 200 µm mesh, it is possible that large *C. gigas* cells were not quantitatively sampled. As a result, their relative contribution to phytoplankton biomass and nutrient uptake over the course of the experiment is unknown.

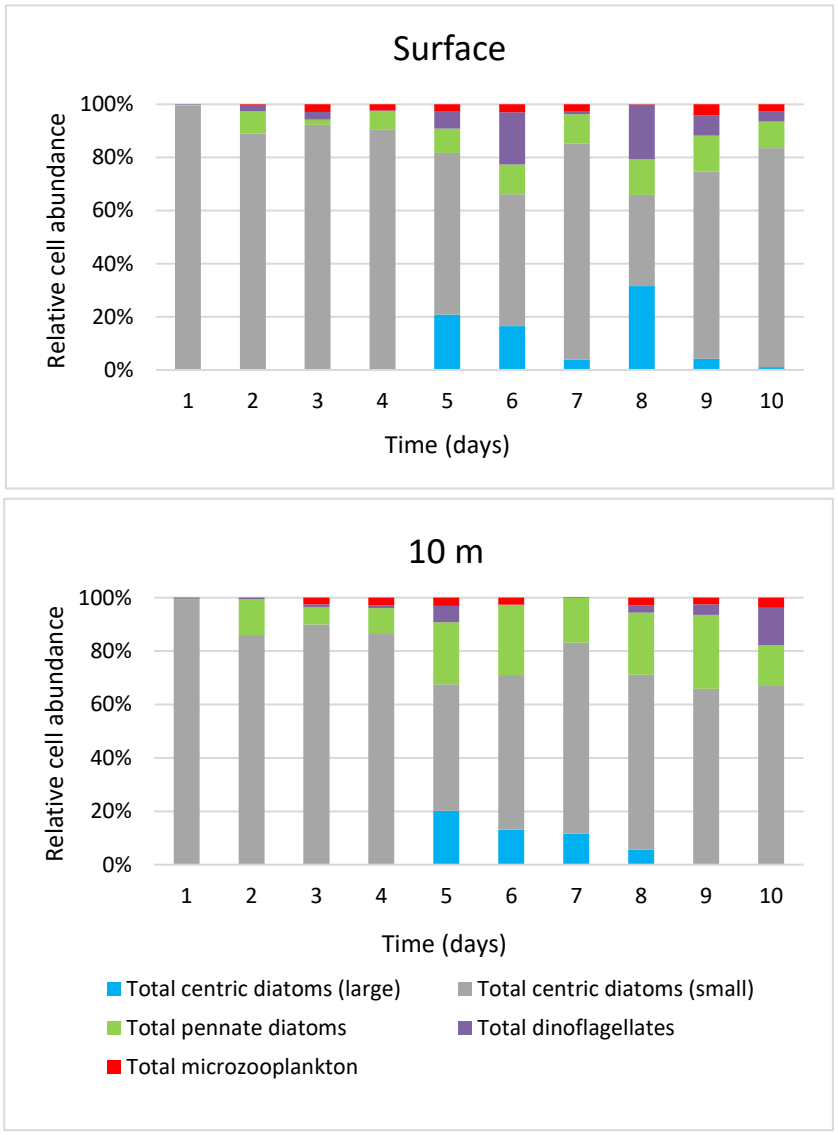

Fig 25. The relative cellular abundance of the main phytoplankton groups identified in St Helena Bay via light microscopy at the surface (top panel) and at 10 m (bottom panel) over the course of the experiment. "Total centric diatoms (large)" includes only the large *Thalassiosira* spp. and *Coscinodiscus gigas.*

During the previous anchor station study conducted in SHB, a *C. gigas* bloom was also observed, although it was far more extensive than that detected in the present study. Extremely high chl-a concentrations were attained, resulting in a pronounced subsurface chl-a maximum layer (CML) that developed quickly after surface waters became nutrient-deplete (Mitchell-Innes & Walker, 1991). This was attributed to a population of *C. gigas* that was initially located in surface waters where it consumed nutrients, but then rapidly sank (Steele & Yentsch, 1960; Smayda, 1970), resulting in the accumulation of biomass deeper in the water column. Within the subsurface CML, rates of primary production were high, and it was estimated that *C. gigas* contributed as much as 67% to 90% of the total water column integrated carbon production (Mitchell-Innes & Walker, 1991). The *C. gigas* bloom was observed at 11 m and 20 m for several days, before finally sinking out of the water column. In the present study, samples for phytoplankton analysis were only collected at 0 m and at 10 m; therefore, if *C. gigas* cells occurred below this depth, they would not have been observed. In section 4.4 below, an attempt is made to use an ecological nutrient phytoplankton model to explore how the addition of a large diatom size class representative of *C. gigas* might have influenced the phytoplankton dynamics and carbon and nutrient cycling in SHB. If a *C. gigas* bloom did occur at the sampling site, it is likely to

have been very short lived given the sinking rate of such large cells (>8 m day^{-1} for live cells; Miklasz & Denny, 2010) and the fact that the bottom depth was only ~30 m, compared to the ~50 m bottom depth of the previous anchor station site.

During the earlier SHB anchor station study, phytoplankton community composition and cell size varied from one upwelling event to the next, and also within a single upwelling event (Pitcher et al. 1991). After the first recorded upwelling event, Pitcher et al. (1991) observed a number of small diatom species belonging to the genera *Minidiscus, Thalassiosira and Nitzschia*, the latter two of which were also observed in the present study. These smaller diatoms were succeeded by larger diatoms like the *Chaetoceros* spp., that were also observed here. Diatom success was attributed to the mixed nature of the water column and the high ambient concentration of DIN (Pitcher et al., 1991). Increasing diatom abundance following NO_3^- input has also been well documented in other upwelling systems, for example in Monterey Bay (Kudela & Dugdale, 2000; Fawcett & Ward, 2011), central Oregon (Wetz and Wheeler 2003), south west Iberia (Domingues et al., 2005), and Lisbon Bay, Portugal (Silva, et al., 2009)

Once upwelling ceased in the earlier study, vertical mixing was reduced and the surface waters warmed. This was followed by a sharp reduction in the ambient DIN concentration, which slowed diatom growth and allowed small flagellate cells to dominate the phytoplankton community (Pitcher et al., 1991). The dominance of diatoms in turbulent waters and flagellate species in stratified waters has been frequently observed in field studies (Smayda, 1980), and Pitcher et al (1991) attribute the increase in flagellate abundance as nutrients decline to the advantage that mobility gives them in the attainment of nutrients. A similar mechanism is likely responsible for the increased appearance of dinoflagellate cells during the relaxation period of the present study.

In the present study, small diatoms dominate throughout the experiment (Fig. 25), and while large diatoms do appear during the relaxation period, small diatoms persist and are never fully succeeded by larger ones. At 10 m, the large diatoms disappear again by day 9. Hydrographic data suggest that days 9 and 10 constitute the beginning of another upwelling cycle. If this is the case, the relaxation period may not have been extensive enough to allow the large diatoms to succeed the small diatoms completely. Similarly, Mitchell-Innes and Walker (1991) suggest that after the second upwelling event studied during their anchor station experiment, succession did not progress beyond the small diatom stage. This, too, was attributed to the shortened duration of the relaxation period following an upwelling event. The broader implications of such a high degree of water column variability and the duration of the active upwelling versus relaxation period are discussed in section 4.5 below.

5 N_3P_3 Ecological Model

5.1. Introduction

The SBUS is highly productive and is regarded as a potential carbon sink (Siegenthaler & Sarmiento, 1993; Gregor & Monteiro 2013), whereby atmospheric CO_2 is exported into the deep ocean after being fixed as organic carbon biomass by phytoplankton in the euphotic zone. Carbon and nitrogen cycling are therefore of great interest in this region. Furthermore, SBUS productivity is governed largely by a high degree of sub-seasonal scale variability (Touratier et al., 2003). For example, it is well established that the SBUS experiences pulsed upwelling cycles in summer that typically last three to ten days (Chapman & Shannon, 1985). Productivity is not only driven by the intensity and duration of active upwelling, but also by the length of the relaxation phase that separates two successive upwelling events (Touratier et al., 2003). According to Pitcher et al. (1992), phytoplankton dynamics are driven largely by chemical and biological processes during water column stabilisation, and the evolution of phytoplankton after upwelling has been widely studied using sized-based ecosystem models (Moloney, 1992; Moloney & Field, 1991; Moloney et al., 1991).

Following the SHB anchor station experiment performed in 1987, Cochrane et al. (1991) constructed a 1D ecosystem model using observations, synthesizing the study's results. This was done in an attempt to highlight important processes and disclose potential gaps in their understanding of ecosystem function. In general, their model was able to simulate the major trends in biomass, although large discrepancies occurred between observations and model results.

Touratier et al. (2003) set out to improve the phytoplankton model for the anchor station study using the recommendations made by Cochrane et al. (1991). Their model resolved all the state variables vertically, and solar radiation was allowed to vary from day to day. In addition, Touratier et al. (2003) did not attempt to simulate the active upwelling phase. As proposed by Cochrane et al. (1991), Touratier et al. (2003) also tried to improve the parameterization of phytoplankton processes like diatom sinking rates. They also set out to determine the ultimate fate of POC during the bloom event captured by the anchor station study, the magnitude of the nutrient supply from the sediments and whether heterotrophy had an important role to play.

In the model constructed by Touratier et al. (2003), most variables were well resolved, such that similar magnitudes, spatial and temporal distributions were achieved in comparison to observations. However, certain aspects such as the patchy phytoplankton distribution and high ammonium concentrations could not be resolved. In addition, NO_3^- uptake and phytoplankton sinking were slightly overestimated. The authors suggested that, even though the model results were good, there remains a lack of estimates for many stocks and flows in the SBUS that are crucial to our ability to resolve major processes and improve our understanding of the system as a whole. Examples include estimates of the concentration of detritus and dissolved organic matter in the water column, processes like phytoplankton mortality and exudation, bacterial grazing, mortality and nitrogen uptake, as well as the decomposition of detritus. This speaks to the necessity of further investigation of the SBUS and highlights the importance of conducting high resolution field studies to provide actual measurements of phytoplankton dynamics so that models can be constrained with observations.

Not only have models enabled us to simulate the response of phytoplankton to upwelling in SHB, but they have also provided insight on the functioning of the ecosystem. For example, model results highlighted the importance of the sedimentary supply of nutrients to the surface in SHB, as suggested by the literature (Bailey & Chapman, 1991). Touratier et al. (2003) showed that roughly two thirds of the NO_3^- assimilated by phytoplankton during the 1987 anchor station study originated from the

sediments as ammonium that was subsequently nitrified in the water column. Furthermore, Touratier et al. (2003) confirmed the high degree of organic matter recycling that occurs during the relaxation phase (Hutchings & Field, 1997), as most fixed carbon was found to be lost through exudation and mortality.

In the present study, a ten-day anchor station experiment was performed in SHB during the upwelling season to improve our understanding of phytoplankton dynamics in the region. The main goal was to determine the drivers of short-term temporal variability in phytoplankton production by characterising the biogeochemistry, productivity and phytoplankton community in SHB over an upwelling cycle. Following the ten-day anchor station study, observational data raised two questions regarding the importance of 1) large diatoms cells and 2) heterotrophic bacteria to the biomass and growth rate of the total assemblage.

In the following section, these questions are investigated through the application of a nutrient-phytoplankton-zooplankton (NPZ) model. NPZ models are ecological models that simulate lower trophic level processes in the euphotic zone. They typically include one or more limiting nutrients, primary producers and grazers (Batchelder et al., 2002). They are designed to evaluate the flow of nutrients between various compartments and have previously been successfully applied to the broader SBUS (Moloney & Field, 1991). More specifically, the present study makes use of a N_3P_3 ecological model whereby three forms of nitrogen and three phytoplankton size classes are simulated, but no zooplankton. Where possible the model was initialised using observations, and mortality rates for each phytoplankton size class were estimated by qualitatively matching the model to data obtained from the field.

5.2. Methods

The model developed for this study is an N_3P_3 ecological model adapted from Evans and Parslow (1985). There are three forms of nitrogen, namely nitrate (NO_3^-), nitrite (NO_2^-) and ammonium (NH_4^+), as well as three phytoplankton size classes, namely picophytoplankton (P_1), nanophytoplankton (P_2) and microphytoplankton (P_3), which range in size from 0 .7 - 2.7 µm, 2.7 - 10 µm and 10 – 200 µm, respectively, consistent with the observational experimental design (section 2). Fig. 26illustrates the main flows of nitrogen between all the state variables of the model. The units of the model are µg N L^{-1} (rather than µmol N L^{-1} as in the observational study). Phytoplankton biomass increases when nutrients are consumed (Fig. 26, Flow 1) and decreases through mortality (Fig. 26, Flow 2) and mixing (Fig. 26, Flow 6) below the base of the mixed layer. Phytoplankton assimilate the bioavailable forms of nitrogen, NO_3^- and NH_4^+. Total nitrogen (Ntotal) is the sum of all bioavailable N species in the model. A proportion of the phytoplankton biomass is remineralized via microbial decomposition after phytoplankton cells die and sink. Remineralization results in a regenerated nitrogen source, which contributes to the total nitrogen pool by increasing the concentration of NH_4^+ (Fig 26, Flow 3). After the stepwise oxidation of NH_4^+ to NO_2^- (Fig 26, Flow 4) and of NO_2^- to NO_3^- (Fig 26, Flow 5), NO_3^- is again available for uptake by phytoplankton. Phytoplankton can also assimilate NH_4^+ before it is oxidised.

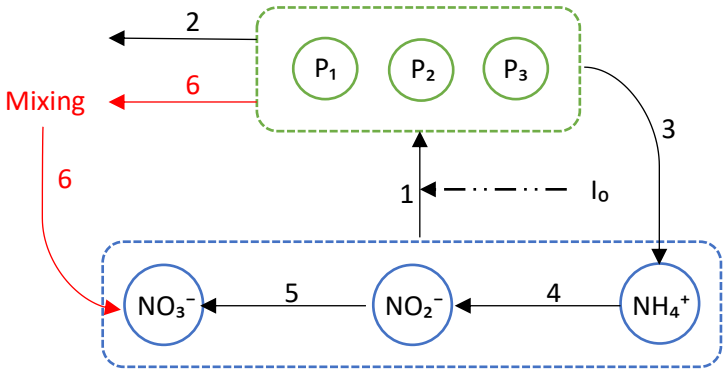

Fig. 26. The major flows of nitrogen into and out of the model compartments, which comprise the state variables. The blue box includes all nitrogen species, the bio-available forms of which (NO_3^- and NH_4^+) constitute total nitrogen (N total). The green box includes all phytoplankton size classes (Ps). Flows are numbered: 1 = nitrogen uptake, 2 = phytoplankton mortality, 3 = nitrogen regeneration, 4 and 5 = oxidation to NO_2^- and NO_3^- and 6 = mixing.

In this model, phytoplankton are considered evenly distributed throughout the mixed layer and absent below the mixed layer. When the base of the mixed layer shallows, phytoplankton are lost and when it deepens, the phytoplankton population is diluted. Below the mixed layer, the nutrient concentration is high and constant (250 µg N L^{-1}). Nutrients can be introduced into the surface mixed layer via mixing. An hourly sequence of mixed layer depths (MLDs) was simulated from an empirical fit to the data as illustrated in Fig. 27. When the MLD at a particular time step is greater than that of the previous time step, mixing is increased. The effect of mixing on the state variables is illustrated by the red arrows in Fig. 26 (Flow 6).

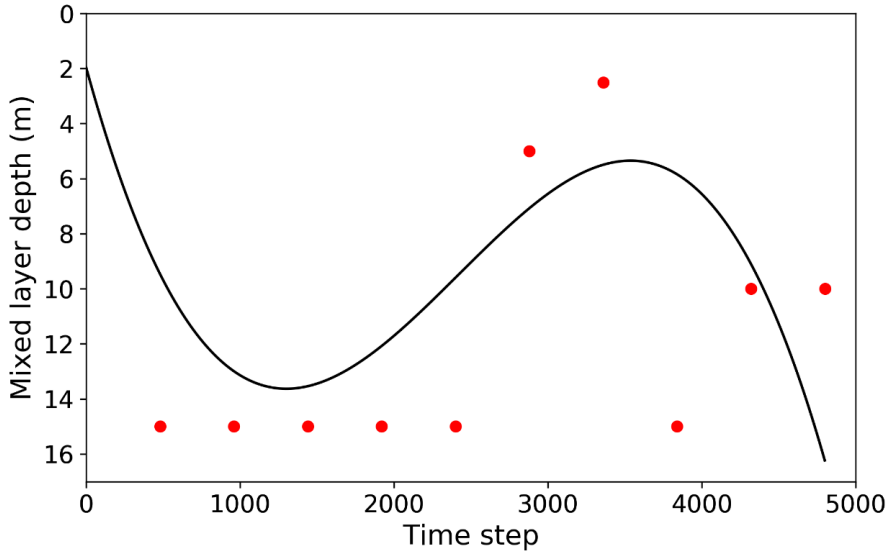

Fig 27. Illustration of the mixed layer depth for every time step in the model, simulated using an empirical fit to the in situ mixed layer depths determined according to de Boyer Montégut et al. (2004) from the CTD data of the ten-day anchor station study. Red dots indicate the in situ mixed layer depth. equation: $y = 1.185*10^{-5}x^3 - 0.0043x^2 + 0.409x + 1.9591$

Phytoplankton growth also depends on light in the model (Fig. 28). Incident light (I_o) is simulated using a normal curve to allow for diurnal variation. For each model day, the equation for incident light is given by:

$$I_o(t) = PARmax * (1/(((2\pi)^{0,5}) * PARsd)) * \exp(-1 * ((hour-PARmean)^2)/(2 * (PARsd^2)))$$

where PARmax is the maximum daytime PAR, PARmean is the mean time of day at which peak PAR occurs and PARsd is the standard deviation of the time of day at which peak PAR occurs. Hour refers to each consecutive timestep at which I_o is calculated. The values of these parameters are given in Table 3.

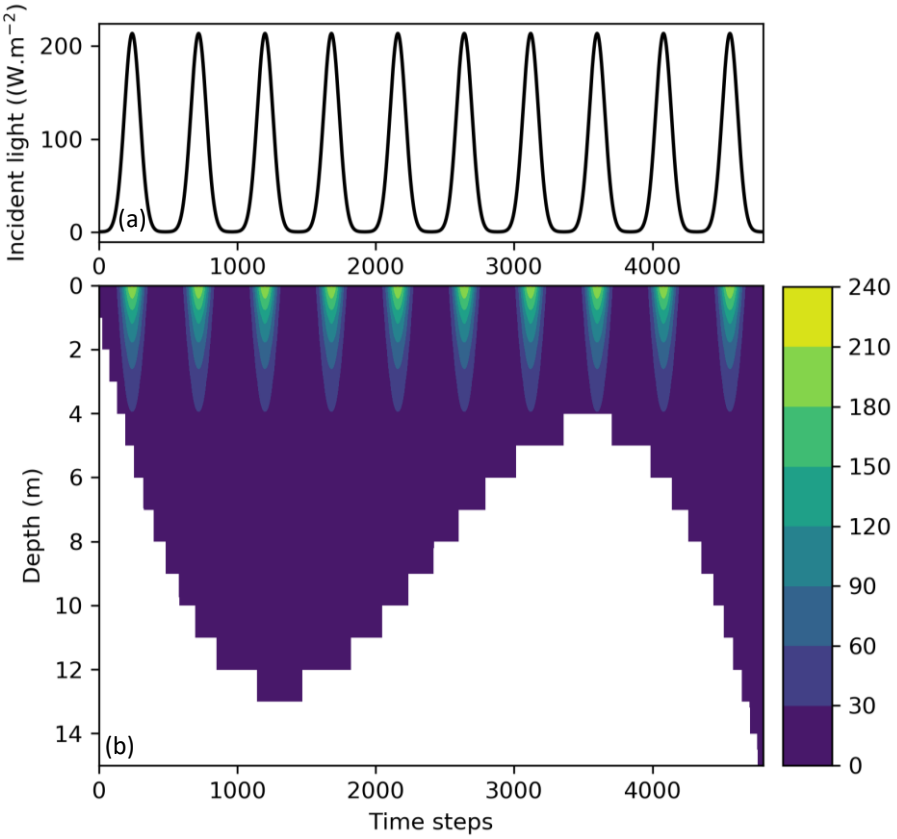

Fig 28. Illustration of (a) the incident light at the surface simulated for every time step and (b) the light environment over depth simulated for every time step in the model.

Light decreases exponentially from the surface to the base of the euphotic zone. The Denman and Pena (1999) function for phytoplankton growth is applied to determine growth based on light and is scaled from 0 to 1 (Miller & Wheeler, 2012). As a result, phytoplankton growth rates can be controlled by nutrients or by light; the slower of the two rates is chosen at each time step, adhering to Liebig's law of the minimum. Production is averaged over the depth of the mixed layer. Changes in the state variables were calculated using the difference equations outlined in Table 2, and the model was programmed using Python, version 3.6 (code available on request).

Table 2: Equations for all state variables in the model. Ntotal is the sum of NO_3^- and NH_4^+, s is the phytoplankton size class (P_1, P_2 and P_3), t is time and Δt is the timestep.

$\mathbf{P(s, t+ \Delta t) = P(s, t) + flow\ 1(t) - flow\ 2(t) - [flow\ 6(t) \times P(s, t)]}$
$\mathbf{NO_3^-(t+ \Delta t) = NO_3^-(t) - \left[\frac{NO_3^-(t)}{Ntotal\ (t)} \times flow\ 1(t)\right] + flow\ 5(t) + [flow\ 6(t) \times [Deep\ N - NO_3^-(t)]]}$
$\mathbf{NO_2^-(t+ \Delta t) = NO_2^-(t) + flow\ 4 - flow\ 5}$
$\mathbf{NH_4^+(t+ \Delta t) = NH_4^+(t) - \left[\frac{NH_4^+(t)}{Ntotal\ (t)} \times flow\ 1(t)\right] + flow\ 3(t) - flow\ 4(t)}$

Table 3: Equations used to describe the processes simulated by the model. The equations are numbered according to the flow to which they are related (Fig. 1). Parameters are in bold, s is phytoplankton size class (P_1, P_2 or P_3), t is time and z is depth. Vmax and Ks are the maximum N uptake rate and half saturation constant for N uptake, respectively, α is the light limitation co-efficient, β is the light extinction co-efficient, M is the mortality rate of phytoplankton, Reg is the proportion of N regenerated from dead phytoplankton, Nit1 is the rate at which NH_4^+ is converted to NO_2^-, Nit2 is the rate at which NO_2^- is converted to NO_3^-, Ω is the diffusion rate and MLDinitial is the MLD at the first timestep.

Related flow	Process	Size-dependent parameters (units)	P_1	P_2	P_3	Size-independent parameters (units)	Values	Source
1	N uptake(s, t) = **Vmax(s)** * min{ N limitation(s, t) and Light limitation(s, t)} * P(s, t)	**Vmax (d^{-1})**	0.8	1.8	0.8			(Marañón et al., 2013)
	N limitation(s, t) = Ntotal(t)/ [**Ks(s)** + Ntotal(t)]	**Ks (μg N L^{-1})**	0.6	4.5	30			(Eppley et al., 1969)
	Light limitation(s, t) = [1 – exp[- **α(s)** * light(t, z)/ **Vmax(s)**]]/depth	**α (h^{-1}/ W. m^{-2})**	0.02	0.02	0.02			Assumed
	light(t, z) = I_o(t) * exp[-1 * **β*** z]					**β (m^{-1})**	0.5	Observed
	I_o(t) = **PARmax** * [1/[[[2π]$^{0.5}$] * **PARsd**]] * exp[-1 * ((hour-**PARmean**]^2]/ [2 * [**PARsd**^{2}]]]					**PARmax (W. m^{-2})**	1500	Assumed
						PARsd (h)	2.8	Assumed
						PARmean (h)	12	Assumed
2	Mortality(s, t) = **M(s)** * P(s, t)^2	**M (h^{-1})**	0.005	0.001	0.0002			Assumed
3	Nregenerated(s, t) = **Reg(s)** * Mortality(s, t)	**Reg**	1	1	1			Assumed
4	Nitrification step 1(t) = **Nit1** * [NH_4^+(t)]^2					**Nit1 (h^{-1})**	0.2	Assumed
5	Nitrification step 2(t) = **Nit2** * [NO_2^-(t)]^2					**Nit2 (h^{-1})**	0.4	Assumed
6	Mixing(t) = [Diffusion(t) + Zeta]/MLD(t)							
	Diffusion(t) = **Ω** * MLD(t)					**Ω (h^{-1})**	0.0025	Assumed
	Zeta = MLD(t) - **MLDinitial**					**MLDinitial (m)**	2	Observed

Table 4 The run time parameters used in the model and initial standing stocks for all state variables.

Run time parameters	Value	Units	Source
Hours per day (nHours)	24		
Number of days (nDays)	10		
Time step (Δt)	0.05	h	
State variables			
P_1 biomass	0.1	µg N L^{-1}	Observations
P_2 biomass	28	µg N L^{-1}	Observations
P_3 biomass	25	µg N L^{-1}	Observations
NO_3^- concentration	227	µg N L^{-1}	Observations
NO_2^- concentration	4	µg N L^{-1}	Observations
NH_4^+ concentration	30	µg N L^{-1}	Observations

For each day of the anchor station study, a number of *in situ* observations were made, including: phytoplankton biomass and growth rates based on N for all three size classes, NO_3^- and NH_4^+ concentrations, and MLD. The model results were used to calculate simulated daily averages of phytoplankton biomass, growth rates and NO_3^- and NH_4^+ concentrations. All *in situ* measurements were made at roughly midday (except for the MLD, which was determined four times each day), such that it is reasonable to assume that observations represented the average state of phytoplankton for that day as opposed to the maximum biomass or growth rate achieved on each day. It is also reasonable to assume that observations represented the average NO_3^- and NH_4^+ concentrations for each day. It should be noted that there are no reliable estimates of picophytoplankton growth rates from the field component of this study, because subtraction of nanophytoplankton and microphytoplankton growth rates from those of the total community resulted in small negative value. However, observed growth rates at fixed depths throughout the water column (Section 3; Fig 14. and Fig. 15) suggest that the contribution of picophytoplankton to the total community growth rates was very small, such that the low modelled growth rates for this size class is justified.

Application of the model: First, a standard model run was performed in order to compare simulated phytoplankton and nutrient dynamics to the observations. Next, an attempt was made to fit the model to the observational data by altering various parameters as outlined in a series of experiments (Table 5). In experiment 1, the mortality rate was changed for each phytoplankton size class and in experiment 2, the nanophytoplankton mortality rate was further increased. The next two experiments varied light: experiment 3.1 simulated increased light for a shorter duration and experiment 3.2 simulated a stepped light environment. In experiment 4, the Vmax parameter was reduced for each phytoplankton size class, and in experiment 5, the mortality rates were altered over time. The model was then used to investigate phytoplankton and nutrient dynamics in SHB, specifically by determining the potential contributions of large diatoms to biomass and N uptake (experiment 6) and the potential impact of heterotrophic bacteria on the biomass and growth rate of the total phytoplankton community (experiment 7).

5.3. Results and discussion

After running the standard model with the initial starting values and parameter values as indicated in Table 5, a pattern emerged in the nutrient and phytoplankton biomass data that was consistent with the model structure, but that did not perfectly match the data. The NO_3^- concentration declined (Fig. 29A) as the biomass of the pico-, nano- and microphytoplankton increased over the ten-day experiment (Fig. 29B). Similar to what was observed in the field, nanophytoplankton achieved the

highest biomass concentrations while picophytoplankton biomass was very low in comparison to that of the nano- and microphytoplankton (Fig. 29B). In contrast to what was observed in the field, concentrations of NH_4^+ and NO_2^- increased over the ten-day experiment (Fig. 29A). The biomass attained by both nano- and microphytoplankton was roughly double what was observed in the field.

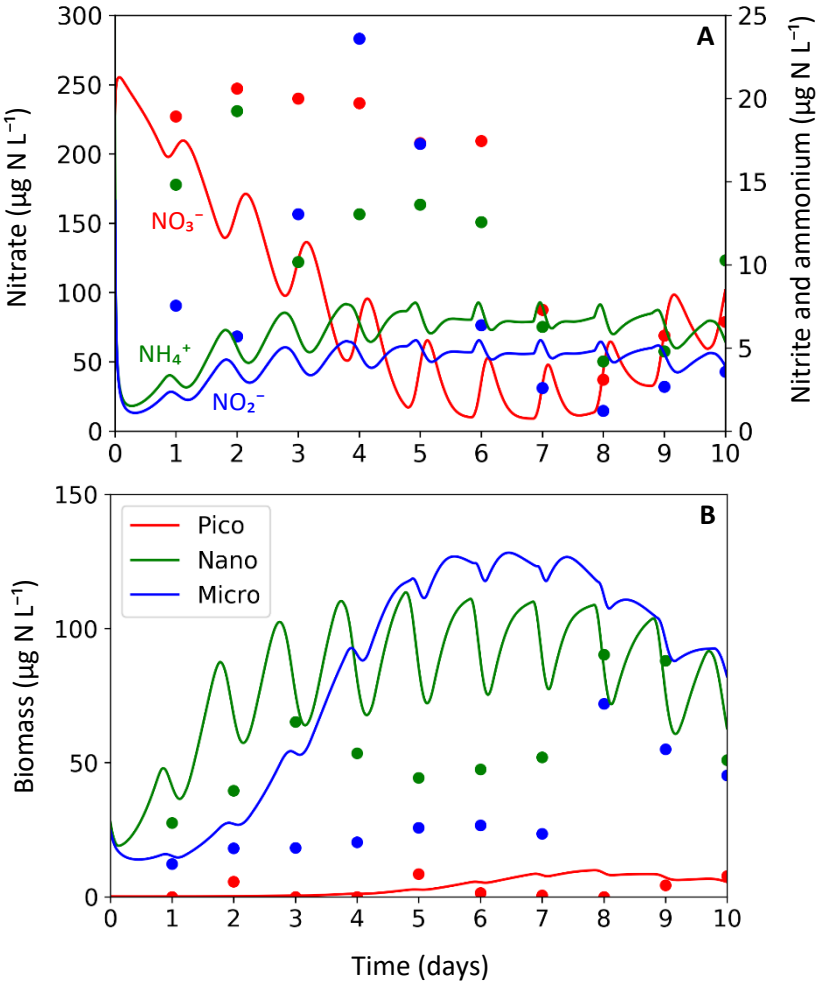

Fig 29. Results from the standard model run showing the N_3P_3 ecological model output for the concentration of all nitrogen species (µg N L^{-1}): nitrate, nitrite and ammonium, the latter two of which are plotted on a secondary y-axis (A), and the biomass of all phytoplankton size classes (µg N L^{-1}): pico-, nano- and microphytoplankton (B) over a ten-day cycle. Lines represent the model output while dots indicate the euphotic zone averages observed *in situ*.

Table 5: Initial and parameter values for each experiment performed using the N_3P_3 ecological model.

	Initial values (µg N L^{-1})	Vmax (day^{-1})	Ks (µg N L^{-1})	Constant mortality rate (hr^{-1})	Time dependent mortality rate (hr^{-1}) for days:		
Standard model					1-2	2-7	7-10
NO_3^-	227						
NO_2^-	4						
NH_4^+	30						
Pico	0.1	0.8	0.6	0.0050			
Nano	28	1.8	4.5	0.0010			
Micro	25	0.8	30	0.0002			
Experiment 1							
Pico	0.1	0.8	0.6	0.0050			
Nano	28	1.8	4.5	**0.0015**			
Micro	25	0.8	30	**0.0006**			
Experiment 2							
Pico	0.1	0.8	0.6	0.0050			
Nano	28	1.8	4.5	**0.0020**			
Micro	25	0.8	30	0.0006			
Experiment 3.1 (light)							
Pico	0.1	0.8	0.6	0.0050			
Nano	28	1.8	4.5	**0.0015**			
Micro	25	0.8	30	**0.0006**			
Experiment 3.2 (light)							
Pico	0.1	0.8	0.6	0.0050			
Nano	28	1.8	4.5	**0.0015**			
Micro	25	0.8	30	**0.0006**			
Experiment 4							
Pico	0.1	**0.70**	0.6	0.0050			
Nano	28	**1.45**	4.5	**0.0015**			
Micro	25	**0.70**	30	**0.0006**			
Experiment 5							
Pico	0.1	0.8	0.6		**0.0050**	**0.0050**	**0.0050**
Nano	28	1.8	4.5		**0.0015**	**0.0020**	**0.0010**
Micro	25	0.8	30		**0.0002**	**0.0017**	**0.0002**
Experiment 6							
Pico	0.1	0.8	0.6		**0.0050**	**0.0050**	**0.0050**
Nano	28	1.8	4.5		**0.0015**	**0.0020**	**0.0010**
Micro	25	0.8	30		**0.0002**	**0.0017**	**0.0002**
C. gigas	**30**	**0.3**	**70**		**0.0002**	**0.0002**	**0.0002**
Experiment 7							
Pico	0.1	0.8	0.6		**0.0050**	**0.0050**	**0.0050**
Nano	28	1.8	4.5		**0.0015**	**0.0020**	**0.0010**
Micro	25	0.8	30		**0.0002**	**0.0017**	**0.0002**
H. bacteria	**0.1**	**0.8**	**0.6**		**0.0050**	**0.0050**	**0.0050**

Experiment 1: Estimating the mortality rate for each phytoplankton size class.

An attempt was made to fit the model to the data by changing the mortality rates of each phytoplankton size class. The mortality rates of both nano- and microphytoplankton were increased to yield the lower biomass observed *in situ* for these two size fractions. The mortality rate for

nanophytoplankton was increased to 0.0015 h^{-1} and the mortality rate for microphytoplankton was increased to 0.0006 h^{-1}, while the mortality rate for the picophytoplankton was maintained at 0.005 h^{-1} (Table 5).

With the slightly elevated mortality rates, the maximum biomass achieved by all phytoplankton size classes was more similar to the observations, while the trend in biomass over time was still poorly captured (Fig. 30B). In addition, the NO_3^-, NO_2^- and NH_4^+ concentrations were all poorly represented. For NO_3^-, observations suggest that concentrations were relatively constant for the first six days of the experiment and decreased rapidly to day 8 before increasing slightly again by day 10. The model however, simulates a gradual decline in NO_3^- concentration to day 8 followed by a gradual increase to day 10. Furthermore, modelled NO_3^- concentrations are never depleted to the same extent that they are in the field.

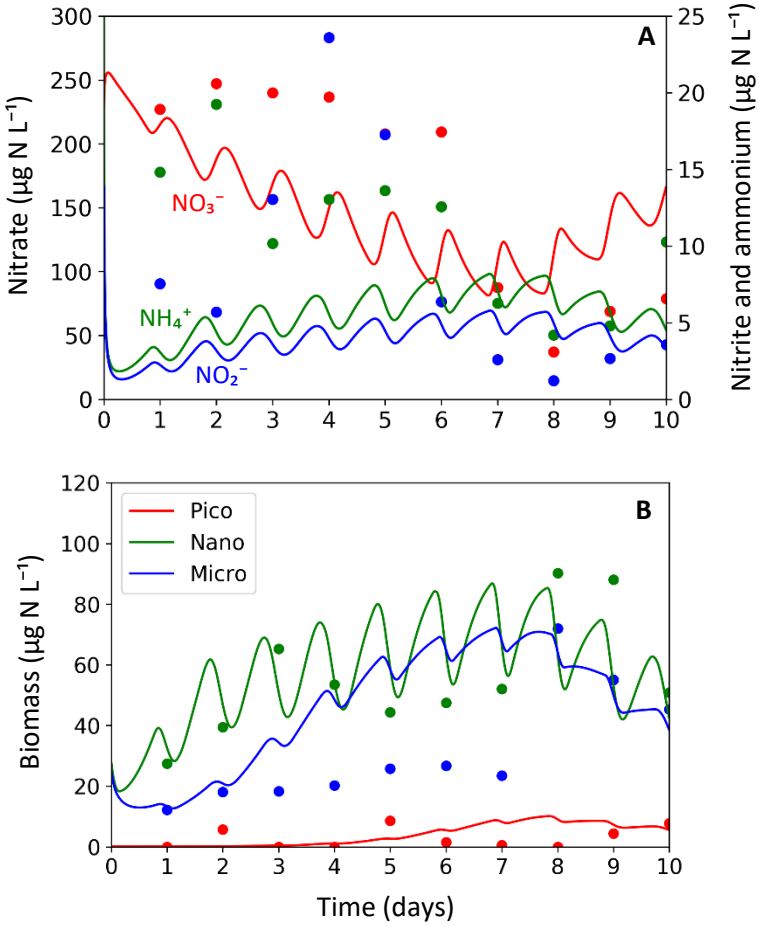

Fig 30. Results of experiment (1) showing the nitrate, nitrite and ammonium concentration (µg N L^{-1}), the latter two of which are plotted on a secondary y-axis (A), and the phytoplankton biomass (µg N L^{-1}) for all three size classes: pico-, nano- and microphytoplankton (B) over the ten-day experiment. Lines represent the model output and dots indicate the euphotic zone averages observed *in situ*.

There is also a large discrepancy between the microphytoplankton biomass simulated by the model and the microphytoplankton biomass observed *in situ* on days 3 to 7. During this time, model-simulated microphytoplankton biomass increases too rapidly compared to observations. In the model, biomass was controlled by the growth and mortality rates of phytoplankton. This suggests that over days 3 to 7, either the mortality rate used for the microphytoplankton size class was too low, or the growth rate was too high. Fig. 31 suggests that the daily average microphytoplankton growth rate estimated by the model corresponds reasonably well with observed growth rates for the size classes

over time (Fig. 31B). However, small discrepancies exist, especially from day 6 onwards. The biggest discrepancy between modelled and observed rates occurred on day 9, when the growth rate was underestimated by 0.05 µg N L^{-1} h^{-1} (30%). The microphytoplankton growth rate was well represented over days 3 to 5, and marginally overestimated from days 6 to 7. This argues against the growth rate as the main cause of the discrepancy between modelled and observed biomass. Therefore, the influence of slightly increasing the mortality rate for microphytoplankton was assessed, as opposed to decreasing the growth rate. This acted to reduce the maximum biomass achieved by microphytoplankton on day 8, without resolving the mismatch between the biomass simulated by the model and the biomass observed in the field over days 3 to 7.

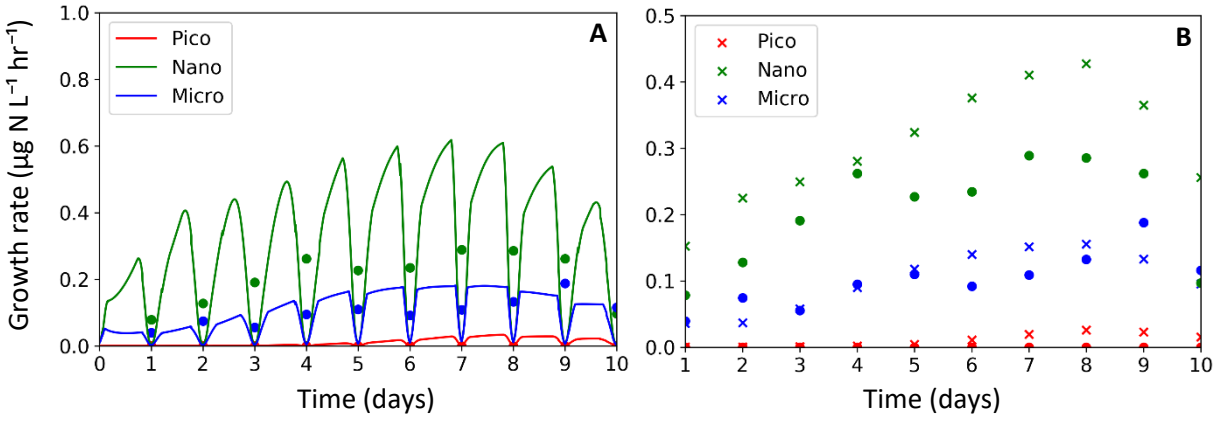

Fig 31. Results of experiment (1) showing the growth rate (µg L^{-1} h^{-1}) for all three phytoplankton size classes: pico-, nano- and microphytoplankton over the course a ten-day experiment. Panel A shows the model output for every time step (lines) and panel B shows the averaged growth rate for each model day (crosses). In both panels, the dots represent the euphotic zone averages observed *in situ*.

Results shown in Fig. 31 also indicate that, while the model was able to resolve the trend in nanophytoplankton growth rate over time (Fig. 31B), it was largely overestimated. The biggest discrepancy between modelled and observed nanophytoplankton growth rates occurred on day 10, when growth was overestimated by 0.16 µg N L^{-1} h^{-1} (> 100%).

In the model, phytoplankton growth rates were controlled by mortality and by light or nutrients such that adjusting mortality rates, light conditions and nutrient uptake parameters could act to reduce the discrepancy in nanophytoplankton and/or microphytoplankton growth rates compared to observations.

Experiment 2: Increasing the nanophytoplankton mortality rate

In a first attempt to better reproduce the observed nanophytoplankton growth rate, the nanophytoplankton mortality rate in the model was slightly increased to 0.002 h^{-1} from 0.0015 h^{-1}. This resulted in a much better representation of the nanophytoplankton growth rate over time (Fig. 32A), such that the largest discrepancy between modelled and observed rates was reduced to an overestimate of 0.09 µg N L^{-1} h^{-1} (93%) on day 10. However, a further consequence of this was a reduction in nanophytoplankton biomass, such that the high biomasses observed on days 8 and 9 were no longer achieved by the model (Fig. 32B).

Therefore, it was decided to explore how changing the light environment might impact phytoplankton growth rates.

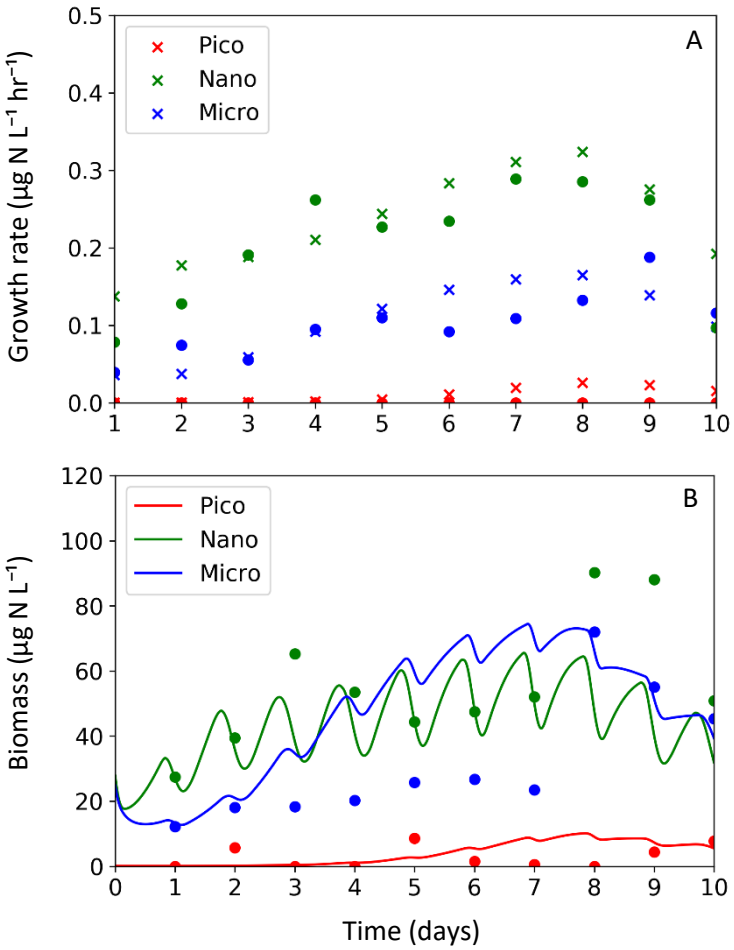

Fig 32. Results of experiment (2) showing the growth rate (µg N L^{-1} h^{-1}) in panel A and the biomass (µg N L^{-1}) in panel B for all three phytoplankton size classes: pico-, nano- and microphytoplankton over the ten-day experiment. Crosses in A represent the average growth rate for each model day, while lines in B represent the simulated biomass at each timestep. In both panels, dots indicate the euphotic zone averages observed *in situ*.

Experiment 3.1: More light for a shorter duration of time

The first experiment involving an alteration of the light field in the model decreased the standard deviation of the time of day at which peak PAR (photosynthetically active radiation) occurred from 2.8 to 2.3 hours. This resulted in a slightly higher incident irradiance experienced by phytoplankton for a shorter duration (Fig. 33E). Decreasing the standard deviation acted to slightly reduce overall nanophytoplankton growth and minimised the largest discrepancy between modelled and observed rates to 0.08 µg N L^{-1} h^{-1} (83%) (Fig. 33A). However, the biggest discrepancy in modelled versus observed rates for the microphytoplankton was almost doubled, such that there was very little improvement overall. Another consequence was a slight reduction in the biomass of both nano- and microphytoplankton, such that the maximum observed biomass was no longer achieved (Fig. 33C).

Experiment 3.2: Stepped light environment

In a second light experiment, the light environment was simulated in such a way that for the first 12 hours of each model day, incident irradiance was 200 W m^{-2}, and for the last 12 hours, incident irradiance was 0 W m^{-2} (Fig. 33F). Introducing a stepped incident light environment, where light is essentially 'on' with a constant irradiance during the day, and 'off' at night, resulted in a reduction of both nano- and microphytoplankton growth rates (Fig. 33B). Indeed, the growth rates for both these

size classes were significantly underestimated for most of the experiment. On the other hand, the biomass of these size classes was reduced such that the first 7 days of the experiment were well represented by the model (Fig. 33D). Again, maximum observed biomass was not achieved.

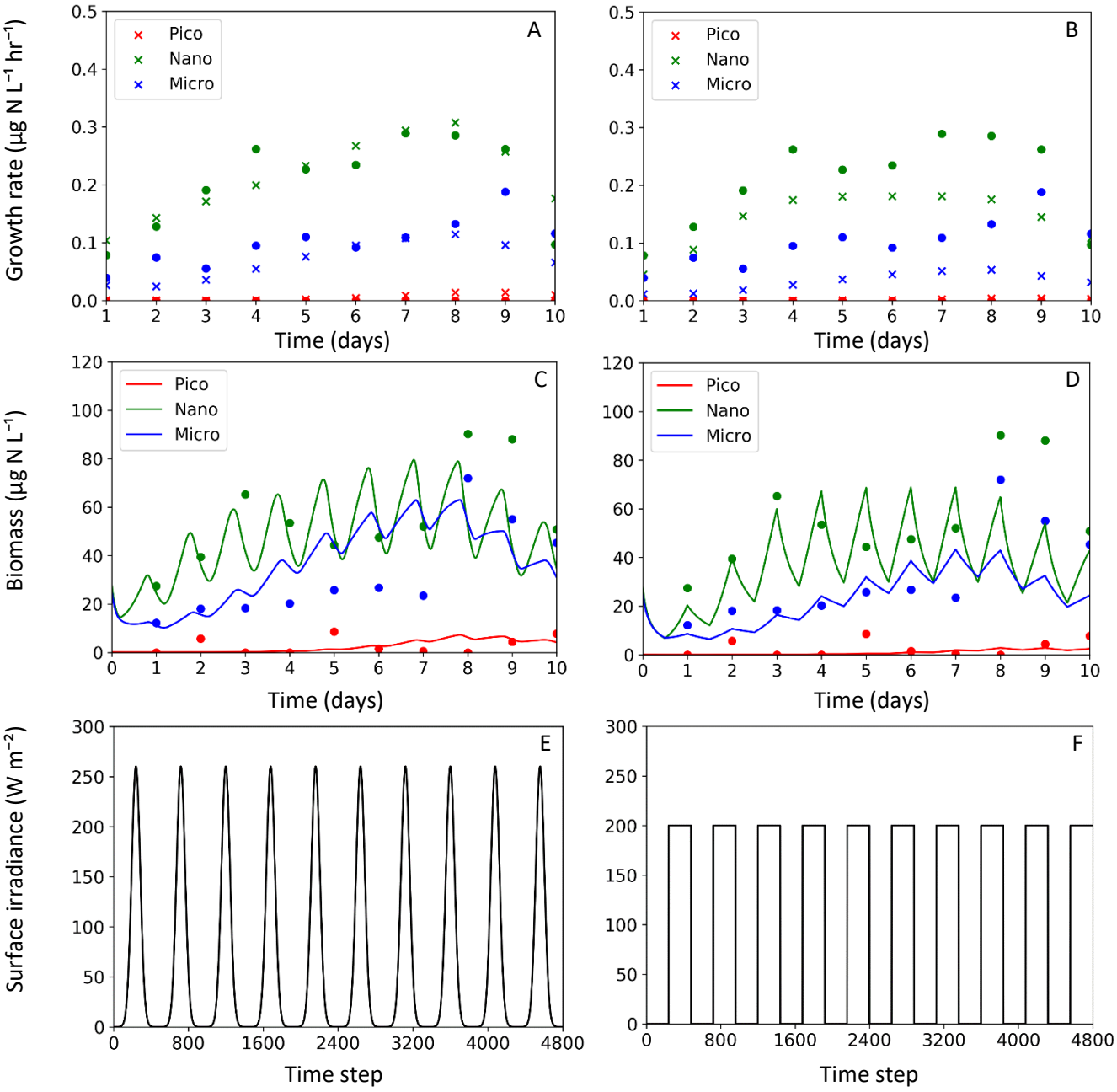

Fig 33. The results of experiments (3.1) and (3.2) showing the growth rate (µg N L^{-1} h^{-1}) in the top row (panels A and B) and the biomass (µg N L^{-1}) in the middle row (panels C and D) for all three phytoplankton size classes: pico-, nano- and microphytoplankton over the ten-day experiment. In both cases, dots indicate the euphotic zone averages observed *in situ* while crosses in panels A and B represent the averaged growth rates for each model day and lines in panels C and D represent the simulated biomass at each timestep. The bottom row (panels E and F) represents the incident light (W m^{-2}) condition experienced by model phytoplankton at each time step. Panels A and C are influenced by the light shown in panel E, while panels B and D are influenced by the light in panel F.

Experiment 4: Reducing the Vmax parameter for each phytoplankton size class

In a final experiment to improve model representation of phytoplankton growth rates, the nutrient uptake parameters were altered. Specifically, the influence of decreasing the maximum specific nitrogen uptake rate (Vmax) for each size class was investigated. Reducing Vmax (Table 5), while still adhering to the unimodal distribution of Vmax versus size described by Marañón et al. (2013), decreased the discrepancy between modelled and observed growth rates over time (Fig. 34A), similar to the experiments that altered the light environment (Fig. 33A). However, the phytoplankton biomass reproduced by the model was still too high duirng the middle of the experiment (days 3 to 7) for microphytoplankton, and too low at the end of the experiment (days 7 to 10) for nanophytoplankton.

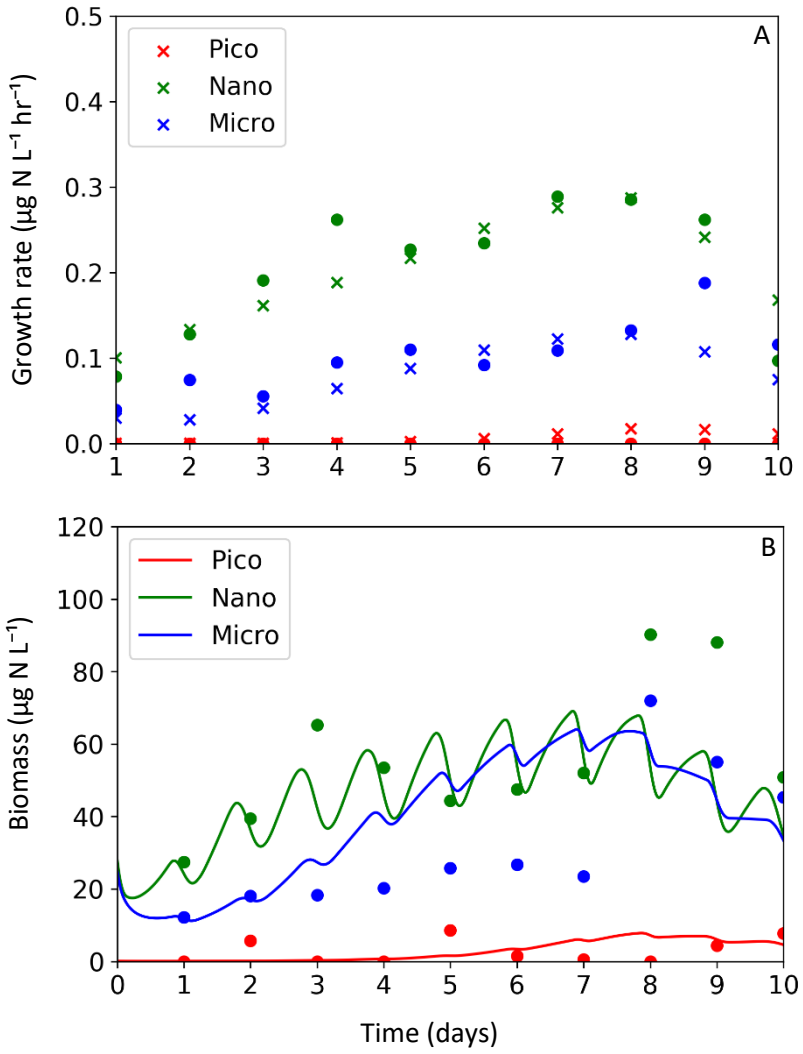

Fig 34. The results of experiment (4) showing the growth rate (µg N L^{-1} h^{-1}) in panel A and the phytoplankton biomass (µg N L^{-1}) in panel B for all three size classes: pico-, nano- and microphytoplankton over the ten-day experiment. Crosses in panel A represent the averaged growth rate for each model day and lines in panel B represent model simulated biomass at every timestep. In both panels, dots indicate the euphotic zone averages observed *in situ*.

The results of the numerical experiments outlined above indicate that, ultimately, to simulate more realistic growth rates using the model and still be able to reproduce the observed trends in biomass, the growth and mortality rates need to be adjusted in unison until the correct balance is achieved.

The phytoplankton biomass observed in the field varied over time (Section 3; Fig. 10), indicating that growth and mortality were not fixed for the duration of the experiment but were changing, likely in response to the hydrographic conditions experienced in the bay. From the hydrographic data, it is possible to differentiate three different sets of conditions ("periods") to which phytoplankton responded, as evidenced by observed changes in biomass over time. The first period was from days 1 to 2, the second period from days 2 to 7 and the last period from days 7 to 10. The first two periods are separated by a localised vertical mixing event and the last two periods are separated by the onset of mixing from below, which characterises the last three days of the experiment, as evidenced by rising isopycnals (Fig. 6).

In light of this, the model was parameterised with a different mortality rate for each period (Table 5), in order to better simulate the trends in phytoplankton biomass. The picophytoplankton mortality rate was kept constant because the biomass of this size class showed little variation over time.

Experiment 5: Altering the mortality rate over time

The mortality rates of nano- and microphytoplankton were increased over the middle of the experiment (days 2 to 7) and reduced at the end of the experiment (days 7 to 10) as outlined in Table 5. When a time varying mortality rate was allowed, the model was able to capture the relatively low and constant biomass that characterised the middle of the experiment, as well as the large increase in biomass over days 7 to 8 and the relatively higher biomass that characterised the end of the experiment (Fig. 35B). This was achieved for both nano- and microphytoplankton (Fig 35B). Additionally, the trend in NO_3^- concentration over time was much better represented by the model (Fig. 35A), although NO_2^- and NH_4^+ concentrations (not shown) remained similar to those produced in the standard model run.

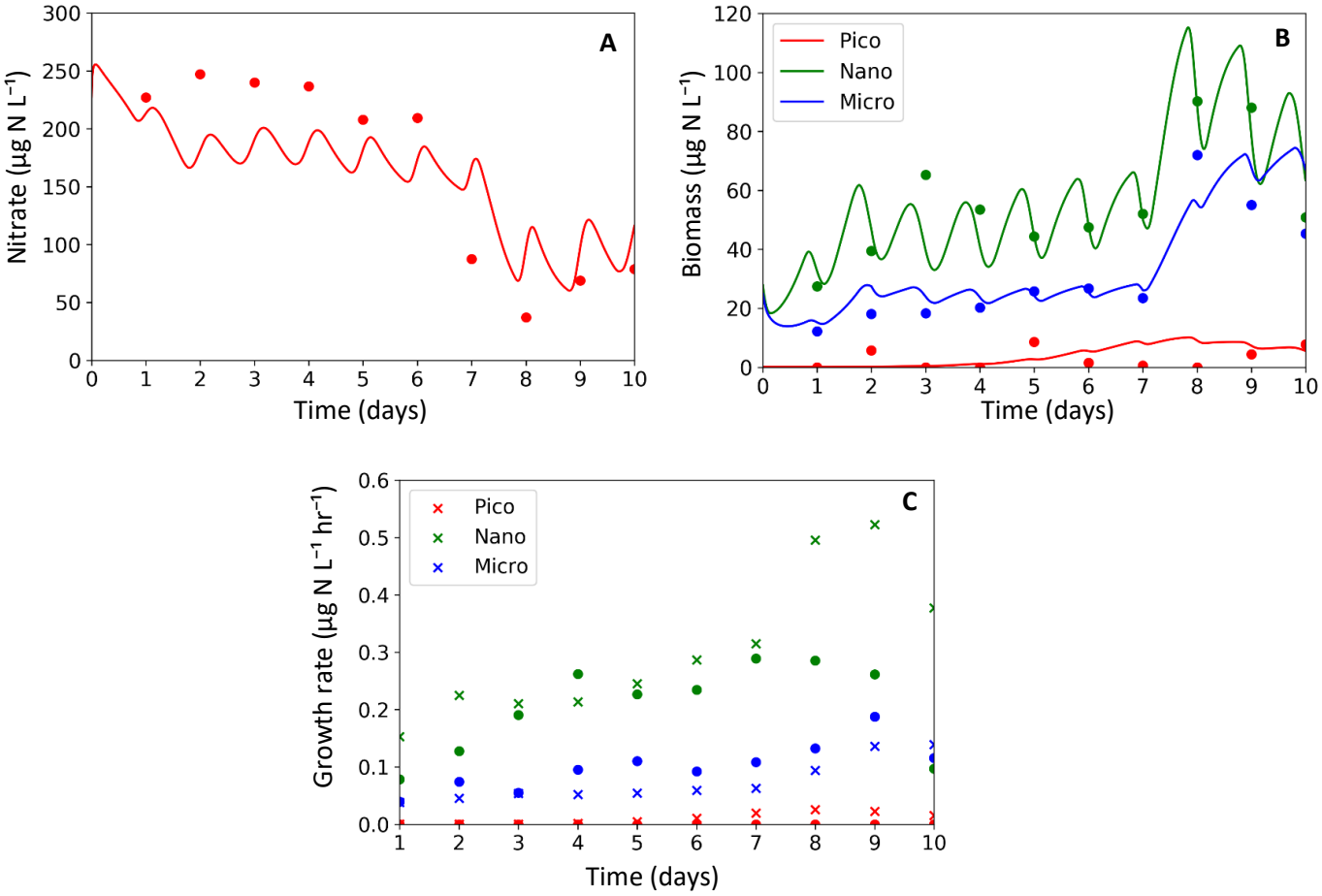

Fig 35. The results of experiment (5) showing the nitrate concentration (µg N L^{-1}) in panel A, the phytoplankton biomass (µg N L^{-1}) in panel B and the growth rate (µg N L^{-1} hr^{-1}) in panel C for all three size classes: pico-, nano- and microphytoplankton over the ten-day experiment. Lines in panels A and B show the model output at each time step, while crosses in panel C represent the average of each model day. In all cases, dots show the euphotic zone averages observed *in situ*.

Adjusting the mortality rates over time is reasonable if zooplankton grazing pressure changed over time, and results in the best model representation of the observed phytoplankton biomass. However, there is little evidence that grazing had a significant role to play in the field experiment. This is because large grazers were actively removed by pre-screening the incubation seawater using a 200 µm mesh, and small grazers (microzooplankton) occurred in low abundance relative to their potential prey (Fig. 25). However, the microzooplankton do respond to periods of high phytoplankton biomass by increasing in number, but without any estimates of zooplankton grazing rates it is difficult to determine whether the low abundance of microzooplankton present could significantly impact the phytoplankton biomass. In this way, the model is not entirely consistent with the observations. One limitation of the lack of complexity in this model is that it assumes all cells are singular and does not account for chain formation. As mentioned in section 4.3.3, chain formation can reduce grazing pressure, which is likely to have been the case in SHB given the high abundances of *Chaetoceros* spp. and *Skeletonema costatum.* That the model is unable to resolve the dynamics of chain forming cells could explain why it suggests that grazing is more important than the field data show. Furthermore, due to the simplicity of the model, mortality encompasses other phytoplankton loss pathways in addition to zooplankton grazing such as cell lysis and sinking, none of which were measured in the

environment. It is therefore possible that a phytoplankton loss process other than grazing did exert a control on biomass accumulation in the environment and that this, rather than grazing, is what the model captured.

In a more complex model developed to understand a similar field experiment from which grazers were removed (Fawcett & Ward 2011), Van Oostende et al. (2015) found that group specific growth rate was critical for appropriately simulating the phytoplankton biomass distribution. In the present study, the group specific growth rate was parameterised using Michaelis-Menten kinetics and the sensitivity of V_{max} parameter was evaluated in model experiment 4. Changing V_{max} had less effect than changing the mortality rate when trying to simulate the observed phytoplankton biomass, which suggests that the control(s) on biomass accumulation in SHB may be different from those in Monterey Bay where the Fawcett & Ward (2011) experiment was conducted. However, the simple model constructed here has not been statistically fitted to the observational data, such that the observations should be considered more correct than the model output. There is clearly room for improving the model, as well as a need for further field-based experimentation. For example, while it was possible to estimate what the mortality rates needed to be in order to reproduce the observed phytoplankton biomass of each size class in the model, zooplankton grazing experiments in the field are really the only way to better understand the role zooplankton play in maintaining size-varying phytoplankton communities. Nonetheless, regardless of the mechanism behind phytoplankton loss, changing the modelled mortality rates over time gave the best representation of biomass. Therefore, even though grazing might not be the primary control on phytoplankton biomass accumulation in the environment, the model set-up depicted in Fig. 35 remains the most appropriate version to use to address two different questions raised by the observational data (experiments 6 and 7; see below).

When the mortality rates were altered in the model, the general trend observed in the phytoplankton growth rates over time was adhered to, but the microphytoplankton growth rates were consistently slightly underestimated and the nanophytoplankton growth rates were severely overestimated, especially during the last three days of the experiment (Fig. 35C). The observational data suggest that SHB is a highly variable system such that there are many important processes not simulated by the model that could very well be responsible for the discrepancies between the model and observations. Examples of processes not resolved by the model that could potentially have important implications for phytoplankton growth rates and biomass are as follows: Firstly, size varying sinking velocities. Due to their size, large cells sink faster than small cells and therefore require turbulence to remain suspended in the euphotic zone (Kiørboe, 1993). Secondly, light limitation, which while parameterised in the model, is also known to be dependent on cell size, with large cells being less adapted than small cells to low light or variable light conditions (Geider, 1987). Thirdly, lateral advection of phytoplankton cells. Water mass circulation in SHB usually favours retention, at least during active upwelling, but cells may have been advected to or from the anchor station site (Margalef, 1978; Malone, 1980). Lastly, the observational data suggest that phytoplankton engaged in luxury NO_3^- uptake, assimilating more N than required according to Redfield stoichiometry. Parameterization of this preferential consumption of NO_3^-, even while there is NH_4^+ available, may improve the model output in future.

It should also be noted that the model experiments above were performed in an attempt to explore the phytoplankton dynamics over a ten-day anchor station study. However, a better statistical fit to the data is required to more accurately estimate parameters like the mortality rate, as well as the times at which these parameters change. Nevertheless, as previously mentioned, the model depicted in Fig. 35 can still be used to probe two questions raised by the observational data.

Experiment 6: the addition of a large diatom size class, *Coscinodiscus gigas* (*C. gigas*).

During a previous anchor station study undertaken in SHB, large diatom cells (*C. gigas*) were present and were responsible for a significant percentage of total phytoplankton biomass and primary production. Light microscopy data from the present study suggest that *C. gigas* was also present, although in very low abundance. These cells range in size from 100 µm to 300 µm (Mitchell-Innes & Walker, 1991), and because samples were pre-screened through a 200 µm mesh to remove grazers, it is possible that many of these large phytoplankton cells were not sampled. For experiment 6, a large diatom size class was added to the model to assess how important *C. gigas* might have been to the biomass and overall growth rate of the total assemblage. The initial standing stock of *C. gigas* was estimated from the abundance data, while the Vmax parameter for *C. radiatus* and *C. wailesii* reported by Marañón et al. (2013) was used as an estimate of Vmax for *C. gigas*. The Ks parameter was taken from Moloney & Field (1991).

Fig. 36 shows that when *C. gigas* is included in the model, there is no change in the overall trend observed in phytoplankton biomass or growth rate. The contribution of *C. gigas* to the biomass of the whole assemblage was greater than its contribution to the total community growth rate. The largest contribution of *C. gigas* to total community phytoplankton biomass occurred on day 1 and was equivalent to 23.2%, while its largest contribution to the total community growth rate, also on day 1, amounted to 5.7%. It thus appears as if not sampling these large diatom cells during the anchor station study may have resulted in an underestimation of the total biomass of the assemblage. However, the relative contribution of *C. gigas* to biomass was on average very similar to that of the picophytoplankton (10-day average ~15%), and as a result may be considered unimportant in comparison to the contributions of both the nano- and microphytoplankton. The contribution of *C. gigas* to the total community growth rate was also similar to that of the picophytoplankton (10-day average ~3%), and can be considered similarly unimportant in comparison to the contribution made by the other two size classes.

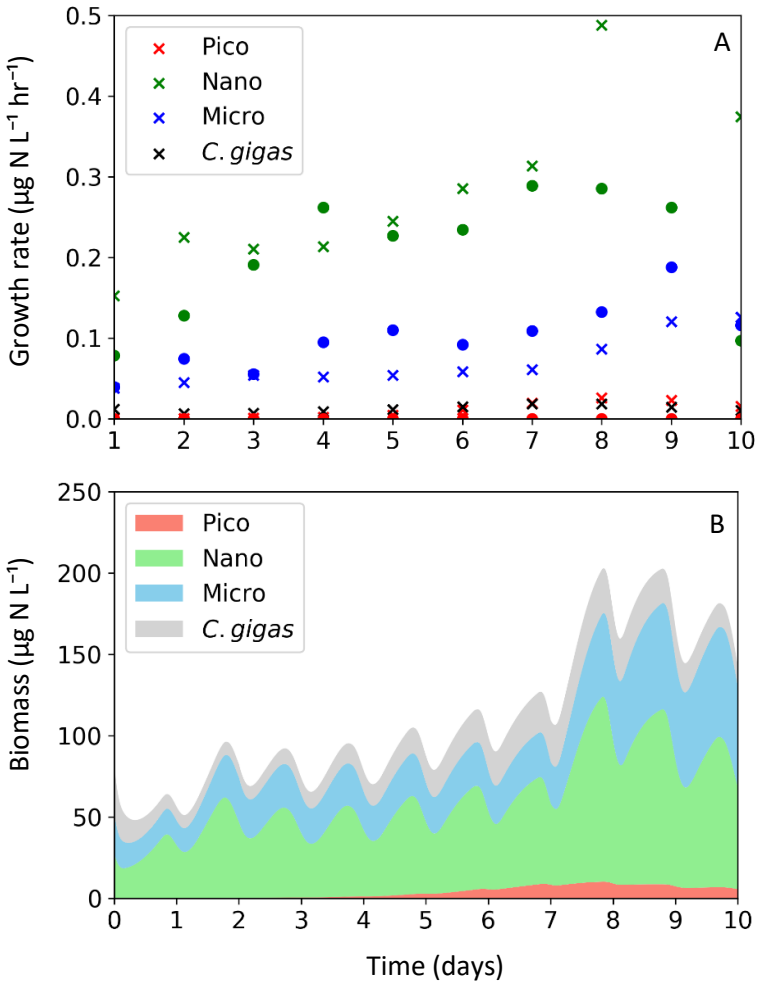

Fig 36. The results of experiment (6) showing the growth rate (µg N L^{-1} hr^{-1}) in panel A and the stacked biomass (µg N L^{-1}) in panel B for each size class: pico-, nano-, and microphytoplankton, with the addition of *C. gigas* black crosses and grey shading). Crosses in panel A represent the average for each model day, while dots indicate the euphotic zone averages observed *in situ*. For this experiment, the model was run in the configuration leading to the outputs shown in Fig. 9 (see text for details).

Experiment 7: the addition of heterotrophic bacteria.

The observational data from the anchor station study suggested that phytoplankton N uptake was decoupled from phytoplankton carbon fixation, whereby phytoplankton assimilated more N than predicted by Redfield stoichiometry. In studies conducted by Bronk et al. (1998) in Chesapeake Bay, ratios of C:N uptake below that of Redfield proportions were also documented. Bronk et al. (1998) attributed this to either phytoplankton assimilating N in excess of their growth requirements, light limitation of carbon fixation, or N uptake by heterotrophic bacteria. In this experiment, heterotrophic bacteria were added to the model to assess their influence on phytoplankton growth. In the model, heterotrophs simply act as a competitor to phytoplankton because they too consume inorganic N. Additionally, the growth rate of heterotrophic bacteria is unaffected by light. Based on the assumption that heterotrophic bacteria are similar in size to small picophytoplankton, the same parameters were used for both groups (Table 5).

As Fig. 37 shows, including heterotrophic bacteria in the model had minimal effect on the model output. The biomass of nano- and microphytoplankton was reduced slightly, especially over the last 3

days of the experiment, and the growth rates of both these size classes were also reduced, again most significantly over the last 3 days. The biomass of heterotrophic bacteria was very low and followed a similar trend to that of the picophytoplankton. Heterotrophic biomass was initially 0.24 µg N L^{-1}, then increased to 13.2 µg N L^{-1} on day 6, after which it remained fairly constant until the end of the experiment.

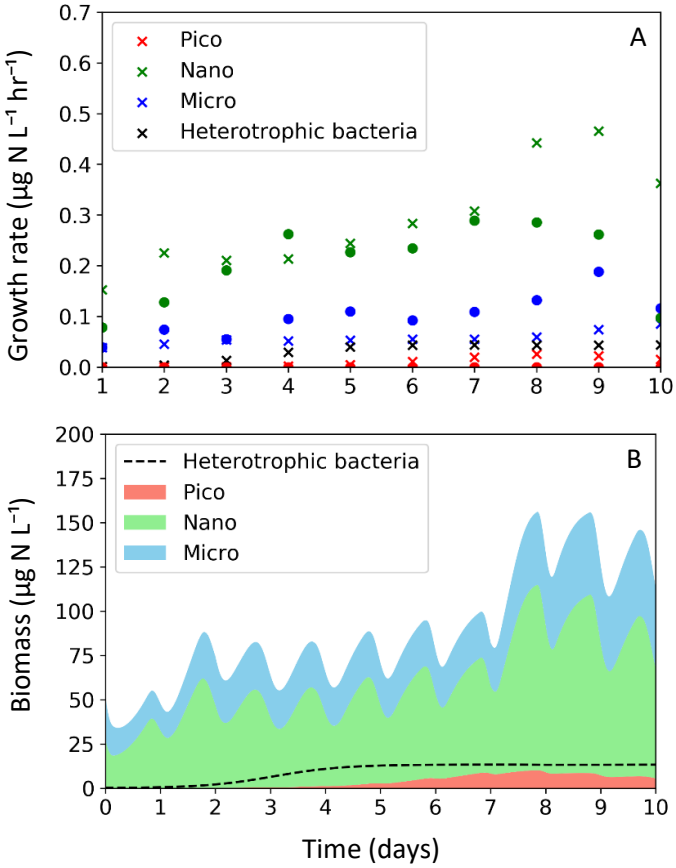

Fig 37. The results of experiment (7) showing the growth rate (µg N L^{-1} hr^{-1}) in panel A and the stacked biomass (µg N L^{-1}) in panel B for each size class: pico-, nano-, and microphytoplankton over the ten-day experiment. Crosses in A represent the average for each model day, while dots indicate the euphotic zone average, observed in situ. The black crosses in panel A and dashed black line in panel B represent the heterotrophic bacteria. For this experiment, the model was run in the configuration leading to the outputs shown in Fig. 9 (see text for details).

The fact that nanophytoplankton growth rates observed in the field were lower than those simulated by the model over the last 3 days of the experiment might be attributed to the presence of heterotrophic bacteria in SHB. This was supported by the model results, where simulated nanophytoplankton growth rates declined after heterotrophic bacteria were introduced. As a result, it is possible that heterotrophic bacteria were unknowingly sampled during the anchor station study. However, in section 4.3.2 other possible causes for the decoupling of C and N uptake are discussed and it is hypothesised that phytoplankton were probably engaging in luxury N uptake.

To conclude, while this model is far simpler than previously-constructed models for the same region (Cochrane et al., 1991; Moloney et al., 1991; Touratier et al., 2003), important questions raised by the observational data, which have potentially large implications for the biogeochemistry of SHB, could still be addressed. Overall, the major trends observed in the nutrient and phytoplankton data during the anchor station study were well captured by the model. This study is unique is that the model-

simulated growth rates for each size class could be compared with direct measurements of size-fractionated growth based on N from the field. The model highlights the importance of medium sized phytoplankton cells, which is consistent with the observational data, as well as the ability of phytoplankton in SHB to respond rapidly to inputs of new N.

This model is limited, however, by the lack of information regarding zooplankton and grazing pressure on phytoplankton. This would help to constrain estimates of phytoplankton mortality rates, which clearly have an important role to play in the phytoplankton dynamics of SHB. Furthermore, because N is used as the model currency, investigation of the C:N:P elemental stoichiometry of phytoplankton and its implications for the ecosystem in SHB was not possible.

6 Conclusions

The broad goal of this study was to investigate the drivers of short-term temporal variability in phytoplankton production in a coastal embayment in the shadow of a major upwelling system. To address this, the biogeochemistry, productivity and phytoplankton community composition in SHB in the SBUS were characterised throughout the upper water column at high resolution over an upwelling cycle. The results of the study clearly show that SHB is a highly variable system in which the major control on productivity switches rapidly between light and nutrient availability. Both these drivers of productivity, as well as the interactions between them, are heavily influenced by the physical water column dynamics, with phytoplankton experiencing light limitation during active upwelling and mixing and nutrient limitation when the water column stratifies.

This study also illustrates that SHB phytoplankton are able to respond rapidly to changes in their environment. A good example of this is the apparent capacity for luxury NO_3^- uptake during active upwelling when light levels are insufficient to support high rates of NPP. This NO_3^- is stored in large intracellular vacuoles to be used when light levels become favourable for photosynthesis and NO_3^- reduction, and/or ambient nutrients are depleted. Luxury NO_3^- uptake appears to aid the success of phytoplankton in an environment characterised by an intermittent and variable nutrient supply because more NO_3^- than is required to fulfil the immediate nutritional requirements of the cell can be taken up during active upwelling and stored for later use during periods of relaxation when NO_3^- deplete conditions persist.

Medium-sized phytoplankton (2.7 – 10 µm) dominate the biomass and rates of NPP and N uptake in SHB during active upwelling and stratification. This is attributed to the ability of these phytoplankton to rapidly increase their NO_3^- uptake rates in response to an input of nutrients. Additionally, they can maintain an elevated rate of NO_3^- uptake for longer than both the small and large phytoplankton. The medium phytoplankton size class is composed mainly of small diatoms (*Chaetoceros* spp. and *Skeletonema Costatum*) that are frequently observed in the SBUS. Their success in SHB seems to be at least partly due to them being the ideal size to avoid predation while also remaining suspended in the surface even when turbulence is reduced.

Measurements of NO_3^- and NH_4^+ uptake suggest that productivity in SHB is predominantly supported by "new" nitrogen, which is often used as an indicator of the potential for an oceanic region to sequester atmospheric CO_2. However, the study site is situated in a very shallow embayment, such that export of organic carbon biomass to the seafloor without resuspension is unlikely, especially given that the entire water column can be mixed during active upwelling. An unknown (but significant) proportion of sinking organic carbon biomass is likely recycled in these shelf waters, rendering any NO_3^- uptake-based estimates of carbon export highly questionable. This is compounded by the observation that there are clearly additional external inputs of N to SHB (Appendix A), the fluxes of which are currently unconstrained.

Understanding the drivers of phytoplankton variability in SHB has implications for the greater SBUS. For example, rapid cycling between light and nutrient limitation as induced by a turbulent versus stratified water column may ultimately advance our capacity to predict the occurrence of HABs. Water-column stratification is a precondition for the rapid growth of most dinoflagellate species (Pitcher & Weeks, 2006) including those that constitute HABs (Smayda, 1997; 2000), and HABs are fairly common in the SBUS (Pitcher & Calder, 2000). In upwelling systems, the typical succession of phytoplankton can be partially reset by the vertical advection of cold, nutrient-rich water to the surface (Estrada & Blasco, 1979). This may act to interrupt the growth of dinoflagellate species and, by extension, the development of HABs. In the present study, it appears as if the stratification period

was too short-lived for dinoflagellates to come to dominate the community before the onset of the next upwelling cycle, which may have prevented HAB formation. Therefore, the duration of the relaxation period during an upwelling cycle could serve as an indicator of the likelihood of HAB formation, with longer periods of stratification favouring the development of HABs.

The duration of turbulence versus stratification during an upwelling cycle also has implications for the phytoplankton size class that comes to dominate this region. For example, turbulence increases the persistence of large cells by decreasing their sinking rate. Being able to predict the dominant cell size based on the hydrographic conditions would be useful because cell size has implications for the dynamics of the pelagic food web (Pitcher et al., 1991). Furthermore, the feeding success of small pelagic fish (sardine and anchovy) is determined by the size of phytoplankton cells. Sardine are dominantly filter-feeders, such that they are most efficient at consuming small copepods that graze on small phytoplankton cells. By contrast, the dominant feeding mode of anchovy is particulate-feeding, which means that they are more efficient at consuming larger copepods that graze on large phytoplankton cells (Van der Lingen et al., 2010). Therefore, understanding the hydrographic variability that characterises SHB is key to understanding, and possibly even predicting, phytoplankton community composition and size distribution (Crichton et al., 2013). This, in turn, provides insights into the feeding habitat available to juvenile and adult small pelagic fish, such that we may ultimately be able to anticipate recruitment and species shifts between sardines and anchovy (Crichton et al., 2013). This is economically and ecologically relevant to South African because together, sardine and anchovy contribute substantially to the country's marine fish catch (Van der Lingen et al., 2010) and also occupy a critical mid-trophic-level position in the food chain, mediating the transfer of energy to higher trophic levels (Cury et al. 2000).

7 Appendix A

On days 3 to 6 of the experiment, unusually high concentrations of NO_2^- were observed at 0 m and 5 m, coinciding with relatively high Si and PO_4^{3-} concentrations. The accumulation of such high NO_2^- is unusual given that NO_2^- is an intermediate species in the N cycle, existing temporarily during nitrification or denitrification (Wada & Hattori, 1971). Additionally, ammonia oxidising bacteria and archaea that facilitate the conversion of NH_4^+ to NO_2^- during nitrification are inhibited by high light conditions like those experienced at the surface (Hooper & Terry, 1974; Guerrero & Jones, 1996; Beman et al., 2008). The lack of evidence for a biologically produced NO_2^- pool in the surface, along with the relatively high coincident Si and PO_4^{3-} concentrations, which could derive from terrestrial sources, argues for an external input of NO_2^- to SHB. In this section, the natural abundance isotopes of NO_3^- are used to investigate the possible sources of N to the bay. The $\delta^{15}N$ of NO_3^- is low at 0 m on days 2 and 4, and low at both 0 m and 5 m on days 5 to 7. This low $\delta^{15}N\text{-}NO_3^-$ signal coincides with the high observed NO_2^- concentrations. A low $\delta^{15}N\text{-}NO_3^-$ signal could derive from N_2 fixation (Carpenter et al., 1997), atmospheric N deposition (Hastings et al., 2003) or terrestrial runoff (Brandes & Devol, 2002). Ultimately, the most likely explanation for the low $\delta^{15}N\text{-}NO_3^-$ signal seems to be submarine groundwater discharge, which could be high in NO_2^- due to either nitrification or denitrification (more likely the former given the very low oxygen requirement of the latter) that occurred prior to its input to the surface of SHB.

7.1 The natural abundance isotopes of NO_3^- in seawater

There are two stable isotopes of nitrogen, ^{14}N and ^{15}N. ^{14}N is far more abundant, comprising 99.63% of all naturally occurring N in the environment. Chemical, physical and biological processes can discriminate between the two isotopes, which results in subtle but detectable differences in the ratio of ^{15}N to ^{14}N, observable in the various reservoirs of N in the ocean. N is required by all phytoplankton for growth, therefore constituting an essential component of marine biomass. Marine N_2 fixation supplies most of the biologically available N to the ocean, while the process of denitrification removes it (Gruber, 2004). Because of its importance to oceanic primary producers, biologically available N records fundamental biogeochemical processes in the marine environment. As a result, the N isotopic composition of any N pool in the ocean contains information about the N cycle processes that have acted on that pool as well as the origin of the N in that pool (Sigman et al., 2009).

The ratio of ^{15}N to ^{14}N of a sample relative to the constant isotopic ratio of a N reference standard (i.e., atmospheric N_2; $^{15}N/^{14}N \approx 0.367\%$) can be determined with high precision via mass spectrometry (Sigman et al., 2009). The isotopic ratio of seawater samples deviates slightly from the standard and these small deviations are expressed in δ notation as follows:

$$\delta^{15}N(‰ \text{ vs. } N_2 \text{ in air}) = \left(\frac{(^{15}N/^{14}N)_{sample}}{(^{15}N/^{14}N)_{standard}} - 1\right) \times 1000$$

The magnitude of isotopic fractionation that certain processes cause is termed the isotope effect and is denoted by ε. Isotopic fractionation can result from equilibrium processes and unidirectional reactions. The latter typically dominate in the ocean (i.e., N is converted from one form ("reactant") to another ("product")) and lead to "kinetic fractionation". The kinetic isotope effect of a particular reaction is defined as the ratio of the rates at which the two isotopes of N transform from reactant to product:

$$\varepsilon(‰ \text{ vs. } N_2 \text{ in air}) = (1 - {}^{15}k/{}^{14}k) \times 1000$$

where ^{14}k and ^{15}k are the rate coefficients of the reaction for reactants that contain ^{14}N and ^{15}N, respectively. When ε <<1000‰, it can be approximated by the $\delta^{15}N$ of the reactant minus the $\delta^{15}N$ of its instantaneous product (Mariotti et al., 1981; Sigman et al., 2009).

7.2 Analysis of nitrate $\delta^{15}N$

In the present study, NO_3^- isotope samples were collected on each day of the experiment and at five depths spanning the euphotic zone (0 m, 5 m, 10 m, 15 m and 20 m). During sample collection, 50 mL HDPE bottles were rinsed three times with seawater before being filled, then frozen at -20°C until analysis.

All NO_3^- isotope samples were filtered using a 0.2 µm syringe filter, after which 15 mL of sample was aliquoted into clean, acid washed 50 mL HDPE bottles and prepared for NO_2^- removal using sulfamic acid. In brief, 10 µL of 2 N sulfamic acid was added per 1 mL of sample to yield a pH of ~3. Samples were shaken and left to react for about 10 minutes then neutralised with 2N NaOH to yield a final pH of ~7.5 (Granger & Sigman, 2009). Following NO_2^- removal, the samples were again frozen at - 20°C until isotope analysis at the University of Massachusetts, Dartmouth.

After NO_2^- removal, the $\delta^{15}N$ of dissolved NO_3^- was measured in duplicate via the "denitrifier method" (Sigman et al., 2001). All the NO_3^- in the seawater sample is quantitatively converted to N_2O gas by cultured denitrifying bacteria (*Pseudomonas chlororaphis* (ATCC #43928)) that do not possess the active N_2O-reductase enzyme. The N_2O gas produced was automatically extracted, purified and then analysed online using a Tracegas-Isoprime preparation system coupled with a continuous flow mass spectrometer (Micromass Isoprime Multiflow) (Bourbonnais et al., 2009). Using this method, the $\delta^{15}N$ of samples with NO_3^- concentrations as low as 1 µmol L^{-1} can be measured. The isotope values were calibrated using an international KNO_3 reference material (IAEA-N3) with an assigned $\delta^{15}N$ value of +4.7‰, and N isotope ratios are reported in ‰ relative to atmospheric N_2. The analytical precision of the method is usually ~0.2‰.

7.3 N cycle processes impacting the subsurface nitrate $\delta^{15}N$

Fig. 1 shows the $\delta^{15}N$ of NO_3^- during the anchor station study. Below 5 m, the $\delta^{15}N$ of NO_3^- ranges from 6‰ to 8‰. The main source of upwelled water in the SHB region of the SBUS is Subantarctic Mode Water (SAMW; Lamont et al., 2015), which has a $\delta^{15}N$ of ~6‰ (Tuerena et al. 2015). To raise the $\delta^{15}N$ of this nitrate above 6‰ requires a fractionating biological process. One possibility is nitrate assimilation. When phytoplankton assimilate N, they preferentially consume the light isotope, leaving the ambient NO_3^- pool enriched in $\delta^{15}N$ (Wada & Hattori, 1978; Mariotti et al., 1981; Waser et al., 1998). The main form of biologically available N for phytoplankton growth in the SBUS is deep-water NO_3^- supplied to the surface via upwelling. Most estimates for the isotope effect of NO_3^- assimilation determined in the field range between 5‰ and 8‰ (Horrigan et al., 1990; Altabet et al., 1991; Wu et al., 1997); the expression of such an isotope effect during the assimilation of SAMW NO_3^- could easily drive its $\delta^{15}N$ above 6‰. Thus, one possible explanation for the high $\delta^{15}N$ of subsurface SHB nitrate is varying degrees of NO_3^- assimilation by phytoplankton. NO_3^- uptake rates suggest that assimilation was mostly occurring at 0 m and 5 m with very low rates below 10 m compared to that of the surface. Water column mixing over the first half of the study could have mixed the signal to greater depths resulting in the elevated $\delta^{15}N$ observed overs days 1 to 5. However, the water column is stratified over the second half of the experiment, such that the elevated $\delta^{15}N$ signal below 5 m probably did not result from the combination of assimilation in the surface and mixing of the signal to greater depths over days 5 to 10.

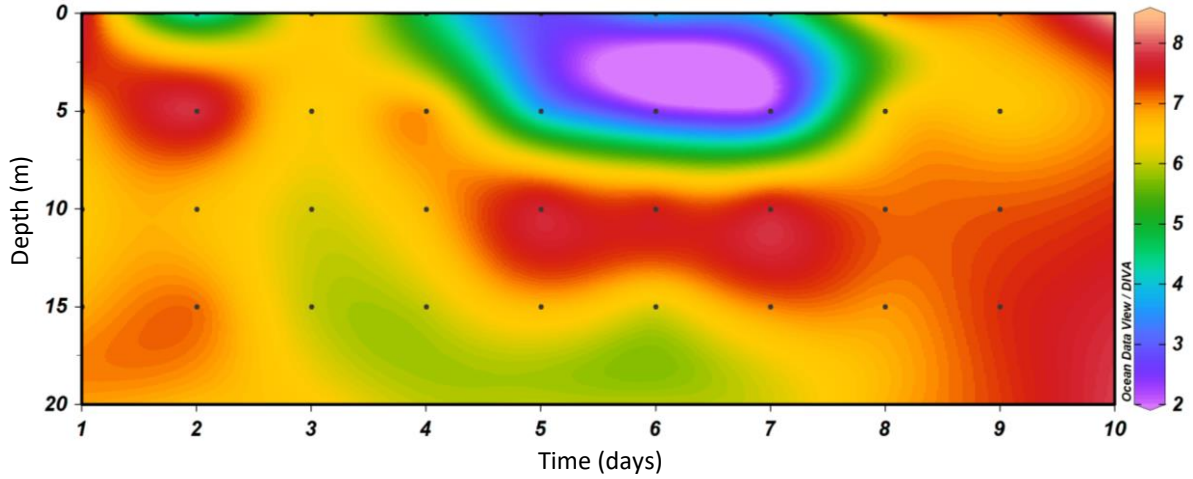

Fig 1. The $\delta^{15}N$ (‰ vs N_2) of NO_3^- in seawater measured throughout the water column over the course of the experiment. Black dots indicate the locations of sample collection.

Another possible explanation for the high subsurface NO_3^- $\delta^{15}N$ observed in the present study is water column denitrification. Denitrification is performed by heterotrophic and facultatively-anaerobic bacteria. When little to no oxygen (O_2) is available, these bacteria will use NO_3^- or NO_2^- as an electron acceptor during the oxidation of particulate organic matter, producing nitric oxides (NO), nitrous oxides (N_2O) and dinitrogen gas (N_2) (Seitzinger 1988). As a result, this process only occurs in areas of the ocean that are characterised by extremely low oxygen (O_2) concentrations. The isotope effect of water column denitrification is 20‰ to 30‰ (Altabet et al., 1999; Granger et al. 2008) such that as fixed N is lost from the system, the remaining NO_3^- pool becomes enriched in $\delta^{15}N$ (Sigman et al., 2009). High rates of denitrification occur in the ocean sediments of the continental margins (Devol 1991; Glud et al. 2009), as well as in the water column in particular regions (Deutsch et al., 2001; Devries et al., 2012). Water column denitrification typically occurs in EBUS that are either supplied with O_2 deplete upwelled water (e.g., the southern California current system; Bograd et al., 2008) and the northern Benguela current system; Nagel et al., 2013), or that develop O_2 deplete water due to high levels of productivity (e.g., the southern Benguela current system).

Fig. 2 shows that bottom water O_2 concentrations are low (< 50 µmol L^{-1}) in SHB. However, denitrifying bacteria will only take over the remineralisation of organic matter when dissolved O_2 concentrations fall below ~5 µmol L^{-1} (Devol, 1978; Jayakumar et al., 2009), and the lowest O_2 concentration recorded during the present study was 25 $\pm$ 5.1 µmol L^{-1}. However, sampling was only conducted between the surface and 20 m, while the bottom depth is ~ 30 m. Therefore, it is possible that lower O_2 concentrations would have been observed in SHB bottom waters as low oxygen water (LOW) is a widespread characteristic of the BUS (Chapman & Shannon, 1985). According to Monteiro and van der Plas (2006), the O_2 state is considered hypoxic when dissolved O_2 concentrations range from 0.5 to 1 ml L^{-1} (which equates to ~22 to 45 µmol L^{-1}). Under these conditions, marine organisms experience extreme stress or mortality and denitrification may occur. Under anoxic conditions, defined by O_2 concentrations < 0.5 ml L^{-1}, respiration is dominated by anaerobic bacteria (Monteiro & van der Plas ,2006). In a hydrographic study of SHB conducted by Lamont et al., (2014) (years 2000 to 2011), hypoxic water was found at station 2 (i.e., the site of our anchor station study) of the St Helena Bay Monitoring Line throughout the upwelling season (September to April) (Lamont et al. 2014). Therefore, it is possible that bottom water O_2 concentrations were sufficiently low during our study to support N loss and that the elevated $\delta^{15}N$ of subsurface NO_3^- is due to water column denitrification.

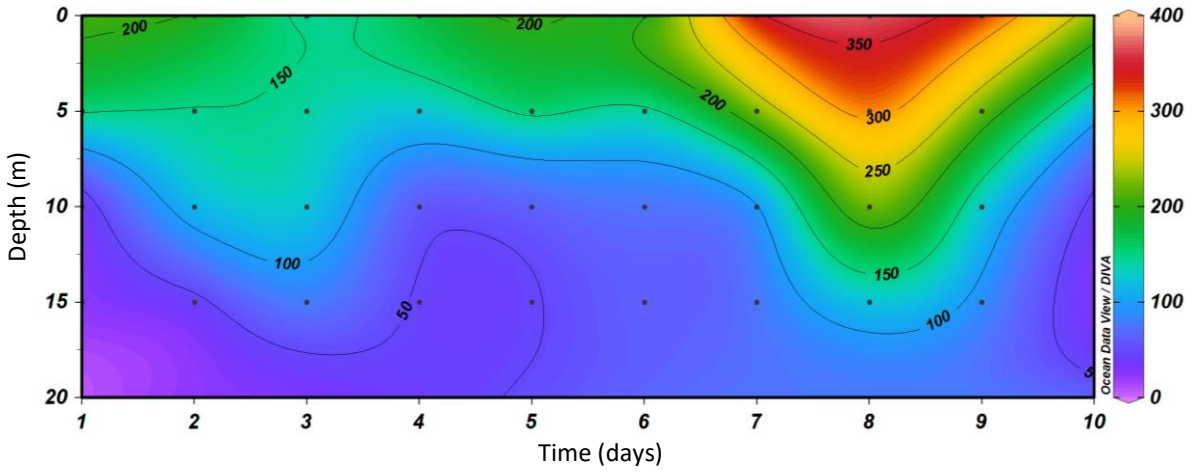

Fig 2. The dissolved oxygen concentration ([O_2]; µmol L^{-1}), measured throughout the water column over the course of the experiment. Black dots indicate the locations of sample collection. In all cases, the average [O_2] (n=2) is shown.

Another option is that the $\delta^{15}N$ of subsurface NO_3^- was driven higher than that of the source water in the region by coupled nitrification-denitrification (Granger et al., 2011). After assimilating NO_3^-, phytoplankton cells die and sink, resulting in the accumulation of organic matter on the seafloor. Here, organic matter is remineralized in the sediments, producing NH_4^+. NH_4^+ is then converted to NO_3^-, through the process of nitrification, which utilises oxygen. Because not all the NH_4^+ in the sediments is completely nitrified to NO_3^-, this process imparts a large isotope effect such that the residual NH_4^+ pool becomes enriched in $\delta^{15}N$, while the newly nitrified NO_3^- is low in $\delta^{15}N$. Upon the onset of oxygen deplete conditions, this newly nitrified NO_3^-, which is low in $\delta^{15}N$, becomes the substrate for sedimentary denitrification (Christensen et al., 1987; Seitzinger, 1988; Devol, 1991; Devol & Christensen, 1993; Jahnke & Jahnke, 2000) producing isotopically light N_2 (Brandes & Devol, 1997) that is released to the atmosphere. At the same time, isotopically heavy NH_4^+ is effluxed into the oxygenated bottom waters of the water column. Here NH_4^+ is nitrified, producing NO_3^- with a higher $\delta^{15}N$ than that of the sinking particles. In this case, denitrification occurs in the sediments as opposed to in the water column, as hypothesised above, and the effect of coupled nitrification-denitrification is communicated to the bottom waters.

Given the lack of evidence that we have of oxygen concentrations low enough to support water-column denitrification, coupled nitrification-denitrification is probably a more realistic hypothesis for the elevated subsurface $\delta^{15}N$ signal observed in the study. We thus conclude that the elevated $\delta^{15}N$ signal observed above ~10 m derived from NO_3^- assimilation in the surface combined with mixing to greater depths, while the elevated $\delta^{15}N$ signal observed below this, likely derived from coupled nitrification-denitrification in the sediments.

7.4 N cycle processes impacting the surface nitrate $\delta^{15}N$

One would expect the surface NO_3^- $\delta^{15}N$ to be high due to assimilation by phytoplankton. The NO_3^- uptake rates measured in the surface suggest that this is true. However, on days 5, 6 and 7 of the experiment, the surface and 5 m are characterised by unusually low $\delta^{15}N$ values that range from 2 $\pm$ 0.8‰ to 4 $\pm$ 0.5‰. Low $\delta^{15}N$ values are also observed at the very surface on days 2 and 4 of the experiment (4‰ and 4.6 $\pm$ 0.6‰, respectively).

There are multiple N cycle processes that can lower the $\delta^{15}N$ of the ambient NO_3^- pool. The first is N_2 fixation. N_2 gas cannot be assimilated by most organisms in the ocean, but some prokaryotes known as diazotrophs possess the enzymes required to convert N_2 to NH_4^+. Once incorporated into

diazotrophic biomass, the ultimate fate of this N is to be recycled into other N forms that can be readily assimilated by non-diazotrophic phytoplankton and bacteria (Knapp, 2012). Most oceanic N_2 fixation is performed by cyanobacteria, particularly of the *Trichodesmium* spp. which are primarily found in warm, stratified and low-nutrient surface environments (Capone et al., 1997; Capone et al., 2005).

Newly fixed N in the surface mixed layer usually has a $\delta^{15}N$ of ~ -2‰ to 0‰ (Carpenter et al., 1997). Remineralisation of diazotrophic biomass at or below the base of the euphotic zone produces NO_3^- that is similarly low in $\delta^{15}N$, which acts to lower the $\delta^{15}N$ of the ambient NO_3^- pool (Knapp et al., 2005; Sigman et al., 2009). For example, NO_3^- $\delta^{15}N$ has been shown to decrease upwards from deep waters into the thermocline of the Sargasso Sea (from ~5‰ at 800 m to 2-3‰ in the thermocline) due to the input of relatively low-$\delta^{15}N$ N attributed to N_2 fixation (Knapp et al., 2005, 2008; Fawcett et al., 2015).

If N_2 fixation were taking place in SHB, one might expect to see the low $\delta^{15}N$ signal near the depth of remineralization as opposed to at the surface, unless remineralisation is occurring throughout the water column. While no N_2 fixation estimates exist for the SBUS, little to no N_2 fixation appears to occur in the surrounding areas (Sohm et al. 2011). This, coupled with evidence of the high energetic cost incurred in breaking the triple bond of N_2 during fixation (as opposed to that required to reduce and assimilate NO_3^-) (Falkowski, 1983) suggests that N_2 fixation in a high-NO_3^- region like the SBUS is unlikely. Numerous culture studies have shown that N_2 fixation is inhibited by high dissolved inorganic nitrogen (DIN) concentrations (e.g., Ohki et al., 1991; Mulholland & Capone, 1999; Mulholland et al., 2001; Fu & Bell, 2003; Holl & Montoya, 2005). However, more recent culture work conducted using concentrations of NO_3^- and PO_4^{3-} typically observed in the surface ocean showed that chronic exposure of *Trichodesmium* and *Crocosphaera* (the latter being a tiny unicellular cyanobacterium) to 5-16 µmol L^{-1} NO_3^- depresses N_2 fixation rates in comparison to cultures grown with no NO_3^-, but that N_2 fixation still occurs even in the presence of as much as 16 µmol L^{-1} NO_3^- (Knapp et al., 2012). Knapp et al. (2012) also suggest that higher PO_4^{3-} concentrations can counteract NO_3^- inhibition of N_2 fixation by increasing the abundance of diazotrophs. This, coupled with a reduction in the inhibitory effect of NO_3^- on N_2 fixation due to lower NO_3^- concentrations can result in significant rates of N_2 fixation in regions characterised by low dissolved N:P ratios. It also suggests that N_2 fixation may not be strictly limited to oligotrophic marine environments but may also occur in high nutrient environments (e.g., in surface waters above oxygen deficient zones, where denitrification results in N loss and thus lower N:P ratios) (Knapp, 2012). Therefore, we cannot rule out N_2 fixation as a possible cause of the low $\delta^{15}N$ signal observed at the surface in the middle of the experiment.

Perhaps a more compelling argument against N_2 fixation as the cause of the low $\delta^{15}N$ of NO_3^- is that the signal is present in the surface and at 5 m. If the low-$\delta^{15}N$ NO_3^- was due to N_2 fixation, low-$\delta^{15}N$ biomass would have to be rapidly remineralised and nitrified in the surface in order for the signal to be observed in the NO_3^- pool. This is unlikely because nitrification is a slow process. In addition, while nitrification may occur in as much as 5 to 10% of surface light intensity, it is generally inhibited by the high light environment of the surface ocean (Dore & Karl, 1996; Ward, 2005; Ward et al., 1989). We thus conclude that N_2 fixation is not the cause of this low $\delta^{15}N$ signal.

The second possible explanation for the low-$\delta^{15}N$ NO_3^- is that it was introduced into SHB via terrestrial runoff or atmospheric deposition. The N isotopic composition of both of these sources is poorly constrained, with most work focused on heavily polluted systems. The small amount of literature that exists on the $\delta^{15}N$ of NO_3^- in pristine rivers, give a value of ~4‰ (Brandes & Devol, 2002; Sweeney & Kaplan, 1980) . However multiple biological processes take place as water flows from its source to the sea, such that the final $\delta^{15}N$ introduced to the marine system may have quite different from the up-river value (Kendall et al., 2007; Sigman et al., 2009). Furthermore, there are no rivers that flow directly into SHB. SHB is boarded by the Berg River to the South and the Olifants River to the North, both of

which are sufficiently far from the study site such that their influence can be ruled out. In addition, the density data show no evidence of any fresh water inputs to SHB (Section 3; Fig. 6).

Human activities like fossil fuel combustion, as well as natural processes like lightning and biomass burning, result in the release of NO_x (the sum of NO and NO_2) into the atmosphere. Here, NO_x undergoes oxidation to nitric acid (HNO_3). HNO_3 readily dissociates to NO_3^-, which can be deposited at the ocean surface via wet deposition (i.e., rain). Dry deposition can also supply atmospherically derived NO_3^- to the ocean, for example in the form of dry gasses like HNO_3 vapor or dry NO_3^- aerosols (Kendall et al., 2007). In terms of atmospheric NO_3^- deposition, a wide range of $\delta^{15}N$ values have been observed, from -15‰ to 15‰ in remote locations (Hastings et al., 2003; Kendall, 1998; Altieri et al., 2013), such that atmospheric NO_3^- deposition may be responsible for the low $\delta^{15}N$ values observed in the present study.

There have been no studies dedicated to atmospheric N deposition over the SBUS. However, studies conducted by Baker et al. (2008) suggest that very low rates of atmospheric N deposition occur in the region of south Atlantic Ocean closest to the SBUS. To assess the possibility that atmospheric NO_3^- deposition (or reduced N deposition that was subsequently nitrified in surface waters; see above for arguments against this) was the cause of the low-$\delta^{15}N$ NO_3^- observed at the surface on days 5 to 7 of the anchor station study, NOAA's Hybrid Single-Particle Lagrangian Integrated Trajectory model (HYSPLIT) was used to compute air mass back trajectories (AMBT) for each day of the experiment, using meteorological data sourced from the NCEP Global Data Assimilation System (GDAS). Using this meteorological data and a simple particle dispersion model, HYSPLIT yields the trajectory of a suspended particle backward in time from a pre-defined point, which in this case is the anchor station. Through this, we can determine where the air over SHB originated from on each day of the experiment.

For this study, 36-hour back trajectories were computed for every hour of the day (i.e., 24 hours) prior to sampling. 36 hours was chosen because it is representative of the lifetime of NO_x in the atmosphere (Altieri et al. 2013). An altitude of 0 m was used because theconditions at the sea surface were of interest. Next, a cluster analysis was performed for each day whereby mean trajectories were generated from a larger number of single trajectories. Single AMBTs are effectively grouped together based on their similarity. Fig. 3 displays the output of the HYSPLIT analysis for day 4 of the anchor station study, which is used as an example as the AMBTs on each day of the experiment are very similar. Fig. 3 suggests that the air mass originated in the southeast Atlantic Ocean and travelled over the city of Cape Town before reaching SHB. It is thus very likely that air reaching SHB contained a significant amount of NO_x such that atmospheric NO_3^- deposition was possible. However, if atmospheric deposition were responsible for the low-$\delta^{15}N$ signal, we would expect to observe it on every day of study given that the air originates from the same place and follows the same path on each day. Another possibility is that there was an unrecorded event such as biomass burning that occurred near SHB during or prior to our sampling on days 5 to 7 that could have resulted in the atmospheric deposition of low-$\delta^{15}N$ NO_3^- only on these days. It is also possible that atmospheric deposition occurred elsewhere and that the low $\delta^{15}N$ signal was advected into SHB. Regardless, in order to decrease the $\delta^{15}N$ of deep nitrate (6‰) to that observed in the surface (3‰ on average), would require the fraction of NO_3^- to derive from atmospheric deposition, to be 38% of the total input of NO_3^- to the top 5 m of the water column. This amounts to 3.8 $\mu mol\ L^{-1}$ on day 5 and would require an atmospheric deposition rate of 19 $mmol\ m^{-2}\ day^{-1}$, which is an order of magnitude larger than estimates of atmospheric deposition in the south Atlantic ocean (Baker et al., 2003), and in regions of the ocean adjacent to heavily polluted main lands like the East China Sea (Kodama et al., 2011).

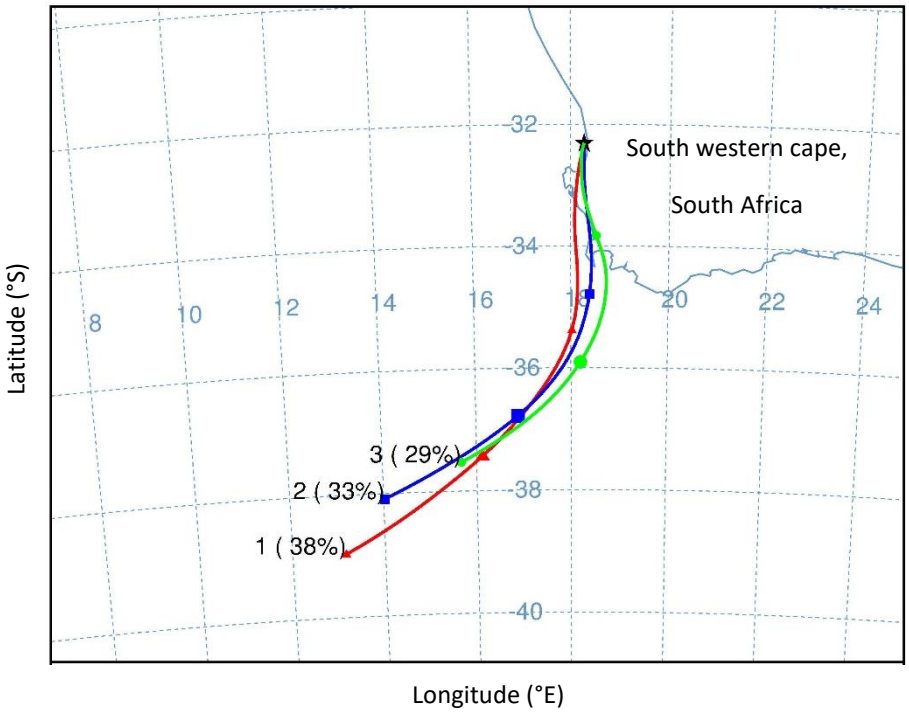

Fig 3. The cluster mean of a 36-hour air mass back trajectory, run for each hour of the day (i.e., 24 hours) prior to sampling at 12:00 pm on the 4th day of the anchor station study using HYSPLIT. The black star indicates the location of the anchor station and the blue, green and red lines each represent the origin of the air mass in SHB. The analysis was performed at a height of 0 m. Meteorological data sourced from the "Global Data Assimilation System" (GDAS).

Furthermore, PO_4^{-3} usually comprises a very small component of aerosols (and atmospheric deposition in general) compared to NO_3^-, such that wet and dry atmospheric deposition are typically characterized by relatively high N:P ratios (>100:1) (Duce, 1986; Sandroni et al., 2007; Kanikadou et al. 2012). For example, Baker et al. (2003) measured the N:P ratios of atmospheric deposition in the Atlantic Ocean and found values much higher than Redfield (on the order of 1000). In the present study, N:P ratios on days 5 to 7 were much lower than Redfield (2.5 - 8; Fig. 4), which further argues against atmospheric deposition as the source of the low-$\delta^{15}N$ NO_3^-.

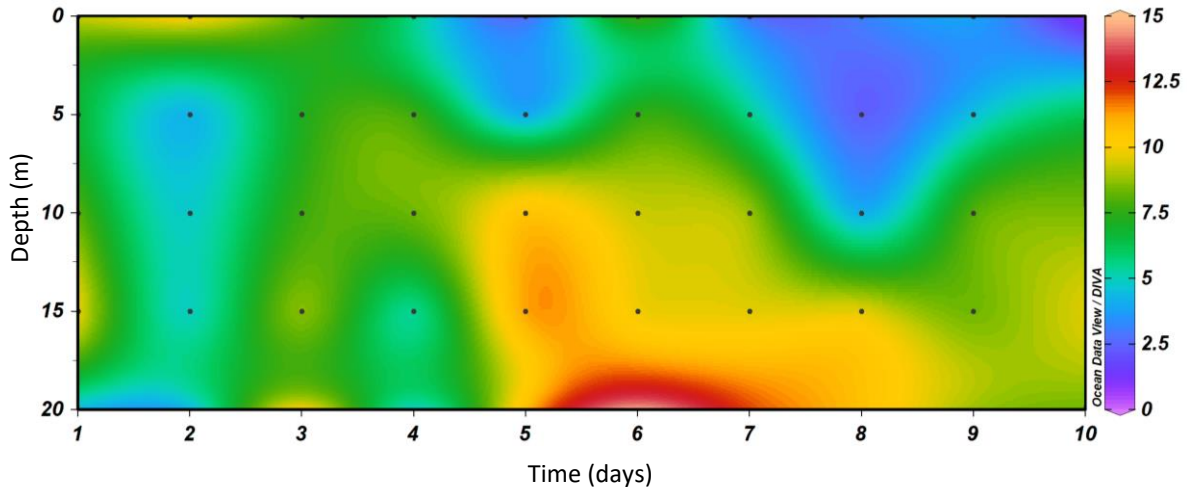

Fig 4. The nitrate to phosphate ratio (N:P), determined from the average nitrate and phosphate concentrations (n = 2) measured throughout the water column at 0 m, 5 m, 10 m, 15 m and 20 m over the course of the experiment. Black dots indicate the locations of sample collection.

Finally, atmospheric deposition should strongly increase the $\delta^{18}O$ of NO_3^- in surface waters because atmospheric NO_3^- has a $\delta^{18}O$ on the order of 70‰ (Hastings et al., 2003; Altieri et al. 2013). For example, an input of atmospherically-derived NO_3^- to surface waters of Monterey Bay in the Californian upwelling system led to a low $\delta^{15}N$ of 2.5‰ coupled with a high $\delta^{18}O$ of ~34‰ (Wankel et al., 2007). While the $\delta^{18}O$ of NO_3^- measured in this study is not shown here, preliminary data suggest that the oxygen isotope ratios do not support atmospheric deposition as the source of the low- $\delta^{15}N$ NO_3^-.

The fact that the low-$\delta^{15}N$ NO_3^- signal observed on days 5 to 6 is coupled with relatively high concentrations of PO_4^{3-} and Si, both of which are not typically considered large or important components of atmospheric deposition(Sandroni et al. 2007; Liss & Johnson, 2014), suggests that the input was most likely terrestrially derived. One potential source of such an input that we have not yet considered is submarine ground water discharge (SGD).

The Verlore is the only river system in Elands Bay, the closest town to our study site. The Verlore River is ~100 km long with a catchment area of ~1895 km². The river flows into a coastal lake (the Verlorenvlei), which is intermittently connected to the ocean by an estuarine channel. During winter, the lake can fill up and potential outflow to the ocean is possible. However, sampling was conducted in summer when high evaporation rates usually result in low water levels. Furthermore, a rocky, sand-covered bar at the mouth of the estuary separates the Verlore River from the sea, making it a virtually closed system almost all year round (Harrison, 1997). During extreme storm events or under strong tidal conditions, the sand barrier can be broken allowing seawater to flow into the system and vice versa (Harrison, 1997). Given the time of year during which sampling took place, it is unlikely that such conditions were met.

The Verlorenvlei catchment area includes the southern extent of the Sandveld, a coastal plain on the southwest coast of South Africa characterised by particularly sandy and nutrient-poor soils. The catchment ranges from its highest point, the Picketberg Mountains to the east, down to Elands Bay on the West Coast. The Sandveld region also comprises of granular primary aquifers and deeper fractured rock sedimentary aquifers that together store approximately 500 Mm³ of water (Knüppe et al., 2016). The Verlorenvlei estuarine lake transports “semi-fresh” water to the sea when the estuary is not obstructed by a sand barrier. However, during periods of reduced flow from rivers (i.e., during drought years, such as at present), the ecology and biodiversity of natural wetlands like the Verlorenvlei are supported by baseflow from the Sandveld aquifers (Watson et al., 2018). The baseflow of an aquifer is in turn influenced by the rate at which the groundwater is recharged (Watson et al. 2018), although groundwater recharge is one of the most difficult components of any hydrological cycle to quantify (Conrad et al., 2004).

There are very few studies investigating the Sandveld aquifers, although Conrad et al. (2004) suggests that the general flow direction is westward towards the coast. Nonetheless, coastal watersheds like the Verlorenvlei that possess a high hydraulic conductivity and coastal aquifers characterised by permeable sediments have the potential to transport fresh water to the ocean. This fresh water typically flows down-gradient from a surficial aquifer to the coastal marine environment and discharges from a seepage face located near the intertidal zone or even farther offshore (Kroeger et al., 2007). Discharge of ground water into the ocean at the coastline is referred to as SGD (Kroeger et al., 2007), irrespective of the force causing the flow or the composition of the water (Moore, 2010). While rivers remain the major hydrological cycle pathway for discharge of water from land to sea, they are highly visible, which makes their contribution to the coastal ocean easier to quantify. Input of continental water from SGD typically occurs at or below the sea surface making this process much more difficult to detect. Regardless, SGD per unit length of a particular coastline is a potentially

significant source of continental water to the ocean due to the vast extent of coastline along which SGD is known to occur and the fact that SGD occurs irrespective of whether rivers are present or not (Taniguchi et al., 2002). Scientists now recognise SGD as an important component of the global water cycle, not only because of its volumetric importance, which is considered to be similar to that of the riverine flux in the Atlantic Ocean (Moore et al., 2008), but also because it is often characterised by higher concentrations of carbon, nutrients and metals than river water. As a result, SGD is potentially as important as rivers for the oceanic budgets of the above-mentioned nutrients (Moore, 2010).

While there is no evidence in our density data of a freshwater input at the coast (Section 3; Fig. 6), many studies that have directly measured SGD suggest that it can have salinity close to that of the surrounding seawater (Kim & Lee, 2003; Smith & Zawadzki, 2003; Taniguchi et al., 2005). Thus, if SGD was occurring at the time of sampling, it would not have been possible to differentiate between groundwater and seawater using the salinity data. To our knowledge, there are no studies investigating SGD off the west coast of South Africa. While SGD has not been documented in the SBUS, if it is occurring near SHB it could represent an additional potential source of low $\delta^{15}N$ NO_3^- to the anchor station site.

NO_3^- in soils and groundwater can originate from natural and anthropogenic sources (Bouchard et al., 1992). Some bacteria, free-living or those that live in association with the roots of higher plants, blue-green algae, and some fungi have the ability to fix atmospheric N_2. Indeed, animals and higher order plants attain N for reproduction and tissue growth from the organisms that fix it. Nitrogenous plant tissue is broken down by microbes in the soil, releasing NH_4^+ and NO_3^- that can then be re-assimilated by organisms in the soil or transported away from their source in the air or water (Bouchard et al., 1992). NO_3^- also occurs naturally as NO_3^- salts in geological deposits, which can leach into groundwater. Additionally, significant amounts of NH_4^+ and NO_3^- from the atmosphere can be transferred to soils and eventually into groundwater via precipitation (Bouchard et al., 1992). Under natural conditions, the NO_3^- concentration of groundwater usually remains low and stable. This is because most natural environments like forests retain NO_3^-, which is only leached into the groundwater system when the environment is disturbed. Natural groundwater NO_3^- concentrations are typically <48 mg L^{-1}, but can increase due to human activities like agriculture, industrial and food processing operations as well as improper waste disposal (Bouchard et al., 1992).

NO_3^- in groundwater usually has a $\delta^{15}N$ similar to that of its source (Kreitler 1979; Wassenaar 1995). For example, the $\delta^{15}N$ of atmospheric NO_3^- and NH_4^+ ranges between -15‰ and 15‰ while the $\delta^{15}N$ of NO_3^- in synthetic fertilisers can range between -4‰ and 4‰ (Kendall, 1998). On the other hand, organic fertilisers generally have a higher $\delta^{15}N$ and exhibit a larger range (i.e., 2‰ to 30‰). NO_3^- sourced from animal waste typically has a high $\delta^{15}N$ ranging between 10‰ and 20‰ (Kreitler 1979), while the $\delta^{15}N$ of NO_3^- in soil can vary from -10‰ to 15‰, depending on its source and subsequent processing (Kendall & Aravena, 2000). Percolation of recharge water through the soil transports NO_3^- into the groundwater (Kreitler and Browning 1983). Once in the subsurface, groundwater NO_3^- can be altered via various chemical, physical and biological processes, which likely alter the $\delta^{15}N$ that eventually reaches the sea via SGD. In a study conducted by Kroeger and Charette (2008), the N biogeochemistry in nearshore fresh, brackish and saline groundwater was examined in Waquoit Bay, Massachusetts, using N concentrations and natural abundance stable isotope ratios. Kroeger and Charette (2008) found the $\delta^{15}N$ of NO_3^- in the freshwater aquifer to be 2.1‰ on average, which they interpreted as indicating an atmospheric deposition or fertiliser source (Kroeger & Charette, 2008). SGD does not require a high N:P ratio and serves as a good explanation for the relatively high Si and PO_4^{3-} concentrations that likely derive from a terrestrial source. Furthermore, it does not require a

salinity lower than that of seawater. In conclusion, SGD is possible explanation for the low $\delta^{15}N$ of NO_3^- observed over days 5 to 7 in the present study.

While it is notoriously difficult to measure groundwater as it flows towards the coast, terrestrially-derived material in SGD has been shown to be an important source of nutrients to the coastal ocean environment (Paytan et al. 2006). While the role of SGD as a nutrient source has not been extensively investigated, some studies suggest that as much as 90% of the DIN input to coastal embayment's could derive from SGD (Kim et al., 2011). As a result, SGD has the potential to initiate the development of phytoplankton blooms and cause eutrophication in coastal waters by introducing large amounts of new nutrients to the system (Paerl, 1997).

References

Abe, K., Imamaki, A., and Hirano, M. 2002. Removal of Nitrate, Nitrite, Ammonium and Phosphate Ions from Water by the Aerial Microalga *Trentepohlia Aurea*. *Journal of Applied Phycology.* 14: 129–134.

Alcaraz, M., Saiz, E. and Estrada, M. 1994. Excretion of Ammonia by Zooplankton and Its Potential Contribution to Nitrogen Requirements for Primary Production in the Catalan Sea (NW Mediterranean). *Marine Biology.* 119: 69–76.

Allen, A. E., Howard-Jones, M. H., Booth, M. G., Frischer, M. E., Verity, P.G., Bronk, D. A. and Sanderson, M. P. 2002. Importance of heterotrophic bacterial assimilation of ammonium and nitrate in the Barents Sea during summer. *Journal of Marine Systems*. 38(1-2): 93-108.

Almeida, J. S., Julio, S.M., Reis, M.A.M. and Carrondo, M. J. T. 1995. Nitrite Inhibition of Denitrification by Pseudomonas Fluorescens. *Biotechnology and Bioengineering.* 46: 194–201.

Altabet, M. A., Deuser, W. D., Honjo, S. and Stienen, C.. 1991. Seasonal and Depth-Related Changes in the Source of Sinking Particles in the North Atlantic. *Letters to Nature.* 354: 136–319.

Altabet, M. A., Pilskaln, C., Thunell, R., Pride, C., Sigman, D., Chavez, F. and Francois, R. 1999. The Nitrogen Isotope Biogeochemistry of Sinking Particles from the Margin of the Eastern North Pacific. *Letters to Nature*.46: 655–679.

Altieri, K. E., Hastings, M. G., Gobel, A. R., Peters, A. J. and Sigman, D. M. 2013. Isotopic Composition of Rainwater Nitrate at Bermuda : The Influence of Air Mass Source and Chemistry in the Marine Boundary Layer. *Journal of Geophysical Research: Atmopheres.* 118 (3): 304–316.

Andrews, W. R. H. and Hutchings, L. 1980. "Upwelling in the Southern Benguela Current." *Progress in Oceanography.* 9: 1–81.

Anning, T., MacIntyre, H. L., Pratt, S. M., Sammes, P. J., Gibb, S. and Geider, R. J. 2000. Photoacclimation in the Marine Diatom Skeletonema Costatum. *Limnology and Oceanography.* 45 (8): 1807–1817.

Azam, F., Fenchel, T., Field, J. G., Gray, J. S., Meyer-Reil, L. A. and Thingstad, F. 1983. The Ecological Role of Water-Column Microbes in the Sea. *Marine Ecology Progress Series.* 10: 257–263.

Babin, M., Therriault, J., Legendre, L. and Condal, A. 1993. Variations in the Specific Absorption Coefficient for Natural Phytoplankton Assemblages: Impact on Estimates of Primary Production. *Limnology and Oceanography.* 38: 154–177.

Bailey, G. W. 1991. Organic carbon flux and development of oxygen deficiency on the modern Benguela continential shelf south of 22^{o}S: spatial and temporal variability. *Geological Society Special Publication*.58: 171–183.

Bailey, G. W. and Chapman, P. 1991. Short-term variability during an anchor station study in the southern Benguela upwelling system: Chemical and physical oceanography. *Progress in Oceanography*. 28: 9-37.

Baker, A.R. and Croot, P.L. 2010. Atmospheric and marine controls on aerosol iron solubility in seawater. *Marine Chemistry*. 120(1-4): 4-13.

Baker, A. R., Kelly, S. D., Biswas, K. F., Witt, M. and Jickells, T.D. 2003. Atmospheric Deposition of Nutrients to the Atlantic Ocean. *Geophysical Research Letters.* 30 (24): 2–5.

Bakun, A., Black, B. A., Bograd, S.J., Garcia-Reyes, M., Miller, A. J., Rykaczewski, R. R. and Sydeman, W. J. 2015. Anticipated Effects of Climate Change on Coastal Upwelling Ecosystems. *Current Climate Change Reports*. 1: 85–93.

Banse, K. 1976. Rates of Growth, Respiration and Photosynthesis of Unicellular Algae as Related to Cell Size. *Journal of Phycology.* 12: 135–140.

Batchelder, H.P., Edwards, C.A. and Powell, T.M. 2002. Individual-based models of copepod populations in coastal upwelling regions: implications of physiologically and environmentally influenced diel vertical migration on demographic success and nearshore retention. *Progress in Oceanography*. 53(2-4): 307-333.

Beman, J. M., Popp, B. N. and Francis, C. A. 2008. Molecular and Biogeochemical Evidence for Ammonia Oxidation by Marine Crenarchaeota in the Gulf of California. *The International Society for Microbial Ecology Journal*. 1–13.

Bender, M., Grande, K., Johnson, K., Marra, J., Williams, P. J. L., Sieburth, J., Pilson, M., Langdon, C. et al. 1987. A Comparison of Four Methods for Determining Planktonic Community Production. *Limnology and Oceanography.* 32 (5): 1085–1098.

Benschneider, K. and Robinson, R. J. 1952. New Spectrophotometric Method for the Determination of Nitrite in Sea Water. *Journal of Marine Research*. 8: 1-14.

Bograd, S. J., Castro, C. G., Di Lorenzo, E., Palacios, D. M., Bailey, H., Gilly, W. and Chavez, F. P. 2008. Oxygen Declines and the Shoaling of the Hypoxic Boundary in the California Current. *Geophysical Research Letters.* 35: 1–6.

Bouchard, D. C., Williams, M. K. and Surampalli, R. Y. 1992. Nitrate Contamination of Groundwater : Sources and Potential Health Effects. *American Water Works Association.* 84 (9): 85–90.

Bourbonnais, A., Lehmann, M. F., Waniek, J. J. and Schulz-bull, D. E. 2009. Nitrate Isotope Anomalies Reflect N_2 Fixation in the Azores Front Region (Subtropical NE Atlantic). *Journal of Geophysical Research.* 114: 1–16.

Boyd, P., LaRoche, J., Gall, M., Frew, R. and Mckay, R. M. L. 1999. Role of Iron, Light, and Silicate in Controlling Algal Biomass in Subantarctic Waters SE of New Zealand." *Journal of Geophysical Research*. 104: 13395–13408.

Bradley, P.B., Sanderson, M.P., Frischer, M.E., Brofft, J., Booth, M.G., Kerkhof, L.J. and Bronk, D.A. 2010. Inorganic and organic nitrogen uptake by phytoplankton and heterotrophic bacteria in the stratified Mid-Atlantic Bight. *Estuarine, Coastal and Shelf Science. 88*(4): 429-441.

Brandes, J. A,. and Devol, A. H. 1997. Isotopic Fractionation of Oxygen and Nitrogen in Coastal Marine Sediments. *Geochimica et Cosmochimica Acta.* 61 (9): 1793–1801.

Brandes, J. A., and Devol, A. H. 2002. A Global Marine-Fixed Nitrogen Isotopic Budget: Implications for Holocene Nitrogen Cycling. *Global Biogeochemical Cycles.* 16 (4): 1-14.

Bronk, D. A., Glibert, P. M. and Ward, B. B. 1994. Nitrogen Uptake, Dissolved Organic Nitrogen Release, and New Production. *Science.* 265: 1843–1846. https://doi.org/10.1126/science.265.5180.1843.

Bronk, D. A., and Glibert, P. M. 1993. Application of a ^{15}N Tracer Method to the Study of Dissolved Organic Nitrogen Uptake during Spring and Summer in Chesapeake Bay. *Marine Biology.* 508 (115): 501–508.

Bronk, D. A., and Glibert, P. M. 1994. The Fate of the Missing ^{15}N Differs among Marine Systems. *Limnology and Oceanography.* 39 (1): 189–195.

Bronk, D. A., and Ward, B. B. 1999. Gross and Net Nitrogen Uptake and DON Release in the Euphotic Zone of Monterey Bay, California. *Limnology and Oceanography.* 44 (3): 573–585.

Bronk, D. A., Glibert, P. M., Malone, T. C., Banahan, S. and Sahlsten, E. 1998. Inorganic and Organic Nitrogen Cycling in Chesapeake Bay: Autotrophic versus Heterotrophic Processes and Relationships to Carbon Flux. *Aquatic Microbial Ecology.* 15: 177–189.

Bronk, D.A. 2002. Dynamics of DON. *Biogeochemistry of marine dissolved organic matter.* 384: 153-247.

Brown, P.C. and Field, J.G., 1986. Factors limiting phytoplankton production in a nearshore upwelling area. *Journal of Plankton Research*. 8(1): 55-68.

Brown, P.C., 1984. Primary production at two contrasting nearshore sites in the southern Benguela upwelling region, 1977—1979. *South African Journal of Marine Science*. 2(1): 205-215.

Brzezinski, M. A., Phillips, D. R., Chavez, F. P., Friederich, G. E. and Dugdale, R. C. 1997. Silica Production in the Monterey, California, Upwelling System. *Limnology and Oceanography.* 42 (8): 1694–1705.

Capone, D. G., Burns, J. A., Montoya, J. P., Subramaniam, A., Mahaffey, C., Gunderson, T., Michaels, A. F. andCarpenter, E. J. 2005. Nitrogen Fixation by *Trichodesmium* Spp.: An Important Source of New Nitrogen to

the Tropical and Subtropical North Atlantic Ocean. *Global Biogeochemical Cycles.* 19 (2): 1-17.

Capone, D. G., Zehr, J. P., Paerl, H. W., Bergman, B. and Carpenter, E. J. 1997. *Trichodesmium*, a Globally Significant Marine Cyanobacterium. *Science.* 276 (5316): 1221–1229.

Carlucci, A. F., Hartwig, E. O. and Bowes, P. M. 1970. Biological Production of Nitrite in Seawater. *Marine Biology.* 7: 161–166.

Carpenter, E. J., Harvey, R. H., Fry, B. and Capone, D. G. 1997. Biogeochemical Tracers of the Marine Cyanobacterium *Trichodesmium*. *Deep Sea Research 1* 44 (1): 27–38.

Carr, M.E. 2001. Estimation of Potential Productivity in Eastern Boundary Currents Using Remote Sensing. *Deep-Sea Research Part II.* 49: 59–80.

Cermeno, P., Maranon, E., Perez, V., Serret, P., Fernandez, E. and Gastro, C. G. 2006. Phytoplankton Size Structure and Primary Production in a Highly Dynamic Coastal Ecosystem (Ria de Vigo, NW-Spain): Seasonal and Short-Time Scale Variability. *Estuarine, Coastal and Shelf Science.* 67: 251–266.

Cermeno, P., Maranon, E., Rodriguez, J. and Fernandez, E. 2005. Large-Sized Phytoplankton Sustain Higher Carbon-Specific Photosynthesis than Smaller Cells in a Coastal Eutrophic Ecosystem. *Marine Ecology Progress Series.* 297: 51–60.

Chapman, P. and Bailey, G. W. 1991. Short-Term Variability during an Anchor Station Study in the Southern Benguela Upwelling System: Introduction. *Progress in Oceanography.* 28: 39–64.

Chapman, P., and Shannon, L. V. 1985. The Benguela Ecosystem Part II. Chemistry and Related Processes. *Oceanography Marine Biology Annual Review.* 23: 183–251.

Chavez, F. P. and Messié, M. 2009. "A Comparison of Eastern Boundary Upwelling Ecosystems." *Progress in Oceanography*. 83: 80-86.

Chen, W., Zhang, Q. and Dai S. 2009. Effects of Nitrate on Intracellular Nitrite and Growth of *Microcystis Aeruginosa*. *Journal of Applied Phycology.* 21: 701–706.

Chrisholm, S. W. 1992. Phytoplankton Size. In *Primary Productivity and Biogeochemical Cycles in the Sea.* P. G. Falkowski and A. D. Woodward, Eds. New York: Plenum Press. 213–237

Christensen, J. P., Murray, J. W., Devol, H. and Codispoti, L. A.. 1987. Denitrification in Continental Shelf Sediments has Major Impact on the Oceanic Nitrogen Budget. *Global Biogeochemical Cycles.* 1(2): 97–116.

Clark, D. R., Rees, A. P. and Joint, I. 2008a. Ammonium Regeneration and Nitrification Rates in the Oligotrophic Trophic Atlantic Ocean : Implications for New Production Estimates. *Limnology and Oceanography.* 53 (1): 52–62.

Cochlan, W.P. and Harrison, P.J., 1991. Inhibition of nitrate uptake by ammonium and urea in the eucaryotic picoflagellate Micromonas pusilla (Butcher) Manton et Parke. *Journal of Experimental Marine Biology and Ecology*. 153(2): 143-152.

Cochrane, K. L., James, A. G., Mitchell-Innes, B. A., Pitcher, G. C., Verheye, H. M. and Walker, D. R. 1991. Short-Term Variability during an Anchor Station Study in the Southern Benguela Upwelling System: A Simulation Model. *Progress in Oceanography.* 28: 121–152.

Codispoti, L. A., and Christensen, J. P. 1985. Nitrification, Denitrification and Nitrous Oxide Cycling in the Eastern Tropical South Pacific Ocean. *Marine Chemistry.* 16: 277–300.

Conrad, J., Nel, J. and Wentzel, J. 2004. The Challenges and Implications of Assessing Groundwater Recharge: A Case Study – Northern Sandveld, Western Cape, South Africa. *Water SA.* 30 (5): 75–81.

Crichton, M., Hutchings, L., Lamont, T. and Jarre, A. 2013. From Physics to Phytoplankton: Prediction of Dominant Cell Size in St Helena Bay in the Southern Benguela. *Journal of Plankton Research.* 35: 526–541.

Cury, P., Bakun, A., Crawford, R. J. M., Jarre, A., Quin, R. A., Shannon, L. J. and Verheye, H. M. 2000. Small Pelagics in Upwelling Systems: Patterns of Interaction and Structural Changes in '" Wasp-Waist " Ecosystems.

ICES Journal of Marine Science. 57: 603–618.

De Baar, H.J.W. 1994. Von Liebig's law of the minimum and plankton ecology (1899–1991). *Progress in oceanography*. *33*(4): 347-386.

De Boyer Montegut, C., Madec, G., Fischer, A.S., Lazar, A. and Iudicone, D. 2004. Mixed layer depth over the global oean: An examination of profile data and a profile-based climatology. *Journal of Geophysical Research*. 109: 1-20.

Demanche, J. M., Curl, H. C., Lundy, D. W. and Donaghay, P. L. 1979. The Rapid Response of the Marine Diatom *Skeletonema Costatum* to Changes in External and Internal Nutrient Concentration. *Marine Biology.* 53: 323–33.

Demarcq, H., Barlow, R. and Hutchings, L. 2007. Application of a Chlorophyll Index Derived from Satellite Data to Investigate the Variability of Phytoplankton in the Benguela Ecosystem. *African Journal of Marine Science*. 29(2): 271-282.

Denman, K.L. and Pena, M.A. 1999. A coupled 1-D biological/physical model of the northeast subarctic Pacific Ocean with iron limitation. *Deep Sea Research Part II: Topical Studies In Oceanography*. 46(11-12): 2877-2908.

Deutsch, C., Gruber, N., Key, R. M., Sarmiento, J. L. and Ganachaud, A. 2001. Denitrification and N_2 Fixation in the Pacific Ocean. *Global Biogeochemical Cycles.* 15 (2): 483–506.

Deutsch, C., Sarmiento, J. L., Sigman, D. M., Gruber, N. and Dunne, J. P. 2007. Spatial Coupling of Nitrogen Inputs and Losses in the Ocean. *Nature.* 445 (7124): 163–167.

Devol, A. H. 1978. Bacterial Oxygen Uptake Kinetics as Related to Biological Processes in Oxygen Deficient Zones of the Oceans. *Deep Sea Research.* 25 (2): 137–146.

Devol, A. H . 1991. Direct Measurement of Nitrogen Gas Fluxes from Continental Shelf Sediments. *Letters to Nature.* 349: 319–321.

Devol, A. H . 2003. Solution to a Marine Mystery. *Nature.* 422: 575–576.

Devol, A. H. and Christensen, J. P. 1993. Benthic Fluxes and Nitrogen Cycling in Sediments of the Continental Margin of the Eastern North Pacific. *Journal of Marine Research.* 51: 345–732.

Devries, T., Deutsch, C., Primeau, F., Chang, B. and Devol, A. 2012. Global Rates of Water-Column Denitrification Derived from Nitrogen Gas Measurements. *Nature Geoscience.* 5 (8): 547–550.

Domingues, R. B., Barbosa, A. and Galva, H. 2005. Nutrients, Light and Phytoplankton Succession in a Temperate Estuary (the Guadiana , South-Western Iberia). *Estuarine Coastal and Shelf Science.* 64: 249–260.

Dore, J. E., Brum, J. R., Tupas, L. M. and Karl, D. M. 2002. Seasonal and Interannual Variability in Sources of Nitrogen Supporting Export in the Oligotrophic Subtropical North Pacific Ocean. *Limnology and Oceanography.* 47 (6): 1595–1607.

Dore, J. E. and Karl, D. M. 1996. Nitrification in the Euphotic Zone as a Source for Nitrite, Nitrate, and Nitrous Oxide at Station ALOHA. *Limnology and Oceanography.* 41 (8): 1619–1628.

Dortch, Q. 1990. The Interaction Between Ammonium and Nitrate Uptake in Phytoplankton. *Marine Ecology Progress Series.* 61: 183–201.

Duce, R.A., LaRoche, J., Altieri, K., Arrigo, K.R., Baker, A.R., Capone, D.G., Cornell, S., Dentener, F., Galloway, J., Ganeshram, R.S. and Geider, R.J. 2008. Impacts of atmospheric anthropogenic nitrogen on the open ocean. *Science*. 320(5878): 893-897.

Duce, R.A., 1986. The impact of atmospheric nitrogen, phosphorus, and iron species on marine biological productivity. In *The role of air-sea exchange in geochemical cycling.* 497-529. Dordrecht: Springer.

Ducklow, H.W., Steinberg, D. K. and Buesseler, K. O. 2001. “Upper Ocean Carbon Export and the Biological Pump.” *Oceanography.* 14 (4): 50-58.

Dugdale, R. C. 1967. Nutrient Limitation in the Sea: Dynamics, Identification, and Significance.” *Limnology and*

Oceanography. 12 (4): 685–95.

Dugdale, R. C. and Goering, J.J. 1967. Uptake of New and Regenerated Forms of Nitrogen in Primary Productivity. *Limnology and Oceanography.* 12 (2): 196–206.

Dugdale, R. C., Wilkerson, F. P., Hogue, V. E. and Marchi, A. 2006. Nutrient Controls on New Production in the Bodega Bay, California, Coastal Upwelling Plume. *Deep-Sea Research part II.* 53: 3049–3062.

Dugdale, RC, and FP Wilkerson. 1986. "The Use of 15N to Measure Nitrogen Uptake in Eutrophic Oceans; Experimental Considerations." *Limnology and Oceanography* 31 (July): 673–89.

Ekman, V.W. 1923. *Über Horizontalzirkulation bei winderzeugten Meeresströmungen*. R. Friedländer & Sohn.

Emeis, K. A. E., Flohr, A., Lahajnar, N., Nausch, G., Neumann, A., Rixen, T., Schmidt, M., Van der Plas, A. and Wasmund, N. 2018. Biogeochemical Processes and Turnover Rates in the Northern Benguela Upwelling System. *Journal of Marine Science.* 188: 63–80.

Eppley, R. W. and Thomas, W. H. 1969. Comparison of Half-Saturation Constants for Growth and Nitrate Uptake of Marine Phytoplankton. *Journal of Phycology*.5(4): 375-379

Eppley, R.W. and Peterson, B. J. 1979. Particulate Organic Matter Flux and Planktonic New Production in the Deep Ocean. *Nature.* 282: 677–680.

Eppley, R. W., Rogers, J. N and Mccarthy, J. J. 1969. Half-Saturation Constants for Uptake of Nitrate and Ammonium by Marine Phytoplankton. *Limnology and Oceanography.* 14 (6): 912–920.

Eppley, R. W., Renger, E. H., Harrison, W. G. and Cullen, J. J. 1979. Ammonium Distribution in Southern California Coastal Waters and Its Role in the Growth of Phytoplankton. *Limnology and Oceanography.* 24 (3): 495–509.

Ernst, W. G. 2000. *Earth Systems: Processes and Issues*. Cambridge, United Kingdom: Cambridge University Press.

Estrada, M. and Blasco, D. 1985. Phytoplankton Assemblages in Coastal Upwelling Areas. In *International Symposium on the Upwelling Areas off Western Africa*. 379–402. Barcelona: Instituto de Investigaciones Pesqueras.

Evans, G.T. and Parslow, J.S. 1985. A model of annual plankton cycles. *Biological oceanography*. 3(3): 327-347

Falkowski, P.G., Laws, E.A., Barber, R.T. and Murray, J.W. 2003. Phytoplankton and their role in primary, new, and export production. In *Ocean biogeochemistry.* 99-121. Berlin, Germany: Springer.

Falkowski, P.G. 1983. Light-shade adaptation and vertical mixing of marine phytoplankton: a comparative field study. *Journal of Marine Research*. 41(2): 215-237.

Fawcett, S.E., Ward, B.B., Lomas, M.W. and Sigman, D.M. 2015. Vertical decoupling of nitrate assimilation and nitrification in the Sargasso Sea. *Deep Sea Research Part I: Oceanographic Research Papers*. 103: 64-72.

Fawcett, S. E. and Ward, B. B. 2011. Phytoplankton Succession and Nitrogen Utilization during the Development of an Upwelling Bloom. *Marine Ecology Progress Series.* 428: 13–31.

Fawcett, S. E., Lomas, M. W., Casey, J. R., Ward, B. B and Sigman, D. M. 2011. Assimilation of Upwelled Nitrate by Small Eukaryotes in the Sargasso Sea. *Nature Geoscience.* 4 (10): 717–722.

Fenchel, T.. 2008. The Microbial Loop – 25 Years Later. *Journal of Experimental Marine Biology and Ecology.* 366 (1–2): 99–103.

Fennel, W. 1999. Theory of the Benguela Upwelling System. *Journal of Physical Oceanography.* 29: 177–190.

Fernandez, C., Farias, L. and Ulloa, O. 2011. Nitrogen Fixation in Denitrified Marine Waters. *PLoS ONE* 6 (6): 1-9.

Flohr, A., van der Plas, A. K., Emeis, K. C., Mohrholz, V. and Rixen, T. 2014. Spatio-Temporal Patterns of C : N : P Ratios in the Northern Benguela Upwelling System" *Biogeosciences* 11: 885–97.

Flynn, R.F., Burger, J. M., Pillay, K. and Fawcett, S. E. 2018. Wintertime Rates of Net Primary Production and Nitrate and Ammonium Uptake in the Southern Benguela Upwelling System.*South African Journal of Marine Science* 40 (3): 253–266.

Fu, F. and Bell, P. R. F. 2003. Effect of Salinity on Growth, Pigmentation, N_2 Fixation and Alkaline Phosphatase Activity of Cultured *Trichodesmium* Sp." *Marine Ecology Progress Series.* 257: 69–76.

García-Reyes, M., Sydeman, W. J., Schoeman, D. S., Rykaczewski, R. R., Black, B. A., Smit, A. J. and Bograd, S. J. 2015. Under Pressure: Climate Change, Upwelling, and Eastern Boundary Upwelling Ecosystems. *Frontiers in Marine Science.* 2: 1–10.

Garrison, D. L. 1979. Monterey Bay Phytoplankton I. Seasonal Cycles of Phytoplankton Assemblages. *Journal of Plankton Research.* 1 (3): 241–266.

Garside, C. 1981. Nitrate and Ammonia Uptake in the Apex of the New York Bight. *Limnology and Oceanography.* 26 (4): 731–39.

Geider, R. J., MacIntyre, H. L. and Kana, T. M. 1997. Dynamic Model of Phytoplankton Growth and Acclimation: Responses of the Balanced Growth Rate and the Chlorophyll a:Carbon Ratio to Light, Nutrient-Limitation and Temperature. *Marine Ecology Progress Series.* 148 (1–3): 187–200.

Geider, R. J. 1987. Light and Temperature Dependence of the Carbon to Chlorophyll a Ratio in Microalgae and Cyanobacteria: Implications for physiology and growth of phytoplankton. *New Phytology.* 106: 1–34.

Geider, R. J., Osborne, B. A. and Raven, J. A. 1986. Growth, Photosynthesis and Maintenance Metabolic Cost in the Diatom *Phaeodactylum Tricornutum* at Very Low Light Levels. *Journal of Phycology*.22: 39–48.

Geider, R. J. and Osborne, B. A. 1987. Light Absorption by a Marine Diatom: Experimental Observations and Theoretical Calculations of the Package Effect in a Small *Thalassiosira* Species." *Marine Biology.* 96: 299–308.

Geider, R. J., La Roche, J., Greene, R. M. and Olaizola, M. 1993. Photosynthetic Apparatus of *Phaeodactylum Tricornutum* (Bacillariophyceae) to Nitrate, Phosphate or Iron Starvation . *Journal of Phycology* 29 (6): 755–766.

Glibert, P.M., Goldman, J.C. and Carpenter, E.J. 1982. Seasonal Variation in the Utilization of Ammonium and Nitrate by Phytoplankton in Vinyard Sound, Massachusetts, USA. *Marine Biology*. 70: 237-249.

Glover, H. E., Garside, C. and Trees, C. C. 2007. Physiological Responses of Sargasso Sea Picoplankton to Nanomolar Nitrate Perturbations. *Journal of Plankton Research.* 29 (3): 263–274.

Glud, R. N., Thamdrup, B., Stahl, H., Wenzhoefer, F., Glud, A., Nomaki, H., Oguri, K., Revsbech, P. and Kitazato, H. 2009. Nitrogen Cycling in a Deep Ocean Margin Sediment (Sagami Bay, Japan). *Limnology and Oceanography.* 54 (3): 723–34.

Goering, J. J., Wallen, D.D. and Nauman, R.M. 1970. Nitrogen Uptake by Phytoplankton in the Discontinuity Layer of the Eastern Subtropical Pacific Ocean. *Limnology and Oceanograph.y* 15 (5): 789–96.

Goldhammer, T., Brüchert, V., Ferdelman, T. G. and Zabel, M. 2010. Microbial Sequestration of Phosphorus in Anoxic Upwelling Sediments. *Nature Geoscienc.e* 3 (8): 1–5.

Granger, J., Prokopenko, M. G., Sigman, D, M., Mordy, C. W., Morse, Z. M., Morales, L. V., Sambrotto, R. N. and Plessen, B. 2011. Coupled Nitrification - Denitrification in Sediment of the Eastern Bering Sea Shelf Leads to ^{15}N Enrichment of Fixed N in Shelf Waters." *Journal of Geophysical Research.* 116: 1–18.

Grasshoff, K., Kremling, K. and Ehrhardt, M. 1983. Methods of Seawater Analysis. *Verlag Chemia*, Florida Grasshoff, K. 1976. Methods of seawater analysis. *Verlag Chemie*, Weinheim and New York

Granger, J. and Sigman, D. M. 2009. Removal of Nitrite with Sulfamic Acid for Nitrate N and O Isotope Analysis with the Denitrifier Method. *Rapid Communications in Mass Spectrometry.* 23: 3753–3762.

Gregor, L. and Monteiro, P. 2013. Is the southern Benguela a significant regional sink of CO_2? *South African Journal of Science*. 109(5-6): 1-5.

Gruber, N. 2004. The Dynamics of the Marine Nitrogen Cycle and Its Influence on Atmospheric CO_2 Variations. In *The Ocean Carbon Cycle and Climate*, 97–148. Dordrecht: Springer.

Gruber, N., and Sarmiento, J. L. 1997. Global Pattern of Marine Nitrogen Fixation and Denitrification. *Global Biogeochemical Cycles.* 11 (2): 235–266.

Guerrero, M. A. and Jones, R. D. 1996. Photoinhibition of Marine Nitrifying Bacteria . I . Wavelength-Dependent Response. *Marine Ecology Progress Series.* 141 (1): 183–92.

Guidi, L., Stemmann, L., Jackson, G. A., Frederic, I., Claustre, H., Legendre, L., Picheral, M. and Gorsky, G. 2009. Effects of Phytoplankton Community on Production, Size and Export of Large Aggregates: A World-Ocean Analysis. *Limnology and Oceanography.* 54 (6): 1951–1963.

Hamersley, M. R., Lavik, G., Woebken, D., Rattray, J. E., Lam, P., Hopmans, E. C., Damste, J. S. S. et al. 2007. "Anaerobic Ammonium Oxidation in the Peruvian Oxygen Minimum Zone. *Limnology and Oceanography.* 52 (3): 923–33.

Harrison, T. D. 1997. A Preliminary Survey of Coastal River Systems on the South African West Coast, Orange River-Groot Berg, with Particular Reference to the Fish Fauna. *Transactions of the Royal Socieyt of South Africa.* 52 (2): 277–321.

Harrison, W. G., Harris, L. R. and Irwin, B. D. 1996. The Kinetics of Nitrogen Utilization in the Oceanic Mixed Layer: Nitrate and Ammonium Interactions at Nanomolar Concentrations. *Limnology and Oceanography.* 41 (1): 16–32.

Hastings, M. G., Sigman, D. M. and Lipschultz, F. 2003. Isotopic Evidence for Source Changes of Nitrate in Rain at Bermuda. *Journal of Geophysical Research.* 108 (2): 1–12.

Hoffmann, L. J., Peeken, I. and Lochte, K. 2008. Iron, Silicate, and Light Co-Limitation of Three Southern Ocean Diatom Species. *Polar Biology.* 31: 1067–1680.

Holl, C. M. and Montoya, J. P. 2005. Interactions between Nitrate Uptake and Nitrogen Fixation in Continuous Cultures of the Marine Diazotroph *Trichodesmium* (Cyanobacteria). *Journal of Phycology.* 1183: 1178–1183.

Holmes, R.M., Aminot, A., Kérouel, R., Hooker, B.A. and Peterson, B.J. 1999. A simple and precise method for measuring ammonium in marine and freshwater ecosystems. *Canadian Journal of Fisheries and Aquatic Sciences*. 56(10):1801-1808.

Hooper, A. B. and Terry, K. R. 1974. Photoinactivation of Ammonia Oxidation in *Nitrosomonas*. *Journal of Bacteriology.* 119 (3): 899–906.

Horrigan, S. G., Montoya, J. P., JNevins, J. L. and McCarthy, J. J. 1990. Natural Isotopic Composition of Dissolved Inorganic Nitrogen in the Chesapeake Bay. *Estuarine, Coastal and Shelf Science.* 30: 393–410.

Horrigan, S.G., Carlucci, A.F. and Williams, P.M. 1981. Light inhibition of nitrification in sea-surface films [California]. *Journal of Marine Research*. 39(3): 557-566.

Howarth, R.W, Marino, R., Lane, J. and Cole, J. J. 1988. Nitrogen Fixation in Freshwater, Estuarine, and Marine Ecosystems . 1 . Rates and Importance. *Limnology and Oceanograph.y* 33: 669–687.

Hutchings, L. 1992. "Fish Harvesting in a Variable, Productive Environment — Searching for Rules or Searching for Exceptions?" *South African Journal of Marine Science.* 12 (1): 297–318.

Hutchings, L. and Field, J.G. 1997. Biological oceanography in South Africa, 1896-1996: Observations, mechanisms. Monitoring and modelling. *Transaction of the Royal Sicety of South Africa.* 52(1): 81-120.

Hutchings, L., Pitcher, G.C., Probyn, T.A. and Bailey, G.W., 1995. The chemical and biological consequences of coastal upwelling. *Environmental Sciences Research Report Es*. 18: 65-82.

Hutchins, D. A., Sedwick, P. N., DiTullio, G. R., Boyd, P. W., Queguiner, B., Griffiths, F. B. and Crossley, C. 2001. Control of Phytoplankton Growth by Iron and Silicic Acid Availability in the Subantarctic Southern Ocean: Experimental Results from the SAZ Project. *Journal of Geophysical Research.* 106: 31559–31572.

Iriberri, J., Unanue, M., Barcina, I. and Egea, L. Seasonal Variation in Population Density and Heterotrophic Activity of Attached and Free-Living Bacteria in Coastal Waters. *Applied and Environmental Microbiology*. 53(10): 2308-2314.

Idso, S. B., and Gilbert. R. G. 1974. On the Universality of the Poole and Atkins Secchi Disk-Light Extinction Equation. *Journal of Applied Ecology.* 11 (1): 399–401.

IOC and SCOR and IAPSO, 2010. *Intergovernmental Oceanographic Commission, Manuals and Guide, 56, UNESCO.* Available: http://www.teos-10.org/pubs/TEOS-10_Manual.pdf [2019, February 4].

Jahnke, R. A. and Jahnke, D. B. 2000. Rates of C, N, P and Si Recycling and Denitrication at the US Mid-Atlantic Continental Slope Depocenter. *Deep Sea Research part 1.* 47: 1405–1428.

Jayakumar, A., Mullan, G. D. O., Naqvi, S. W. A. and Ward, B. B. 2009. Denitrifying Bacterial Community Composition Changes Associated with Stages of Denitrification in Oxygen Minimum Zones. *Microbial Ecology.* 58 (2): 350–362. https://doi.org/10.1007/s00248-009-9487-y.

Karl, D., Letelier, R., Tupas, L., Dore, J., Christian, J. and Hebel, D. 1997. The Role of Nitrogen Fixation in Biogeochemical Cycling in the Subtropical North Pacific Ocean. *Nature.* 388: 533-538.

Karl, D., Michaels, A., Bergman, B., Capone, D., Carpenter, E., Letelier, R., Lipschultz, F., Paerl, H., Sigman, D and Stal, L. 2002. Dinitrogen Fixation in the World 's Oceans. *Biogeochemistry.* 57(58): 47–98.

Kendall, C. 1998. Tracing Nitrogen Sources and Cycling in Catchments. In *Isotope Tracers in Catchment Hydrology*, C. Kendall and J. J. McDonnell, Eds. Amsterdam, Netherlands: Elsevier.

Kendall, C. and Aravena, R. 2000. Nitrate Isotopes in Groundwater Systems. In *Environmental Tracers in Subsurface Hydrology*. 261–95. Boston: Springer.

Kendall, C.,Elliott, E. M. and Wankel, S. D. 2007. Tracing Anthropogenic Inputs of Nitrigen to Ecosystems. In *Stable Isotopes in Ecology and Environmental Science*. R. Michener and K. Lajtha, Eds. 375–435. Oxford, United Kindom: Blackwell Publishing.

Kim, G., Kim, J. and Hwang, D. 2011. Submarine Groundwater Discharge from Oceanic Islands Standing in Oligotrophic Oceans: Implications for Global Biological Production and Organic Carbon Fluxes. *Limnology and Oceanography.* 56 (2): 673–682.

Kim, G. and Lee, K. 2003. Large Submarine Groundwater Discharge (SGD) from a Volcanic Island. *Geophysical Research Letters.* 30 (21): 1–4.

Kiørboe, Thomas. 1993. Turbulence, Phytoplankton Cell Size, and the Structure of Pelagic Food Webs. *Advances in Marine Biology.* 29: 2–61. 7.

Kirchman, D. L. and Wheeler, P.A. 1998. Uptake of Ammonium and Nitrate by Heterotrophic Bacteria and Phytoplankton in the Sub-Arctic Pacific. *Deep Sea Research Part I: Oceanographic Research Papers.* 45(2-3): 347-365.

Kirchman, D.L., Suzuki, Y., Garside, C. and Ducklow, H.W. 1991. High turnover rates of dissolved organic carbon during a spring phytoplankton bloom. *Nature*. *352*(6336): 612.

Kirchman, D.L., Ducklow, H.W., McCarthy, J.J. and Garside, C. 1994. Biomass and nitrogen uptake by heterotrophic bacteria during the spring phytoplankton bloom in the North Atlantic Ocean. *Deep Sea Research Part I: Oceanographic Research Papers.* 41(5-6): 879-895.

Kirk, J. T. O. 1994. *Light and Photosynthesis in Aquatic Ecosystems*. Cambridge, United Kingdom: Cambridge university press.

Kirk, J. T. O. 1976. A Theoretical Analysis of the Contribution of Algal Cells to the Attenuation of Light within Natural Waters. *New Phytology* 77: 341–358.

Knap, A. H., Jickells, T. D., Pszenny, A. and Galloway, J. 1986. Significance of Atmospheric-Derived Fixed Nitrogen on Productivity of the Sargasso Sea." *Nature*. 320: 158–160.

Knapp, A. N. 2012. The Sensitivity of Marine N_2 Fixation to Dissolved Inorganic Nitrogen. *Frontiers in Microbiology.* 3: 1–14.

Knapp, A. N., Casciotti, K. L., Berelson, W. M., Prokopenko, M. G. and Capone, D. G. 2016. Low Rates of Nitrogen Fixation in Eastern Tropical South Pacific Surface Waters. *Proceedings of the National Academy of Sciences.* 113 (16): 4398–4403.

Knapp, A.N., Dekaezemacker, J., Bonnet, S., Sohm, J. A and Capone, D. G. 2012. Sensitivity of *Trichodesmium Erythraeum* and *Crocosphaera Watsonii* Abundance and N_2 Fixation Rates to Varying NO_3^- and PO_4^{3-} Concentrations in Batch Cultures. *Aquatic Microbial Ecology*. 66: 223–236.

Knapp, A.N., DiFiore, P.J., Deutsch, C., Sigman, D.M. and Lipschultz, F. 2008. Nitrate isotopic composition between Bermuda and Puerto Rico: Implications for N_2 fixation in the Atlantic Ocean. *Global Biogeochemical Cycles*. 22(3).

Knapp, A. N., Sigman, D. M. and Lipschultz, F. 2005. N Isotopic Composition of Dissolved Organic Nitrogen and Nitrate at the Bermuda Atlantic Time-Series Study Site. *Global Biogeochemical Cycles.* 19: 1–15.

Knüppe, K., Pahl-wostl, C. and Vinke-de Kruijf, J. 2016. Sustainable Groundwater Management: A Comparative Study of Local Policy Changes and Ecosystem Services in South Africa and Germany. *Environmental Policy and Governance.* 72 : 59–72.

Kodama, T., Furuya, K., Hashihama, F., Takeda, S. and Kanda, J. 2011. Occurrence of Rain - Origin Nitrate Patches at the Nutrient - Depleted Surface in the East China Sea and the Philippine Sea during Summer. *Journal of Geophysical Research* 116: 1–14.

Kokkinakis, S.A., and Wheeler, P. A. 1987. Nitrogen Uptake and Phytoplankton Growth in Coastal Upwelling Regions. *Limnology and Oceanography* 32 (5): 1112–1123.

Korner, H., and Zumft, W. G. 1989. Expression of Denitrification Enzymes in Response to the Dissolved Oxygen Level and Respiratory Substrate in Continuous Culture of Pseudomonas Stutzeri. *Applied and Environmental Microbiology.* 55 (7): 1670–1676.

Kreitler, C. W. 1979. Nitrogen-Isoptope Ratio Studies of Soils and Groundwater Nitrate from Alluvial Fan Aquifers in Texas. *Journal of Hydrology.* 42: 147–170.

Kreitler, C. W. and Browning, L. A. 1983. Nitrogen-Isotope Analysis of Groundwater Nitrate in Carbonate Aquifers: Natural Sources versus Human Pollution. *Journal of Hydrology.* 61: 285–301.

Kroeger, K.D. and Charette, M. A. 2008. Nitrogen Biogeochemistry of Submarine Groundwater Discharge. *Limnology and Oceanography.* 53 (3): 1025–1039.

Kroeger, K. D., Swarzenski, P. W., Greenwood, W. J. and Reich, C. 2007. Submarine Groundwater Discharge to Tampa Bay: Nutrient Fluxes and Biogeochemistry of the Coastal Aquifer. *Marine Chemistry.* 104: 85–97.

Kudela, R. M. and Dugdale, R. C. 2000. Nutrient Regulation of Phytoplankton Productivity in Monterey Bay, California. *Deep Sea Research Part II.* 47: 1023–1053.

Kuypers, M. M. M., Lavik, G., Woebken, D., Schmid, M., Fuchs, B. M.,Amann, R., Jørgensen, B. B. and Jetten, M. S. M. 2005. Massive Nitrogen Loss from the Benguela Upwelling System through Anaerobic Ammonium Oxidation. *Proceedings of the National Academy of Sciences of the United States of America* 102 (18): 6478–6483.

Lamont, T., Barlow, R. G. and Kyewalyanga, M. S. 2014. Physical Drivers of Phytoplankton Production in the Southern Benguela Upwelling System. *Deep-Sea Research Part I.* 90: 1–16.

Lamont, T., Hutchings, L., van den Berg, M. A., Goschen, W. S., and Barlow, R. G. 2015. Hydrographic Variability in the St. Helena Bay Region of the Southern Benguela Ecosystem. *Journal of Geophysical Research: Oceans.* 120 (4): 2920–2944.

Legendre, L. and Gosselin, M. 1989. New Production and Export of Organic Matter to the Deep Ocean: Consequences of Some Recent Discoveries. *Limnology and Oceanography.* 34 (7): 1374–1380.

Legendre, L. and Gosselin, M. 1996. Estimation of N or C Uptake Rates by Phytoplankton Using ^{15}N or ^{13}C : Revisiting the Usual Computation Formulae. *Journal of Plankton Research.* 19 (2): 263–271.

Legendre, L. and Rassoulzadegan, F. 1995. Plankton and Nutrient Dynamics in Marine Waters. *Ophelia.* 41: 153–172.

Legendre, L. and Rassoulzadegan, F . 1996. Food-Web Mediated Export of Biogenic Carbon in Oceans: Hydrodynamic Control. *Marine Ecological Progress Series.* 145: 179–193.

Van der Lingen, C. D., Hutchings, L., and Field, J. G. 2010. Comparative Trophodynamics of Anchovy *Engraulis Encrasicolus* and Sardine *Sardinops Sagax* in the Southern Benguela: Are Species Alternations between Small Pelagic Fish Trophodynamically Mediated? *South African Journal of Marine Science.* 28 (3&4): 465–477.

Lipschultz, F. 2008. Isotope Tracer Methods for Studies of the Marine Nitrogen Cycle. *Nitrogen in the Marine Environment, 2nd Edition, Academic Press: Burlington, MA, USA*. 1345-1384.

Liss, P.S. and Johnson, M.T. eds. 2014. *Ocean-atmosphere interactions of gases and particles*. Springer.

Litchman, E. 2007. Resource Competition and the Ecological Success of Phytoplankton. In *Evolution of Primary Producers in the Sea*, 351–376. Amsterdam: Elsevier.

Lomas, M. W. and Glibert, P. M. 1999. Temperature regulation of nitrate uptake: A novel hypothesis about nitrate uptake and reduction in cool-water diatoms. *Limnology and Oceanography.* 44(3): 556-572.

Lomas, M. W., Rumbley, C. J. and Glibert, P. M. 2000. Ammonium Release by Nitrogen Sufficient Diatoms in Response to Rapid Increases in Irradiance. *Journal of Plankton Research.* 22 (12): 2351–2366.

Loranger, C. and Carpentier, R. 1994. A Fast Bioassay for Phytotoxicity Measurements Using Immobilized Photosynthetic Membranes. *Biotechnology and Bioengineering.* 44: 178–183.

Losada, M. and Guerrero, M.G., 1979. The photosynthetic reduction of nitrate and its regulation. *Photosynthesis in relation to model systems.* Amsterdam: Elsevier. 365-408.

Lutjeharms, J. R. E. and Meeuwis, J. M. 1987. The Extent and Variability of South-East Atlantic Upwelling. *South African Journal of Marine Scienc.e* 5 (1): 51–62.

Macintyre, H.L., Kana, T. M.,Anning, T. and Geider, R. J. 2002. Review Photoacclimation of Photosynthesis Irradiance Response Curves and Photosynthetic Pigments in Microalgae and Cyanobacteria. *Journal of Phycology.* 38: 17–38.

MacIsaac, J. J. and Dugdale, R. C. 1972. Interactions of Light and Inorganic Nitrogen in Controlling Nitrogen Uptake in the Sea. *Deep-Sea Research.*19 (3): 209–232.

MacIsaac, J. J. 1978. Diel Cycles of Inorganic Nitrogen Uptake in a Natural Phytoplankton Population Dominated by Gonyaulax Polyedra. *Limnology and Oceanography.* 23 (1): 1–9.

MacIsaac, J. J. and Dugdale, R. C. 1969. The Kinetics of Nitrate and Ammonia Uptake by Natural Populations of Marine Phytoplankton. In *Deep Sea Research*. 16:45–57.

Malone, T. C. 1980. Size-Fractionated Primary Productivity of Marine Phytoplankton. In *Primary Productivity in the Sea*. 301–319. Springer.

Marañón, E., Steele, J., Thorpe, A. and Turekian, A. 2009. Phytoplankton Size Structure. In *Elements of Physical Oceanography: A Derivative of the Encyclopedia of Ocean Sciences.* 85.

Marañón, E., Cermeno, P., Lopez-Sandoval, D. C., Rodriguez-Ramos, T., Sobrino, C., Huete-Ortega, M., Blanco, J. M. and Rodriguez, J. 2013. Unimodal Size Scaling of Phytoplankton Growth and the Size Dependence of Nutrient Uptake and Use. *Ecological Letters.* 16: 371–379.

Margalef, R. 1978. Life-Forms of Phytoplankton as Survival Alternatives in an Unstable Environment. *Oceanologica Acta.* 1 (4): 493–509.

Margeson, J. H., Suggs, J. C. and Midgett, M. R. 1980. Reduction of Nitrate to Nitrite with Cadmium. *Analytical Chemistry*.8: 1955–1957.

Mariotti, A., Germon, J. C., Hubert, P., Kaiser, P., Letolle, R., Tardieux, A. and Tardieux, P. 1981. Experimental Determination of Nitrogen Kinetic Isotope Fractionation: Some Principles; Illustration for the Denitrification and Nitrification Processes. *Plant and Soi.l* 62: 413–430.

Martin, J. H., Knauer, G. A., Karl, D. M. and Broenkow, W.W. 1987. VERTEX: Carbon Cycling in the Northeast Pacific. *Deep Sea Research.* 34 (2): 265–85.

Mcquoid, M. R. and Hobson, L. A. 1996. Diatom Resting Stages. *Journal of Phycology.* 902: 889–902.

Meija, J., Coplen, T. B., Berglund, M., Brand, W. A., De Bièvre, P., Gröning, M., Holden, N. E., et al. 2016. Isotopic Compositions of the Elements 2013 (IUPAC Technical Report). *Pure and Applied Chemistry.* 88 (3): 293–306.

Merbt, S. N., Stahl, D. A., Casamayor, E. O., Marti, E., Nicol, G. W. and Prosser, J. I. 2011. Differential Photoinhibition of Bacterial and Archaeal Ammonia Oxidation. *FEMS Microbiology Letters.* 327: 41–46.

Michaels, A. F., and Silver, M. W. 1988. Primary Production , Sinking Fluxes and the Microbial Food Web. *Deep Sea Research.* 35 (4): 473–490.

Miklasz, K. A. and Denny, M. A. 2010. Diatom Sinking Speeds : Improved Predictions and Insight from a Modified Stokes ' Law. *Limnology and Oceanography.* 55 (6): 2513–2525.

Miller, C. B and Wheeler, P. A. 2012. *Biological Oceanography*. Wiley-Blackwell.

Mitchell-Innes, B. A., Pitcher, G. A. and Probyn, T. A. 2000. Productivity of Dinoflagellate Blooms on the West Coast of South Africa, as Measured by Natural Flourescence. *South African Journal of Marine Science.* 22: 273–284.

Mitchell-Innes, B. A., and Walker, D. R. 1991. Short-Term Variability during an Anchor Station Study in the Southern Benguela Upwelling system: Phytoplankton Production and Biomass in Relation to Species Changes. *Progress in Oceanography.* 28: 65–89.

Moloney, C. L. 1992. Simulation Studies of Trophic Flows and Nutrient Cycles in Benguela Upwelling Foodwebs. *South African Journal of Marine Science.* 12 (1): 457–476.

Moloney, C. L. and Field, J. G. 1989. General Allometric Equations for Rates of Nutrient Uptake , Ingestion, and Respiration in Plankton Organisms. *Limnology and Oceanograph.y* 34 (7): 1290–1299.

Moloney, C.L. and Field, J. G. 1991. The Size-Based Dynamics of Plankton Food Webs . I . A Simulation Model of Carbon and Nitrogen Flows. *Journal of Plankton Research.* 13 (5): 1003–1038.

Moloney, C. L., Field, J. G. and Lucas, M. L. 1991. The Size-Based Dynamics of Plankton Food Webs . II . Simulations of Three Contrasting Southern Benguela Food Webs. *Journal of Plankton Research.* 13 (5): 1039–1092.

Monteiro, P. M. S. and van der Plas, A. K. 2006. Low Oxygen Water (LOW) Variability in the Benguela System: Key Processes and Forcing Scales Relevant to Forecasting." In *Large Marine Ecosystem*s. L.V. Shannon, G. Hempel, P. Malanotte-Rizzoli, C. Moloney, and J. Woods, Eds. 14:92–109. Elsevier B.V. Ltd.

Monteiro, P. M. S. and Roychoudhury, A. N. 2005. Spatial Characteristics of Sediment Trace Metals in an Eastern Boundary Upwelling Retention Area (St . Helena Bay, South Africa): A Hydrodynamic-Biological Pump Hypothesis. *Estuarine Coastal and Shelf Science*.65: 123–134.

Moore, C. M., Mills,M. M., Achterberg, E. P., Geider, R. J., LaRoche, J., Lucas, M. I., McDonagh, E. L., et al. 2009. Large-Scale Distribution of Atlantic Nitrogen Fixation Controlled by Iron Availability. *Nature Geoscience.* 2 (12): 867–871.

Moore, W. S. 2010. The Effect of Submarine Groundwater Discharge on the Ocean. *Annual Review of Marine Science.* 2: 59–88.

Moore, W. S., Sarmiento, J. L. Key, R. M. 2008. Submarine Groundwater Discharge Revealed by 228 Ra Distribution in the Upper Atlantic Ocean. *Nature Geosciences.* 1: 309–311.

Morel, A. and Bricaud, A. 1981. Theoretical Results Concerning Light Absorbtion in a Discrete Medium, and Application to Specific Absorption of Phytoplankton. *Deep Sea Research*. 28 (11): 1375–1393.

Mulholland, M.R. and Capone, D. G. 1999. Nitrogen Fixation, Uptake and Metabolism in Natural and Cultured Populations of *Trichodesmium* Spp." *Marine Ecology Progress Series.* 188: 33–49.

Mulholland, M. R., Ohki, K. and Capone, D. G. 2001. Nutrient Controls on Nitrogen Uptake and Metabolism by Natural Populations and Cultures of *Thrichodesmium* (Cyanobacteria). *Journal of Phycolog*y. 37: 1001–1009.

Murphy, J. and Riley, J. P. 1962. A Modified Single Solution Method for the Determination of Phosphate in Natural Waters. *Analytica Chimica Acta.* 27: 21–36.

Nagel, B., Emeis, K. C., Flohr, A., Rixen, T., Schlarbaum, T., Mohrholz, V. and Van Der Plas, A. 2013. N-Cycling and Balancing of the N-deficit Generated in the Oxygen Minimum Zone over the Namibian Shelf — An Isotope-Based Approach. *Journal of Geophysical Research: Biogeosciences.* 118: 1–11.

Neale, P. J., Cullen, J. J., Lesser, M. P. and Melis, A. 1993. Physiological Bases for Detecing and Predicting Photoinhibition of Aquatic Photosynthesis by PAR and UV Radiation. In *Photosynthetic Responses to the Environment*.H. Y. Yamamoto and C. M. Smith, Eds. 61–77. Maryland, USA: American Society of Plant Physiology.

Needoba, J. A., Foster, R. A., Sakamoto, C., . Zehr, J. P. and Johnson, K. S. 2007. Nitrogen Fixation by Unicellular Diazotrophic Cyanobacteria in the Temperate Oligotrophic North Pacific Ocean. *Limnology and Oceanography.* 52 (4): 1317–1327.

Nelson, G. and Hutchings, L. 1983. The Benguela upwelling area. *Progress in Oceanography*. 12(3): 333-356.

Neumann, A., Lahajnar,N. and Emeis, K. C. 2016. Benthic Remineralisation Rates in Shelf and Slope Sediments of the Northern Benguela Upwelling Margin. *Continental Shelf Research.* 113: 47–61.

Ohki, K., Zehr, J. P., Falkowski, P. G. and Fujita, Y. 1991. Regulation of Nitrogen-Fixation by Different Nitrogen Sources in the Marine Non-Heterocystous Cyanobacterium *Trichodesmium* Sp. NIBB1067." *Archives of Microbiology.* 1067: 335–337.

Olson, R.J. 1981. Differential photoinhibition of marine nitrifying bacteria: a possible mechanism for the formation of the primary nitrite maximum. *Journal of Marine Research*. 39: 227-238.

Owens, N. J. P., Galloway, J. N. and Duce, R. A. 1992. Episodic Atmospheric Nitrogen Deposition to Oligotrophic Oceans. *Nature.* 357: 397-399.

Paerl, H.W. 1997. Coastal eutrophication and harmful algal blooms: Importance of atmospheric deposition and groundwater as "new" nitrogen and other nutrient sources. *Limnology and oceanography*. 42: 1154-1165.

Paerl, H. 1995. Coastal Eutrophication in Relation to Atmospheric Nitrogen Deposition : Current Perspectives. *Ophelia.* 41: 237–259.

Paerl, H. W. and Fogel, M. L. 1994. Isotopic Characterization of Atmospheric Nitrogen Inputs as Sources of Enhanced Primary Production in Coastal Atlantic Ocean Waters. *Marine Biology.* 119: 635–645.

Pauly, D. and Christensen, V. 1995. Primary Production Required to Sustain Global Fisheries. *Nature.* 374: 255–257.

Paytan, A., Shellenbarger, G. G., Street, J. H., Gonneea, M. E., Davis, K., Young, M. B. and Moore, W. S. 2006. Submarine Groundwater Discharge: An Important Source of New Inorganic Nitrogen to Coral Reef Ecosystems. *Limnology and Oceanography.* 51 (1): 343–348.

Pitcher, G. C. 1990. Phytoplankton Seed Populations of the Cape Peninsula Upwelling Plume, with Particular Reference to Resting Spores of *Chaetoceros* (Bacillariophyceae) and Their Role in Seeding Upwelling Waters. *Estuarine, Coastal and Shelf Science.* 31 (3): 283–301.

Pitcher, G. C. 1988. Mesoscale Heterogeneities of the Phytoplankton Distribution in St Helena Bay , South Africa , Following an Upwelling Event. *South African Journal of Marine Science.* 7(1) : 9–23.

Pitcher, G.C. and Calder, D. 2000. Harmful algal blooms of the southern Benguela Current: a review and appraisal of monitoring from 1989 to 1997. *African Journal of Marine Science*. *22*: 255-271.

Pitcher, G.C. and Weeks, S.J. 2006. 7 The variability and potential for prediction of harmful algal blooms in the southern Benguela ecosystem. In *Large marine ecosystems*. 14: 125-146. Elsevier.

Pitcher, G. C., Brown, P. C. and Mitchell-Innes, B. A. 1992. Spatio-Temporal Variability of Phytoplankton in the Southern Benguela Upwelling System. *South African Journal of Marine Science.* 12(1): 439-456

Pitcher, G. C., Walker, D. R., Mitchell-Innes, B. A. and Moloney, C. L. 1991. Short-Term Variability during an Anchor Station Study in the Southern Benguela Upweiling System: Phytoplankton Dynamics. *Progress in Oceanography.* 28: 39–64.

Probyn, T. A. 1992. The Inorganic Nitrogen Nutrition of Phytoplankton in the Southern Benguela: New Production, Phytoplankton Size and Implications for Pelagic Foodwebs. *South African Journal of Marine Science.* 12 (1): 411–420.

Probyn, T. A., Mitchell-Innes, B. A. and Searson S. 1995. Primary Productivity and Nitrogen Uptake in the Subsurface Chlorophyll Maximum on the Eastern Agulhas Bank. *Continental Shelf Research.* 15 (15): 1903–1920.

Probyn, T. A. and Painting, S. J. 1985. Nitrogen Uptake by Size-Fractionated Phytoplankton Populations in Antarctic Surface Waters." *Limnology and Oceanography.* 30: 1327–1332.

Probyn, T.A., Waldron, H. N. and James, A. G. 1990. Size-Fractionated Measurements of Nitrogen Uptake in Aged Upwelled Waters: Implications for Pelagic Food Webs. *Limnology and Oceanography.* 35 (1): 202–210.

Probyn, T. A. 1985. Nitrogen Uptake by Size-Fractionated Phytoplankton Populations in the Southern Benguela Upwelling System. *Marine Ecology Progress Series.* 22(3):249-258.

Probyn, T. A., Waldron, H. N., Searson, S. and Owens, N. J. P. 1996. Diel Variability in Nitrogenous Nutrient Uptake at Photic and Sub- Photic Depths. *Journal of Plankton Research.* 18 (3): 2063–2079.

Raven, J. A. Waite, A. M. 2004. The Evolution of Silicification in Diatoms : Inescapable Sinking and Sinking as Escape? *New Phytologyst.* 162: 45–61.

Redfield, A. C. 1958. The Biological Control of Chemical Factors in the Environment. *American Scientist.* 46 (3): 205–221.

Riemann, B., Simonsen, P. and Stensgaard, L. 1989. The Carbon and Chlorophyll Content of Phytoplankton from Various Nutrient Regimes. *Journal of Plankton Research.* 11 (5): 1037–1045.

Rykaczewski, R. R., Dunne, J. P., Sydeman, W. J., García-Reyes, M., Black, B. A. and Bograd, S. J. 2015. Poleward Displacement of Coastal Upwelling-Favorable Winds in the Ocean's Eastern Boundary Currents through the 21st Century. *Geophysical Research Letters.* 42 (15): 6424–6431.

Ryther, J. H. 1969. Photosynthesis and Fish Production in the Sea. *Science.* 166 (3901): 72–76.

Sabine, C. L., Feely, R. A., Gruber, N., Key, R. M., Lee, K., Bullister, J. L., Wanninkhof, R., et al. 2004. The Oceanic Sink for Anthropogenic CO_2. *Science.* 305: 367–372.

Sandroni, V., Raimbault, P., Migon, C., Garcia, N. and Gouze, E. 2007. Dry Atmospheric Deposition and Diazotrophy as Sources of New Nitrogen to Northwestern Mediterranean Oligotrophic Surface Waters. *Deep-Sea Research Part 1.* 54: 1859–1870.

Sarmiento, J. L. and Gruber, N. 2002. Sinks for Anthropogenic Carbon. *Physics Today.* 55 (8): 30–36.

Sathyendranath, S., Lazzara, L. and Prieur, L. 1987. Variations in the Spectral Values of Specific Absorption of Phytoplankton. *Limnology and Oceanography.* 32 (2): 403–415.

Schön, G.H. and Engel, H. 1962. Der einfluss des lichtes auf Nitrosomonas europaea Win. *Archives of Microbiology*. 42(4): 415-428.

Schulz, H. N. and Jørgensen, B. B. 2001. Big Bacteria. *Annual Review on Microbiology.* 55: 105–137.

Schulz, H. N. and Schulz, H. D. 2005. Large Sulfur Bacteria and the Formation of Phosphorite. *Science.* 307: 416–419.

Seitzinger, S. P. 1988. Denitrification in Freshwater and Coastal Marine Ecosystems: Ecological and Geochemical Significance. *Limnology and Oceanography.* 33(4): 702–724.

Shannon, L. V. and Nelson, G. 1996. The Benguela: Large Scale Features and Processes and System Variability. In *The South Atlantic: Present and Past Circulation*. 163–210. Berlin, Heidelberg: Springer.

Shannon, L. V. and O'Toole, M. J. 1999. Integrated Overview of the Oceanography and Environmental Variability of the Benguela Current Region. In Synthesis and assessment of information on the Benguela Current large marine ecosystem (*BCLME),* Thematic Report NO. 2.

Shannon, L. V. and O'Toole, M. J. 2003. Sustainability of the Benguela: Ex Africa Semper Aliquid Novi. In *Large Marine Ecosystems of the World:Trends in Exploitation, Protection and Research*. 227–253.

Sharp, J. H. 1983. The Distributions of Inorganic Nitrogen and Dissolved and Particulate Organic Nitrogen in the Sea. In *Nitrogen in the Marine Environment*. 1–35.

Shillington, F. A., Reason, C. J. C., Duncombe Rae, C. M., Florenchie, P. and Penven, P. 2006. Large Scale Physical Variability of the Benguela Current Large Marine Ecosystem (BCLME).In *Large Marine Ecosystems.*V. Shannon, G. Hempel, P. Malanotte-Rizzoli, C. Moloney and J. Woods, Eds. 14: 49–70.

Siegenthaler, U. and Sarmiento, J. L. 1993. Atmospheric Carbon Dioxide and the Ocean. *Nature.* 365: 119–125.

Sigman, D. M., Casciotti, K. L., Andreani, M., Barford, C., Galanter, M. and Bohlke, J. K. 2001. A Bacterial Method for the Nitrogen Isotopic Analysis of Nitrate in Seawater and Freshwater. *Analytical Chemistry.* 73 (17): 4145–4153.

Sigman, D. M., Karsh, K. L. and Casciotti, K. L. 2009. *Ocean Process Tracers: Nitrogen Isotopes in the Ocean.* Elsevier Ltd.

Sigman, D. M. and Hain, M. P. 2012. The Biological Productivity of the Ocean. *Nature Education.* 3 (6): 1–16.

Sijbesma, W. F. H., Almeida, J. S., Reis, M. A. M. and Santos, H. 1996. Uncoupling Effect of Nitrite During Denitrification by *Pseudomonas Fluorescens*; An In Vivo 31P-NMR Study." *Biotechnology and Bioengineering.* 52: 176–182.

Silva, A., Palma, S., Oliveira, P.B. and Moita, M. T. 2009. Composition and Interannual Variability of Phytoplankton in a Coastal Upwelling Region (Lisbon Bay, Portugal). *Journal of Sea Research.* 62 (4): 238–249.

Smayda, T. J. 2000. Ecological Features of Harmful Algal Blooms in Coastal Upwelling Ecosystems. *South African Journal of Marine Science.* 22: 219–253.

Smayda, T.J. 1997. Harmful algal blooms: their ecophysiology and general relevance to phytoplankton blooms in the sea. *Limnology and oceanography*. 42: 1137-1153.

Smayda, T.J. 1980. Phytoplankton species succession. *The physiological ecology of phytoplankton.* 493-570.

Smayda, T.J. 1970. The suspension and sinking of phytoplankton in the sea. *Oceanography and Marine Biology Annual Review.* 8: 353-414.

Smetacek, V. S. 1985. Role of Sinking in Diatom Life-History Cycles: Ecological, Evolutionary and Geological Significance. *Marine Science*. 251: 239–251.

Smetacek, V., Klaas, C., Strass, V. H., Assmy, P., Montresor, M., Cisewski, B., Savoye, N., et al. 2012. Deep Carbon Export from a Southern Ocean Iron-Fertilized Diatom Bloom. *Nature.* 487: 313–319.

Smith, J.M., Chavez, F.P. and Francis, C.A. 2014. Ammonium uptake by phytoplankton regulates nitrification in the sunlit ocean. *PLoS One*. 9(9): e108173.

Smith, L. and Zawadzki, W. 2003. A Hydrogeologic Model of Submarine Groundwater Discharge: Florida Intercomparison Experiment. *Biogeochemistry.* 66 (1): 95–110.

Sohm, J. A., Hilton, J. A., Noble, A. E., Zehr, J. P., Saito, M. A. and Webb, E. A. 2011. Nitrogen Fixation in the South Atlantic Gyre and the Benguela Upwelling System. *Geophysical Research Letters.* 38: 1–6.

Sommer, U. 1984. The Paradox of the Plankton : Fluctuations of Phosphorus Availability Maintain Diversity of Phytoplankton in Flow-through Cultures. *Limnology and Oceanograph.y* 29 (3): 633–636.

Spiller, H. and Boger, P. 1997. Photosynthetic Nitrite Reduction by Dithioerythritol and the Effect of Nitrite on Electron Transport in Isolated Chloroplasts. *Photochemistry and Photobiology.* 26: 397–402.

Steele, J. H. and Yentsch, C. S. 1960. The vertical distribution of chlorophyll. *Journal of the Marine Biological Association of the United Kingdom.* 39(2): 217-226.

Strickland, J.D. and Parsons, T.R. 1972. A practical handbook of seawater analysis, 2nd ed. *Fisheries Research Board of Canada*. 167: 1- 310.

Sunda, W. G. and Huntsman, S. A. 1997. Interrelated Influence of Iron, Light and Cell Size on Marine Phytoplankton Growth. *Nature.* 390: 389–392.

Sverdrup, H.U. 1953. On vernal blooming of phytoplankton. *Conseil Exp.* 18: 287-295.

Sweeney, R. E. and Kaplan, I. R. 1980. Natural Abundances of ^{15}N as a Source Indicator for Near-Shore Marine Sedimentary and Dissolved Nitrogen. *Marine Chemistry.* 9 : 81–94.

Sydeman, W. J., Garcia-Reyes, M., Schoeman, D. S., Rykaczewski, R. R., Thompson, S. A., Black, B. A. and Bograd, S. J. 2014. Climate Change and Wind Intensification in Coastal Upwelling Ecosystems. *Science.* 345 : 77–80.

Syrett, P.J., 1981. Nitrogen metabolism of microalgae. *Can. Bull. Fish. Aquat. Sci. 210*: 182-210.

Taguchi, S. 1976. Relationship between Photosynthesis and Cell Size of Marine Diatoms. *Journal of Phycology.* 12: 185–189.

Takahashi, T., Sutherland, S. C., Sweeney, C., Poisson, A., Metzl, N., Tilbrook, B., Bates, N., et al. 2002. Global Sea – Air CO_2 Flux Based on Climatological Surface Ocean pCO_2, and Seasonal Biological and Temperature Effects. *Deep Sea Research Part II.* 49: 1601–1622.

Takahashi, T.,, Sutherland, S. C., Wanninkhof, R., Sweeney, C., Feely, R. A., Chipman, D. W., Hales, B., et al. 2008. Climatological Mean and Decadal Change in Surface Ocean pCO_2, and Net Sea – Air CO_2 Flux over the Global Oceans. *Deep Sea Research Part II.* 56: 554–577.

Taniguchi, M., Burnett, W. C., Cable, J. E. and Turner, J. V. 2002. Investigation of Submarine Groundwater Discharge. *Hydrological Processes.* 16: 2115–2129.

Taniguchi, M., Ishitobi, T. and Saeki, K. I. 2005. Evaluation of Time-Space Distributions of Submarine Ground Water Discharge. *Ground Water.* 43 (3): 336–342.

Touratier, F., Field, J. G. and Moloney, C. L. 2003. Simulated Carbon and Nitrogen Flows of the Planktonic Food Web during an Upwelling Relaxation Period in St Helena Bay (Southern Benguela Ecosystem). *Progress in Oceanography.* 58: 1–41.

Tuerena, R. E., Ganeshram, R. S., Geibert, W., Fallick, A. E., Dougans, J., Tait, A., Henley, S. F. and Woodward, E. M. S. 2015. Nutrient Cycling in the Atlantic Basin: The Evolution of Nitrate Isotope Signatures in Water Masses. *Global Biogeochemical Cycles*. 29: 1–15.

Tyrrell, T. and Lucas, M I. 2002. Geochemical Evidence of Denitrification in the Benguela Upwelling System. *Continental Shelf Research.* 22: 2497–2511.

Tyson, P. D. 1986. *Climatic Change and Variability in Southern Africa*. United States of America: Oxford University Press.

UBC Department of Earth, Ocean and Atmospheric Sciences. 2012. *Phyto'pedia – The Phytoplankton Encyclopaedia Project*. Available: https://www.eoas.ubc.ca/research/phytoplankton/ [2019, February 4].

Van Oostende, N., Dunne, J.P., Fawcett, S.E. and Ward, B.B. 2015. Phytoplankton succesion explains size-partitionaing of new production following upwelling-induced blooms. *Journal of Marine Systems*. 148: 14-25.

Veitch, J., Hermes, J., Lamont, T., Penven, P. and Dufois, F. 2018. Shelf-edge jet currents in the southern Benguela: A modelling approach. *Journal of Marine Systems*. 188: 27-38.

Verheye, H. M. 2000. Decadal-Scale Trends Across Several Marine Trophic Levels in the Southern Benguela Upwelling System off South Africa. *Ambio* 29 (1): 30–34.

Verheye, H. M. and Richardson, A. J. 1998. Long-Term Increase in Crustacean Zooplankton Abundance in the Southern Benguela Upwelling Region (1951 – 1996): Bottom-up or Top-down Control?" *ICES Journal of Marine Science.* 55: 803–807.

Wada, E. and Hattori, A. 1971. Nitrite Metabolism in the Euphotic Layer of the Central North Pacific Ocean. *Limnology and Oceanography.* 16 (5): 766–772.

Wada, E. and Hattori, A . 1978. Nitrogen Isotope Effects in the Assimilation of Inorganic Nitrogenous Compounds by Marine Diatoms. *Geomicrobiology Journal.* 1 (1): 37–41.

Waldron, H. N. and Probyn, T. A. 1992. Nitrate Supply and Potential New Production in the Benguela Upwelling System. *South African Journal of Marine Science.* 12 (1): 29–39.

Waldron, H.N. 1985. Influences on the hydrology of the Cape Columbine/St Helena Bay region. MSc thesis, Univeristy of Cape Town.

Wang, D., Gouhier, T. C., Menge, B. A. and Ganguly, A. R. 2015. Intensification and Spatial Homogenization of Coastal Upwelling under Climate Change. *Nature.* 518: 390–394.

Wang, X. J., Behrenfeld, M., Le Borgne, R., Murtugudde, R. and Boss, E.. 2009. Regulation of Phytoplankton Carbon to Chlorophyll Ratio By Light, Nutrients and Temperature in the Equatorial Pacific Ocean: A Basin-Scale Model. *Biogeosciences.* 6: 391–404.

Wankel, S. D., Kendall, C., Pennington, J. T., Chavez, F. P. and Paytan, A. 2007. Nitrification in the Euphotic Zone as Evidenced by Nitrate Dual Isotopic Composition: Observations from Monterey Bay, California. *Global Biogeochemical Cycles.* 21 (2): 1–13.

Ward, B. B. 2005. Temporal Variability in Nitrification Rates and Related Biogeochemical Factors in Monterey Bay, California, USA. *Marine Ecology Progress Series.* 292: 97–109.

Ward, B.B., 2000. Nitrification and the marine nitrogen cycle. *Microbial ecology of the oceans*. 427-453.

Ward, B. B., Kilpatrick, K. A., Renger, E. H. and Eppley, R. W. 1989. Biological Nitrogen Cycling in the Nitracline. *Limnology and Oceanography.* 34 (3): 493–513.

Ward, B.B. 1985. Light and substrate concentration relationships with marine ammonium assimilation and oxidation rates. *Marine Chemistry*. 16(4): 301-316.

Waser, N. A. D., Harrison, P. J., Nielsen, B., Calvert, S. E. and Turpin, D. H. 1998. Nitrogen Isotope Fractionation during the Uptake and Assimilation of Nitrate, Nitrite, Ammonium, and Urea by a Marine Diatom. *Limnology and Oceanography.* 43 (2): 215–224.

Wasmund, N., Struck, U., Hansen, A., Flohr, A., Nausch, G., Gruttmuller, A. and Voss, M. 2015. Missing nitrogen fixation in the Benguela region. *Deep-Sea Research 1.* 106: 30-41.

Wassenaar, L. I. 1995. Evaluation of the Origin and Fate of Nitrate in the Abbotsford Aquifer Using the Isotopes of ^{15}N and ^{18}O in NO_3^-." *Applied Geochemistry.* 10: 391–405.

Watson, A., Miller, J., Fleischer, M. and De Clercq, W. 2018. Estimation of Groundwater Recharge via Percolation Outputs from a Rainfall/Runoff Model for the Verlorenvlei Estuarine System, West Coast, South Africa." *Journal of Hydrology.* 558: 238–254.

Weeks, S. J., Barlow, R., Roy, C. and Shillington, F. A. 2006. Remotely Sensed Variability of Temperature and Chlorophyll in the Southern Benguela: Upwelling Frequency and Phytoplankton Response. *African Journal of*

Marine Science. 28 (4): 493–509.

Welschmeyer, N.A., 1994. Fluorometric analysis of chlorophyll a in the presence of chlorophyll b and pheopigments. *Limnology and Oceanography*. *39*(8): 1985-1992.

Wetz, M. S. and Wheeler, P. A. 2003. Production and Partitioning of Organic Matter during Simulated Phytoplankton Blooms. *Limnology and Oceanography.* 48 (5): 1808–1817.

Whitledge, T. E. 1981. Nitrogen Recycling and Biological Populations in Upwelling Ecosystems. In *Coastal Upwelling*. 257–273. American Geophysical Union.

Wilkerson, F. P. and Dugdale, R. C. 1987. The Use of Large Shipboard Barrels and Drifters to Study the Effects of Coastal Upwelling on Phytoplankton Dynamics. *Limnology and Oceanography.* 32 (2): 368–382.

Wilkerson, F. P., Dugdale, R. C., Kudela, R. M. and Chavez, F. P. 2000. Biomass and Productivity in Monterey Bay, California: Contribution of the Large Phytoplankton. *Deep-Sea Research Part II.* 47 (5–6): 1003–1022.

Wilkerson, F. P. and Dugdale, R. C. 2008. Coastal Upwelling. In *Nitrogen in the Marine Environment*. 771-807.

Wilkerson, F. P., Dugdale, R. C., Hogue, V. E. and Marchi, A. 2006. Phytoplankton Blooms and Nitrogen Productivity in San Francisco Bay. *Estuaries and Coasts*. 29 (3): 401–416.

Wu, J., Calvert, S. E. and Wong, C. S. 1997. Nitrogen Isotope Variations in the Subarctic Northeast Pacific: Relationships to Nitrate Utilization and Trophic Structure. *Deep Sea Research part I.* 44 (2): 287–314.

Yang, S., Wang, J., Cong, W., Cai, Z. and Ouyang, F. 2004. Utilization of Nitrite as a Nitrogen Source by *Botryococcus Braunii*." *Biotechnology Letters.* 26: 239–243.

Zehr, J. P. and Ward, B. B. 2002. Nitrogen Cycling in the Ocean: New Perspectives on Processes and Paradigms. *Applied and Environmental Microbiology.* 68 (3): 1015–1024.

Zehr, J. P., Waterbury, J. B., Turner, P. J., Montoya, J. P., Omoregie, E., Steward, G. F., Hansen, A. and Karl, D. M. 2001. Unicellular Cyanobacteria Fix N_2 in the Subtropical North Pacific Ocean. *Nature.* 412 : 25–28.

Zentara, S. J. and Kamykowski, D. 1977. Latitudinal Relationship among Temperature and Selected Plant Nutrients along West Coast of North-America and South-America. *Journal of Marine Research.* 35 (2): 321–337.